

© 2018

Maria J. Qadri

ALL RIGHTS RESERVED

Phase Plane Analysis & Morphological Simulation of Intracranial Pressure
Variability for Physiological Monitoring of Acute Severe Brain Injury

By

MARIA JAMAL QADRI

A dissertation submitted to the

School of Graduate Studies

Rutgers, The State University of New Jersey

In partial fulfillment of the requirements

For the degree of

Doctor of Philosophy

Graduate Programs in Biomedical Engineering & Quantitative Biomedicine

Written under the direction of

William Craelius

And approved by

New Brunswick, New Jersey

January 2018

ABSTRACT OF THE DISSERTATION

Phase Plane Analysis & Morphological Simulation of Intracranial Pressure

Variability for Physiological Monitoring of Acute Severe Brain Injury

By MARIA JAMAL QADRI

Dissertation Director: William Craelius, Ph.D.

After severe acute brain trauma, cerebrovascular autoregulation (AR) can be impaired, but the performance of this homeostatic mechanism cannot be interrogated directly due to the complexity of the vascular system and existing challenges in assessing cerebrovascular phenomena. When indicated by the severity of brain trauma, clinicians continuously monitor intracranial pressure (ICP) to assess cerebral perfusion as a proxy measure for neural tissue oxygenation. The Monroe-Kellie doctrine states that the sum of the brain tissue, blood in the cerebrovascular bed, and cerebrospinal fluid in the ventricles is held constant within the cranial cavity; the resultant pressure of these volumes within the cranial cavity is ICP which fluctuates during a single cardiac cycle. Where ABP presents two peaks corresponding to systole and diastole, ICP presents three distinct peaks that correspond to cardiac systole (peak 1), cerebrovascular compliance (peak 2), and cardiac diastole (peak 3). Recent research on the

morphology of individual intracranial pressure beats indicates the potential to use transient morphological changes in ICP between cardiac cycles in the time domain to gain greater insight into physiological performance of AR and near-future ICP.

In order to highlight fluctuations in ICP behavior between successive cardiac cycles, this dissertation presents a novel method to analyze ICP morphology by transforming this cerebral pressure data from the time-domain to the phase-domain. Since existing mathematical models of the cerebrovascular performance focus on longer time-scale ICP behavior and clinically measured ICP morphology during cardiac cycles is often erratic, this dissertation demonstrates a novel morphological simulation of ICP to test a phase domain metric, the phase area ratio (PAR) in application to ICP monitoring.

An additive Gaussian simulation of ICP was developed to specifically examine the behavior of ICP Peak 2 that represents cerebral compliance, which is the component of AR that cannot be assessed directly using other existing physiological measures. This dissertation tests the hypothesis that phase domain analysis of ICP is useful as a forecasting tool for intracranial hypertension (IH) after severe acute brain trauma and post-surgical intervention. To test this hypothesis, 300 simulated ICP cycles and over 1 million clinical ICP cycles from 7 patients were analyzed. The simulated data were analyzed in a linear model that showed an R-squared value of no more than 0.76 for PAR and peak 2 amplitude, and the model showed a 0.93 R-squared value or higher between

mICP and peak 2 behavior. The Spearman's correlation presented weak positive correlations between PAR and ICP ranging from 0.4 for the 1-hr time span to -0.1 for the 0.1-hr time span in time segments preceding intracranial hypertension (preIH). Overall in the clinical data examination, PAR was successfully able to differentiate between time periods of intracranial normotension and preIH time periods ranging from 1 to 0.1 hours using a Kolmogorov-Smirnov test for 67.9% of time periods tested in the seven patients. PAR performed with a lower area under the curve (0.53) than the time domain metric, Sample Entropy (SE) (0.71), when tested as a threshold classifier using receiver operator characteristic analysis for all time points in the exemplar patient. When analyzing all patient data, the area under the curve for PAR came out to 0.43 for a 1-hr window. A confusion matrix analysis of all patient data that yielded similar results as the receiver operator curve analysis. Using a logistic regression approach for prediction measurement, the results showed that PAR adds value to the performance of the model, where a longer amount of prior information yields better predictions for shorter times into the future. When PAR was used in conjunction with other metrics in a classifier, PAR-based metrics were more valuable than PAR itself. Overall PAR is a parameter that (1) requires less data for calculation than existing metrics, (2) has a bounded range between 0 to 1, and (3) does not have discontinuities like comparable complexity metrics. Ultimately, this work shows that PAR contributes unique information to existing multi-parameter prediction algorithms to forecast IH.

DEDICATION

"If I have seen further, it is by standing on the shoulders of giants."

– Sir Isaac Newton, 1676

This document is a testament to my family:

genetic and chosen.

past, present, and future.

To my Nani & Nana: Hamida Begum & Muhammad Sultan

To my Dadi & Dada: Maryam Khatoon & M. Afzal H. Qadri

To my Ami: Fahmeeda J. Qadri

To my Abu: Jamal H. Qadri

To my three brilliant brothers, my three encouraging sisters, & their joyful children

To my partner then, now, and forever: Thomas G. Barker

ACKNOWLEDGEMENTS

I am the sum of all of my experiences and all of the people I have encountered in my existence. I cannot thank each of you individually here – you remain an everlasting and vital part of my success.

To my committee members, thank you for your time, your effort, and your insights. I could not have completed this research without you.

To my advisor, **Dr. William Craelius**: thank you for giving me the opportunity to work under your direction with the freedom to further develop my scientific skills and gain the expertise I was seeking in the culmination of my academic training.

Dr. Shabbar Danish: thank you for continuing to do research as a renowned clinician and imparting me with your expertise in everything related to the brain.

Dr. Troy Shinbrot: thank you for your guidance on everything from pedagogy to inclusion to mathematical modeling and your unfailing counsel in times of doubt.

Dr. Michael Wininger: thank you for always picking up the phone, sharing your invaluable perspective on every aspect of this trip, and always guiding me to the most efficient and effective path to sound scientific research.

To my lab mates in the Biomechanics and Rehabilitation Engineering Lab, thank you for your comradery and your scientific contributions to this research.

Nam Kim Ph.D., Kim Moradi Ph.D., Alex Krasner M.S., Bianca Pineda M.S., Todd Alter B.S., Zachary Kappus B.S., Colin Kosinski B.S., Shiv Patel B.S., and Alex Shin B.S.

To my Rutgers University BME, QB & beyond-program family, thank you for always being only a walk, a snack, a beverage, or a message away.

These friendships and memories have sustained me through innumerable grand highs and dark lows. Thank you does not capture the deep appreciation I have for the privilege of being in this place, in this time, with each of you.

To my funding sources: Thank you for the food, shelter, and peace of mind you provided me while I completed this journey. Thank you to the several internal funding resources within **Rutgers University**, particularly the **Institute of Quantitative Biomedicine**, **Division of Life Science** & the **Biomedical Engineering Department** for my teaching assistantships. Thank you to the **New Jersey Commission on Brain Injury Research** for my graduate research assistantship and the continual reminder of my purpose in asking “How?” and “Why?” repeatedly.

My entire academic journey has been an exhilarating rollercoaster that has shaped me as a human being. I would not have realized my potential without all of my peers, mentors, teachers, friends, & family to care for my well-being and inspire me in accomplishing this endeavor. With the deepest sincerity, thank you.

TABLE OF CONTENTS

| | |
|---|------|
| ABSTRACT OF THE DISSERTATION | ii |
| DEDICATION | v |
| ACKNOWLEDGEMENTS | vi |
| TABLE OF CONTENTS | viii |
| TABLE OF FIGURES | xii |
| TABLE OF TABLES | xii |
| TABLE OF EQUATIONS | xvii |
| CHAPTER 1. INTRODUCTION | 1 |
| 1.1 Neurotrauma Incidence, Classification, and Treatment | 1 |
| 1.2 Cardiac Cycle: Vascular and Cerebrovascular Phenomena | 3 |
| 1.3 Models of Intracranial Pressure | 5 |
| 1.4 Intracranial Hypertension Metrics | 7 |
| 1.5 Hypothesis and Approach | 8 |
| CHAPTER 2. PHASE DOMAIN ANALYSIS | 9 |
| 2.1 Phase Domain Description | 9 |
| 2.1.1. Mathematical Foundation | 9 |
| 2.1.2. Previous Applications of Phase-Domain Analysis | 10 |
| 2.2 Definition of Phase Area Ratio | 11 |

| | |
|---|----|
| CHAPTER 3. MORPHOLOGICAL SIMULATION OF INTRACRANIAL PRESSURE | 15 |
| 3.1 Simulation: Primary Development | 15 |
| 3.1.1 ICP Gaussian Decomposition | 15 |
| 3.1.2 Parameters and Performance | 16 |
| 3.2 Simulation: Experimental Design | 20 |
| 3.2.1 Extraction of Time-Domain Features: | 21 |
| 3.2.2 Linear Modeling of Features | 23 |
| 3.2.2.1. Amplitude of Peak 2 | 23 |
| 3.2.2.2. Mean ICP | 23 |
| 3.3 Simulation Results | 24 |
| 3.3.1 Boxplots of Results | 24 |
| 3.3.2 Linear Modeling of Results | 28 |
| 3.3.2.1 Amplitude of Peak 2 | 28 |
| 3.3.2.2 Mean ICP | 29 |
| 3.4 Signal to Noise Ratio Performance of PAR | 30 |
| CHAPTER 4. PHASE AREA RATIO PERFORMANCE IN CLINICAL TRAUMA RECORDINGS | 33 |
| 4.1 Sample Population | 33 |

| | |
|--|----|
| 4.2 Data Collection & Conditioning | 34 |
| 4.3 Analysis Methods and Results | 39 |
| 4.3.1 Identifying preIH Timespans | 39 |
| 4.3.2 Relationship Between PAR and mICP via Linear Regression | 40 |
| 4.3.3 Correlation with ICP | 41 |
| 4.3.4 Separation of preIH and IN Distributions | 46 |
| 4.3.5 Receiver Operator Characteristic Curve | 50 |
| 4.3.6 Classification of Data Across Population | 54 |
| 4.3.7 PAR General Utility in Predicting Hypertensive Events | 56 |
| 4.3.8 PAR Specific Features Useful for Predicting Hypertensive Events | 61 |
| 4.3.9 Simulated Prediction of Hypertensive Events | 64 |
| 4.4 Overall Results | 67 |
| CHAPTER 5. FUTURE DIRECTIONS AND CONCLUSIONS | 70 |
| 5.1 Future Directions | 70 |
| 5.1.1 Alternative Phase Domain Metrics | 70 |
| 5.1.2 Multiparameter Phase Domain Analysis | 70 |
| 5.1.3 Accelerating PAR Score Calculation Time and Increasing SNR | 71 |

| | |
|---|-----|
| 5.1.4 Combinatorial Approach to Cerebrovascular AR Monitoring | 73 |
| 5.2 Conclusions | 74 |
| APPENDIX I. REFERENCES | 77 |
| APPENDIX II. ABBREVIATIONS | 81 |
| APPENDIX III. PEER-REVIEWED MANUSCRIPTS, CONFERENCE PROCEEDINGS, AND PRESENTATIONS | 82 |
| Publications | 82 |
| In Preparation | 82 |
| Peer Reviewed Conference Proceedings | 82 |
| APPENDIX IV. FULL RESULTS OF SIMULATION LINEAR MODEL | 84 |
| Width Modulation | 84 |
| Width variation -- Output:mlCP | 84 |
| Width variation -- Output:peaks2 | 86 |
| Amplitude Modulation | 89 |
| Amplitude variation -- Output:mlCP | 90 |
| Amplitude variation -- Output:peak2 | 92 |
| APPENDIX V. CLINICAL DATA - PATIENT A-F SUMMARIES | 96 |
| APPENDIX VI. MOCK ALARM FOR PATIENTS A-F | 102 |

TABLE OF FIGURES

| | |
|--|----|
| Figure 1. Representation of Relationship between Vascular and Cerebrovascular Cycles. | 3 |
| Figure 2. Sample Ursino Model Output during 5-level Bolus Infusion Study. | 7 |
| Figure 3. Phase Area Ratio Components | 12 |
| Figure 4. ICP in the Time, Velocity Phase Plane and Acceleration Phase Plane for Health And Impaired Signals..... | 14 |
| Figure 5. Exemplar of ICP simulation with Three Gaussian Sub-Components Shown | 18 |
| Figure 6. Exemplar @findpeaks with ICP simulation for Individual Peak Amplitudes and Widths | 19 |
| Figure 7. Simulated ICP Width Modulation Exemplars for Low, Medium, High Time Domain, 1st & 2nd Derivatives, and Acceleration-Velocity Phase Plane | 20 |
| Figure 8. Simulated ICP Amplitude Modulation Exemplars for Low, Medium, High Time Domain, 1st & 2nd Derivatives, and Acceleration-Velocity Phase Plane | 20 |
| Figure 9. Measured Amplitude and Width for Model 1: Width Modulation | 25 |
| Figure 10. Measured Amplitude and Width for Model 2: Amplitude Modulation . | 26 |
| Figure 11. Results from Simulated Width Modulation at Three Levels for Time Domain Features and Phase Domain Features | 26 |
| Figure 12. Results from Simulated Amplitude Modulation at Three Levels for | |

| | |
|---|----|
| Time Domain Features and Phase Domain Features | 27 |
| Figure 13. Experimental SNR Modulation Exemplars for SNR of 20 (top row), 40 (middle row), and 80 (bottom row) with time domain (left column), derivatives (middle column), and acceleration phase plane (right column) | 31 |
| Figure 14. SNR Modulation from 50 to 100 dB in increments of 2dB with the Raw PAR in Blue and the Filtered PAR in Red SNR (Left), PAR1 (Middle), and PAR2 (Right) results | 32 |
| Figure 15. Abbreviated Sample of ICP Recording with Segmented Cardiac Cycles | 35 |
| Figure 16. Exemplar Raw Clinical ICP recording for One Hour | 38 |
| Figure 17. FFT data of the Raw Clinical ICP from Figure 14 | 38 |
| Figure 18. 20-second Window of Raw Clinical ICP Exemplar | 39 |
| Figure 19. Clinical Exemplar of Raw (Blue) versus Filtered (Orange) ICP, dICP, & ddICP in Time Domain and Phase Domain for a single cardiac cycle .. | 39 |
| Figure 20. Exemplar of Data Masking to Identify Onset of IH events & Classify IN (green), preIH (yellow), IH (red), and postIH (pink) time Periods | 40 |
| Figure 21. Patient Exemplar Recorded ICP & Analysis for 24 hours | 42 |
| Figure 22. Patient Exemplar Zoomed In | 43 |
| Figure 23. Spearman's Correlation of PAR and SE to ICP during IN segments for Exemplar Patient at selected time increments | 43 |
| Figure 24. Spearman's Correlation of PAR and SE to ICP during preIH segments | |

| | |
|---|----|
| for Exemplar Patient at selected time increments | 44 |
| Figure 25. Patient Exemplar KS Test of IN & preIH hours at 1-hour interval; Left: Non-parametric distribution fitting of the density histograms for PAR Right: Non-parametric distribution fitting of the density for SE data | 46 |
| Figure 26. Non-parametric distribution fitting of the density histograms for PAR for Patients A-F | 49 |
| Figure 27. Receiver Operator Curves for PAR and SE for Exemplar Patient with 1-hr preIH window. Red circle indicates maximum distance from dashed line and labeled with corresponding PAR or SE value | 52 |
| Figure 28. Receiver Operator Curves for PAR and SE for Patients A-F with 1-hr window. Red circle indicates maximum distance from dashed line and labeled with corresponding PAR or SE value..... | 53 |
| Figure 29. ROC Curve for All Patient Data | 54 |
| Figure 30. Mean Predictive Model Performance for 0.1, 0.25, 0.5, and 1 Hour statistic windows with error bars depicting standard error..... | 60 |
| Figure 31. ROC of 12 Parameter Classifier | 65 |
| Figure 32. Mock Alarm Results in Exemplar Patient. Alarm on, preIH, IH, postIH, IN | 66 |
| Figure 33. Example of Multiple Cycles Aggregated: Individual Cycles, Mean Cycle, Absolute Maximum and Absolute Minimum Values | 72 |
| Figure 34. Acceleration-Velocity Phase Plane of Mean ICP signal from Figure 27 | 73 |

TABLE OF TABLES

| | |
|--|----|
| Table 1. ICP Cycle Components | 5 |
| Table 2. Study Design Parameters..... | 19 |
| Table 3. Summary of features extracted from ICP pulses | 22 |
| Table 4. R-Squared Values for Linear Model Analysis of Peak 2 Amplitude | 29 |
| Table 5. R-Squared Values for Linear Model Analysis of mean ICP | 30 |
| Table 6. Patient Summary Information | 34 |
| Table 7. Linear Regression of PAR predicting ICP for Exemplar Patient | 41 |
| Table 8. Spearman's Rank Correlation between PAR and mICP during IN hours | 45 |
| Table 9. Spearman's Rank Correlation between PAR and mICP during preIH hours | 46 |
| Table 10. Results of Two-sided Kolmogorov Smirnov Test for PAR and SE at 1.0, 0.5, 0.25, and 0.1 preIH time periods versus IN time periods for Exemplar Patient..... | 47 |
| Table 11. Hypothesis Result of Two-Sided Kolmogorov-Smirnov Test for Patient Cohort. 1= PAR during IN and preIH hours are separable | 50 |
| Table 12. Area Under the Curve for PAR, SE, & SE-PAR ROC Curves..... | 53 |
| Table 13. Confusion Matrix Analysis for Exemplar Patient Left Top: Confusion Matrix for PAR; Left Bottom: Confusion Matrix for SE; Right: Summary Statistics..... | 55 |

| | |
|---|----|
| Table 14. Confusion Matrix Analysis for All Patient Data Left Top: Confusion Matrix for PAR; Left Bottom: Confusion Matrix for SE; Right: Summary Statistics..... | 56 |
| Table 15. Feature Matrix Present in Models for All 7 Patients with Average Inclusion Colormap. Green = High Presence and Red = Low Presence | 61 |
| Table 16. Features Present in Models by Number of Patients Using Each Feature | 63 |
| Table 17. 12 Parameter Logistic Regression Coefficients | 65 |
| Table 18. Number of Events with Simulated Alarm before Event | 67 |

TABLE OF EQUATIONS

| | |
|--|----|
| Equation 1. Monroe-Kellie Doctrine | 3 |
| Equation 2. Velocity Series Calculation | 12 |
| Equation 3. Acceleration Series Calculation | 12 |
| Equation 4. Phase Area Ratio | 13 |
| Equation 5. Gaussian Mixture Simulation of ICP for Individual Cardiac Cycles.. | 16 |
| Equation 6. Sample Entropy | 21 |
| Equation 7. Spearman's Correlation Coefficient | 42 |

CHAPTER 1. INTRODUCTION

1.1 Neurotrauma Incidence, Classification, and Treatment

According to the United States Centers for Disease Control, in 2010 there were approximately two and half million emergency visits that included trauma to the head [1, 2]. After initial assessment and treatment, those visits led to over 280,000 hospitalizations and more than 50,000 traumatic brain injury (TBI) related deaths. Of the 130,000 hospitalizations not resulting in death, 85,000 resulted in long-term disabilities. As of 2010, more than five million people in the U.S. live with TBI-related disabilities. In order to reduce the incidence of TBI-related disability and the cost associated with care, this dissertation focuses on neuromonitoring methods immediately after surgical intervention with the mission of reducing secondary injury, which is a subsection of these cases.

Severity of neurotrauma is gauged clinically on the Glasgow coma scale that is the summation of scores for visual, motor, and eye opening assessments on a scale that ranges from 3 to 15 [3, 4]. A lower score is indicative of a more severe injury. Patients on the lower half of the scale that yield a severe classification are typically unconscious and intubated. In the case of severe TBI, a greater risk of elevated intracranial pressure (ICP) exists that corresponds to decreased cerebral perfusion and subsequent inflammatory cascades driven by hypoxic-ischemia [5]. For optimal recovery after a TBI, ICP regulation is maintained to ensure adequate oxygenation of tissues and limiting the risk of secondary injury from inflammation.

For healthy individuals, homeostatic cerebrovascular autoregulatory (AR)

mechanisms control ICP by adjusting the levels of cerebral blood flow and by varying the resistance of blood vessels in response to changes in blood pressure in order to maintain adequate oxygenation of the brain [6]. Positive feedback is a common indicator of impaired AR: ICP elevation can quickly trigger cerebral edema and ischemic tissue damage; therefore, current treatments are focused on maintaining safe levels of ICP in the absence of thorough understanding of the highly complex cerebrovascular AR mechanisms related to cerebral perfusion.

In the presence of capricious cerebrovascular AR mechanisms and the absence of reliable detection of AR status, post-trauma and post-surgical protocols focus on ICP management approaches to reduce immediate ICP hypertension (IH) in order to limit swelling and ensure adequate cerebral perfusion [7-9]. IH impairs cerebral blood flow resulting in ischemic damage and requires immediate physical or chemical intervention [7-10]. The current gold-standard for detecting IH uses continuous monitoring of ICP during post-surgical care and alerts care providers when the value of ICP exceeds a fixed threshold, typically between 20 and 25 mmHg [12,13]. Evidence suggests that reducing IH incidence during in-patient hospital stays will reduce the likelihood of long-term disability after trauma and hypothetically reduce the cost of long-term disability care and rehabilitation [12,13]. Thus, several research laboratories are searching for predictive indices of AR function by focusing on ICP behavior and ensuring longer periods of ICP normotension (IN).

With these factors and existing research in mind, this work lays the

foundation for using a novel approach to identify upcoming IH events by focusing on morphological changes in individual ICP cycles. The ultimate direction of this research is to maintain IN via proactive treatment to prevent IH instead of the modern approach of reactive IH treatment, which risks secondary inflammation.

1.2 Cardiac Cycle: Vascular and Cerebrovascular Phenomena

Intracranial pressure (ICP) is a resultant pressure based on fluctuations in the volume of neural tissue, cerebrospinal fluid, and cerebrovascular blood within the fixed space of the cranial cavity, which is formally referred to as the Monroe-Kellie Doctrine [7].

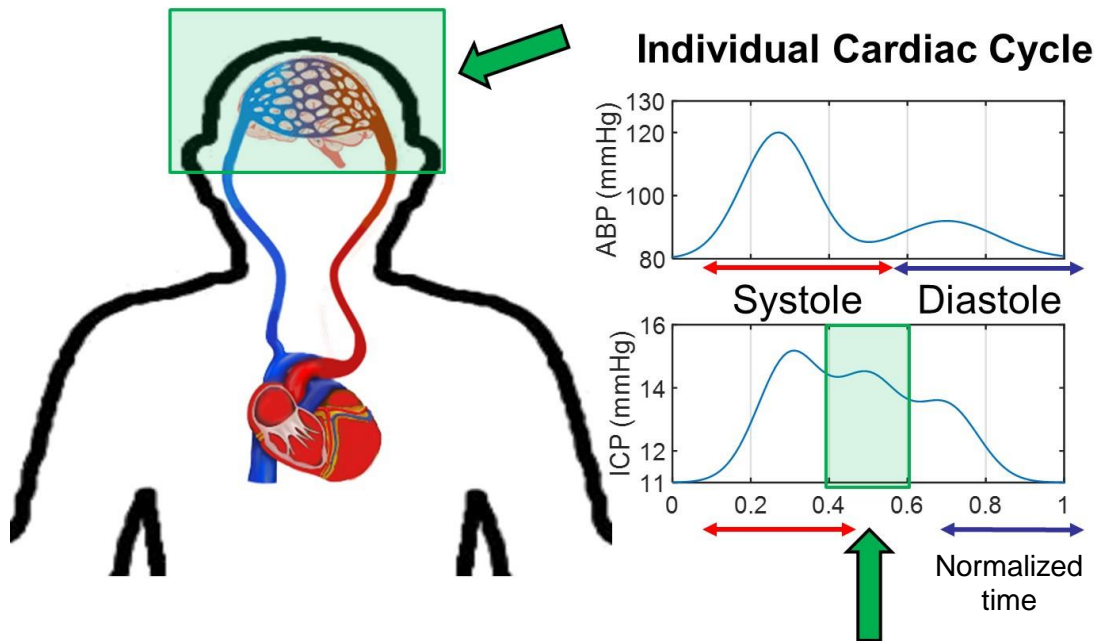
Equation 1. Monroe-Kellie Doctrine

$$Constant = V_{TISSUE} + V_{BLOOD} + V_{CSF}$$

Based on this doctrine, ICP can be identified as a resultant pressure of fluctuations in volume in any of the three components. In TBI cases, contusion is the primary cause of changes in tissue, and infections are the leading cause of over-production of CSF [7]. The overwhelming component to homeostatic ICP fluctuations particularly in relation to AR is the volume of the blood in the cerebral cavity, which is driven by arterial blood pressure (ABP) fluctuations within each cardiac cycle. Figure 1 demonstrates the previously researched relationship between the vascular and cerebrovascular systems that function in similar but distinct manners: only Peak 2 of ICP cannot be explained by the systolic and diastolic fluctuations in ABP. Note that absent in Figure 1 is a noted delay of approximately half a second that exists between the onset of an ABP cycle and ICP cycle, which is also of interest to TBI researchers.

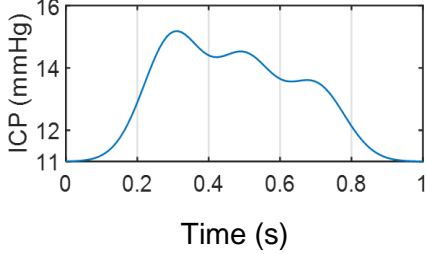
Figure 1. Representation of Relationship between Vascular and

Cerebrovascular Cycles. Left: Closed-loop circulation between heart and brain. Top Right: Arterial Blood Pressure Cycle. Bottom Right: Intracranial Pressure Cycle



A single ICP cycle, which is approximately the duration of a heartbeat, exhibits three distinct peaks that relate to different physiological processes, as summarized in Table 1: a percussive peak, Peak 1, corresponding to the influx of blood driven by the ABP impulse during systole after a transit delay; a tidal peak, Peak 2, relating to the compliance of the cerebrovascular bed, and a dirotic peak, Peak 3, which mirrors the dirotic notch and rebound seen during diastole of ABP [7]. These fluctuations are of interest because Cerebral Perfusion Pressure, which is a proxy measure of oxygen to the brain, is calculated as the difference between mean ABP and mean ICP [7-13]. Note that while ABP can be easily measured with non-invasive sphygmomanometers or mildly-invasive catheters using the vessels of the arm, ICP can only be measured continuously via invasive probe in the cranial cavity.

Table 1. ICP Cycle Components

| | | |
|--------|--|--|
| Peak 1 | Percussive Peak Arterial Blood Pressure Impulse during Systole |  |
| Peak 2 | Tidal Peak Cerebrovascular Compliance | |
| Peak 3 | Dicrotic Peak Arterial Blood Pressure Impulse during Diastole | |

Previous studies indicate that ICP waveform complexity decreases as the risk of IH increases; these decreases in complexity are implicated as the cause to decreased neural vessel compliance, which can indicate dysfunction of cerebral autoregulation [6-15,19-22]. One research team found, “as early as 6 h into monitoring, complexity measures from easily attainable vital signs, such as [heart rate] and [mean arterial pressure], in addition to ICP, can help triage those who require more intensive neurological management at an early stage” [39]. Furthermore, the behavior of these peaks and other morphological features of the ICP pulse have been used to predict rises in ICP up to an hour before the event by using a rule-based clustering and analysis algorithm [15-18]. This forecasting method used a multi-parameter feature vector including up to 24 metrics per cycle that focuses on signal amplitudes, relative position, radius of curvature, and proportional time-domain measures occurring at selected points within the individual ICP cycle [41].

1.3 Models of Intracranial Pressure

The difficulties of modeling intracranial pressure are related to the

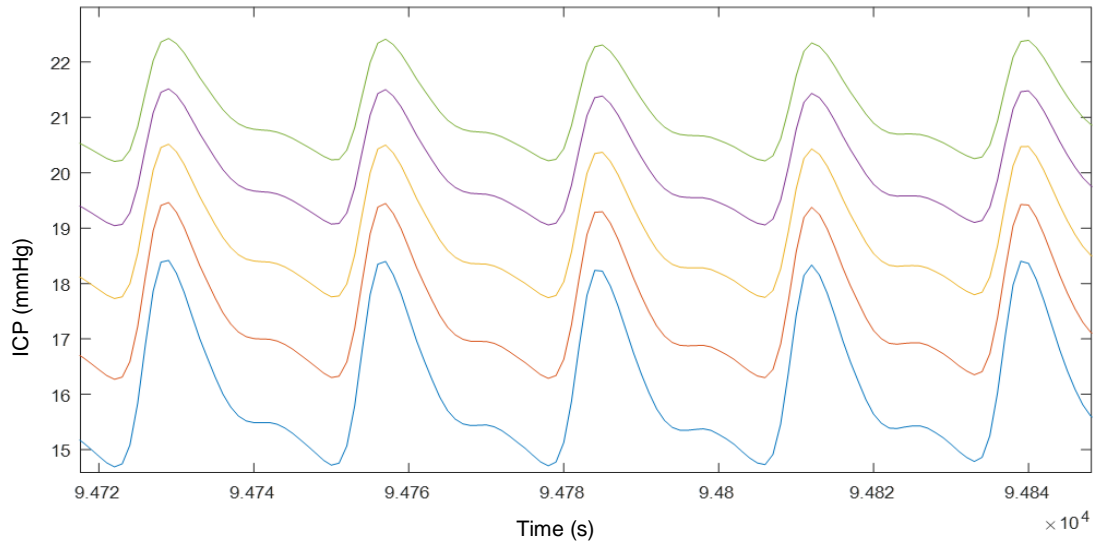
difficulties in assessing a resultant pressure within an enclosed cavity in the human body [7, 10-14, 20, 21]. Human rights and ethics concerns have limited cerebrovascular studies to retrospective investigations of individuals with brain injuries or in prospective animal studies. Consequently, only two models of intracranial pressure have dominated the field since the 1980s: Takamae and Ursino.

The Takamae model (1987) was based on clinical data [23]. Currently, the threshold for clinical IH is between 20 and 25 mmHg and for the Takamae data, the threshold was set at 50 mmHg. The model was based on an electrical circuit called the Agarwal circuit and included resistors for vessel wall stress and capacitors to accommodate the compliance of the arterioles and capillaries leading back to veins. A limitation to implementing this model in this research is the input data – Takamae used cerebral blood flow and CSF flow data which require additional equipment in the ICU beyond the traditional ICP monitors.

The Ursino models are the more comprehensive models and were published in 3 iterations [24, 25]. The first iteration was the most comprehensive and the last was the most simplified. Ursino also include components for the arterioles and arteries and includes many additional variables of vascular and cerebrovascular behavior. The most recent utilitarian version of the model demonstrates appropriate long-term ICP morphology, with the major limitation that the model is non-representative of ICP morphology during cardiac cycles. Figure 2 is an example of ICP during four cardiac cycles and when compared to Figure 1, the waveform morphology shows two peaks akin to the input signal of

ABP instead of three peaks as expected in ICP. This major limitation to the preeminent ICP model necessitates a simulation of ICP morphology during cardiac cycles as presented later in this work.

Figure 2. Sample Ursino Model Output during 5-level Bolus Infusion Study. Each trace is resultant ICP after successive 2 mmHg CSF infusions to model starting from 13mmHg (Blue =13, Red=14, Yellow=15, Purple=16, Green=17)



1.4 Intracranial Hypertension Metrics

There exist several metrics of cerebrovascular AR performance and IH that operate on long timescales [7, 11-15]. The most commonly used metric is pressure reactivity index, PRx, which is calculated as the correlation between the mean arterial pressure and the mean intracranial pressure of over 5 minutes to several hours. Another commonly used method is the correlation coefficient between the fundamental amplitude of ICP and the mean ICP over the course of a minute to several minutes, abbreviated as RAP. The shortest time analysis is sample entropy as a measure of complexity of the ICP signal that has previously been taken from 1 to 5 minute timescales [15]. All of these approaches average

ICP data to ignore the underlying complexity of each individual waveform and require large buffers of data to perform the calculations. Hu et al. analyzed individual cycle metrics and found significant features of individual cycles including mean ICP, ratio of amplitude peak 2 to amplitude peak 1, amplitude peak 2, amplitude peak 3, the time offset of peak 2 from the start of the cycle, the radius of curvature for peak 2, and the slope of peak 1 [16, 41].

1.5 Hypothesis and Approach

Since changes in ICP sub-peaks from cycle-to-cycle are difficult to discern visually during real-time monitoring, this dissertation demonstrates the benefits of phase-domain analysis (PDA) techniques in identifying physiologically relevant features of cerebrovascular AR. PDA differs fundamentally from temporal domain analysis since it focuses on the rate of change of a given signal, more specifically in this examination – ICP. This transformation can enhance discrimination of subtle differences in waveform morphology, which is analogous to waveform complexity.

The central hypothesis evaluated here is that patterns in the rate of change for ICP can be identified by transformation of ICP waves from the time domain to the phase domain, particularly Peak 2 which has previously been identified as a marker of cerebrovascular compliance, and phase domain metrics can forecast IH events. The long-term objective of this body of work is to reduce the likelihood of long-term disability in patients suffering acute severe brain trauma after surgical intervention by identifying the risk of IH and subsequent ischemia proactively; after accomplishing this, future research may elucidate AR

mechanisms and develop new proactive and preventative IH treatments.

A previously established signal processing technique for cyclical behaviors that is based on areas observed in the phase domain yields a distinct numerical measure of PDA: the phase area ratio (PAR), which is detailed in Chapter 2. To test this hypothesis, Peak 2 amplitude and width was modulated within a novel morphological simulation of ICP at the scale of individual cardiac cycles; three Gaussian pulses were added to produce simulated ICP waves with physiologically-relevant morphologies. Chapter 3 captures the simulations and analysis of PAR's response to controlled modulations as well as PAR's performance in the presence of noise. The results of PAR to a comparable time domain analysis method, Sample Entropy (SE), in long-duration clinical recordings are summarized in Chapter 4. The last chapter of this dissertation recapitulates the findings of this work and offers future directions based on this research.

CHAPTER 2. PHASE DOMAIN ANALYSIS

2.1 Phase Domain Description

2.1.1. Mathematical Foundation

Common techniques in mathematical analysis of a waveform are distribution analysis, frequency domain analysis, and derivation or integration of the waveform. Phase domain analysis focuses specifically on derivatives and echoes an aspect extracted from differential calculus: gradient analysis. For gradient analysis of differential equations, a gradient plane is created by plotting the time domain function on the abscissa (x-axis) and the derivative of the time

domain function on the ordinate (y-axis). To extend this principle, phase domain plots are created by plotting the signal or its derivative on the abscissa and a derivative of one higher order on the ordinate axes. If the signal has regular periodicity, the shape created by plotting the points over time will create a closed shape which captures the utilized area of the phase plane plotted; in gradient analysis, this method is used to find the solutions as well as the sources and sinks of the complex differential or partial differential equation. Here, the phase domain plots are used to capture information about the impulse-like forces driving pressure phenomena inside the complex vessel bed of the brain.

2.1.2. Previous Applications of Phase-Domain Analysis

Limitations of time domain processing of physiological signals include both the elimination of artefactual features and the lack of information regarding the driving impulses motivating the signal set. To solve these issues, previous researchers have used phase domain-like analyses in both cardiovascular and in human movement domains.

For several decades, vascular analysis has centered on plotting the volume of blood in the left ventricle against the left ventricle pressure; these pressure-volume relationships are used in conjunction with optical mapping and electrocardiograms to identify weakening muscular components within the heart [26, 27]. The pressure-volume curves yield loop features that serve as a proxy for the work completed by a pump and system efficiency, which is cardiac performance in the case of the heart. Impairment of the left ventricle of the heart can often be identified by signal hysteresis; with many cardiac cycles, hysteresis

and signal behavior can indicate weaknesses in particular fibrous areas near valves, entire chambers of the heart, or even the major and minor vessels that as a whole comprise the mechanism for oxygenating the human body.

In human biomechanics, particularly in human movement of joints and limbs, derivative analysis is a common technique to identify impairments that cannot otherwise be detected [28- 31]. Previous research with the Biomechanics and Rehabilitation Engineering Laboratory exemplified the benefit of quantitative assessment of limb movements through derivative analysis and phase-plane analyses. [30,31]

While use of phase plane analysis to illustrate vascular hemodynamics and human movement can be clearly interpreted via external validation methods like blood flow velocity and optical recordings of human movement, phase plane analysis has not been applied to intracranial pressure previously due to absence of a validation technique, which will be further addressed in Chapter 3.

2.2 Definition of Phase Area Ratio

Moradi previously applied the Phase Area Ratio (PAR) of the acceleration versus velocity phase (AVP) plane in a major body of work and demonstrated that PAR could successfully capture notable differences in movement within recordings of an individual patient and also among multiple patients [31]. While the application of phase-plane analyses has successfully been executed in movement analysis, this work focuses on evaluating this analytical technique specifically upon cerebrovascular phenomena.

While chapter 3 explores both the acceleration vs velocity phase plane

(AVP) and the velocity vs signal phase plane (VSP), this chapter centers on the AVP. Below, equations 2 and 3 are used to construct the AVP portrait,

Equation 2. Velocity Series Calculation

$$\frac{dP}{dt} = \sum_n^c \frac{P(s_{n+1} - s_n)}{t(s_{n+1} - s_n)}$$

Equation 3. Acceleration Series Calculation

$$\frac{d^2P}{d^2t} = \sum_n^c \frac{\left[\frac{P(s_{n+2} - s_{n+1})}{t(s_{n+2} - s_{n+1})} - \frac{P(s_{n+1} - s_n)}{t(s_{n+1} - s_n)} \right]}{t(s_{n+2} - s_{n+1})}$$

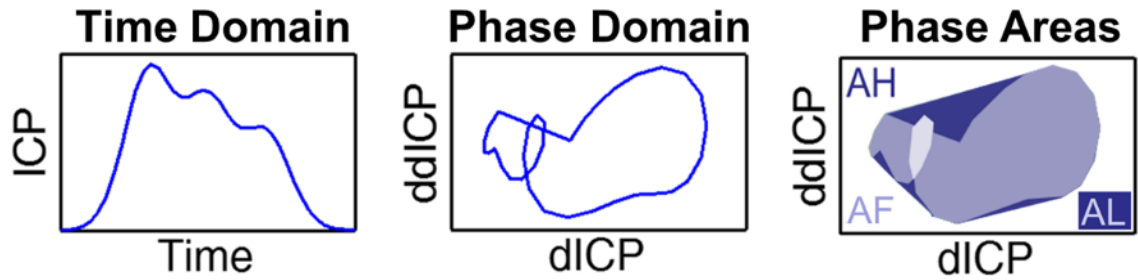
where s_n represents the sample, t represents time, and P represents the intracranial pressure. n represents each point in the cycle, which goes from 1 to length of each cycle, C . Note that the time between successive sample points is uniform due to a fixed sampling rate in data acquisition. Because graphical plots require that plotting vectors be of identical length, the first point of the first derivative is cropped, and the first point of each vector is repeated at the end of the vector to create a bounded region.

To obtain PAR, three separate parameters were computed as shown in Figure 3: 1) the phase footprint, AF, that comprised the total area contained within the outer perimeter; 2) the loop area, AL, that comprised the total area circumscribed by inner loops, including nested loops; and 3) the hull area, AH, that comprised the tightest-fitting convex polygon fit to the perimeter of the phase portrait. PAR was then calculated as shown in Equation 4. A benefit of this metric includes ease of interpretation since the ratio is bounded between 0 and 1.

Figure 3. Phase Area Ratio Components

Left: Idealized ICP Cycle vs Time – approximate time scale of a heartbeat;
Center: Transformation to the Acceleration-Velocity Phase Domain;
Right: Each phase area used in the calculation of PAR where AH refers to

the area of the Convex Hull, AF refers to the area of the footprint, and AL is the sum of the areas of any loops.



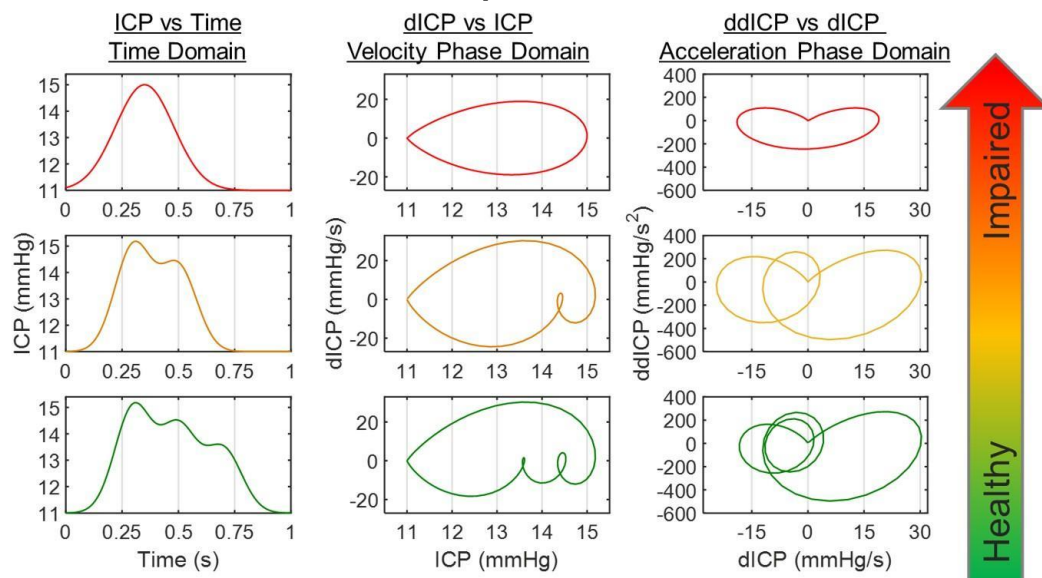
Equation 4. Phase Area Ratio

$$PAR = 1 - \frac{AF}{AL + AH}$$

When applied to intracranial pressure, phase domains present in three major shapes: single loop, bi-loop, or tri-loop. If the time domain is a single peak, the Velocity Phase Plane and Acceleration Phase Plane peaks present smooth, single-loop shape. As more peaks are introduced, more loops appear and overlap as can be seen in Figure 4. This phenomenon dictates that $PAR = 1$ in an ideal case where multiple convex loops were present and overlapping whereas if no loops are present $PAR \sim 0$. Since a specific number of peaks are desirable in healthy representations of ICP, lower values of PAR indicate high potential for AR impairment; note that the most common impairment is occlusion or complete absence of peaks. This phenomenon will be explored further through simulating small fluctuations in Peak 2 amplitude and width in Chapter 3.

Figure 4. ICP in the Time, Velocity Phase Plane and Acceleration Phase Plane for Health and Impaired Signals.

Velocity Phase Plane PAR: Top=0.02; Middle=0.05; Bottom=0.08
Acceleration Phase Plane PAR: Top=0.09; Middle=0.23; Bottom=0.41



CHAPTER 3. MORPHOLOGICAL SIMULATION OF INTRACRANIAL PRESSURE

To interrogate the viability of phase plane analysis in ICP for future clinical use, a novel method for simulating ICP cycle morphology using additive Gaussian functions was proposed. Both phase domain and time domain morphological features were interrogated by modulating the amplitude and width of only Peak 2 within the simulation. The simulated ideal ICP wave was also tested with added white Gaussian noise in order to test the sensitivity of PAR to distortive noise.

3.1 Simulation: Primary Development

3.1.1 ICP Gaussian Decomposition

While many distribution functions could be used including Gamma-, Chi-square, and Weibull-distributions, Gaussian decomposition modeling inspired the approach used in this body of work since the most existing literature was available on this type of function [32]. Alternate methods of signal decomposition have been used for ICP, as inspired by previous limitations on sampling rates that no longer exists with plug-and-play software; similar methods could be applied concurrently with the phase plane analysis method presented in this work to overcome sampling limitations in less-advanced hardware configurations [33, 34]. Additionally, Gaussian processes have been previously implemented in intracranial pressure analyses; however, these have been applied over longer time intervals [35]. Polynomial decomposition may be a viable technique in future iterations of this work.

In order to identify realistic parameters, Gaussian distribution decomposition was used on brief signal recordings available on Physionet and abbreviated samples of clinical recordings available from the Rutgers Biomechanics and Rehabilitation Laboratory [34]. To decompose individual ICP cycle recordings, custom Matlab code was developed to add three Gaussian functions and minimize the root mean square error between the clinically recorded cycle and the additive Gaussian simulation. Since all ICP recordings in humans occur in impaired individuals, values to recreate idealized morphology was also empirically derived by iterative testing to recreate shapes as identified in literature [7, 9, 12, 16, 41]. Based on a cohort of 50 randomly sampled clinical cycles from 2 patients where three peaks could be visually identified and recreating literature-based tripartite morphologies, parameters were empirically derived through iterative testing to establish an idealized ICP waveform as described further in Equation 5 and Figure 6.

3.1.2 Parameters and Performance

Artificial ICP signals were synthesized using a finite additive Gaussian approach using three separate Gaussian functions to individually emulate each of the three-peaks of ICP. The model used is:

Equation 5. Gaussian Mixture Simulation of ICP for Individual Cardiac Cycles

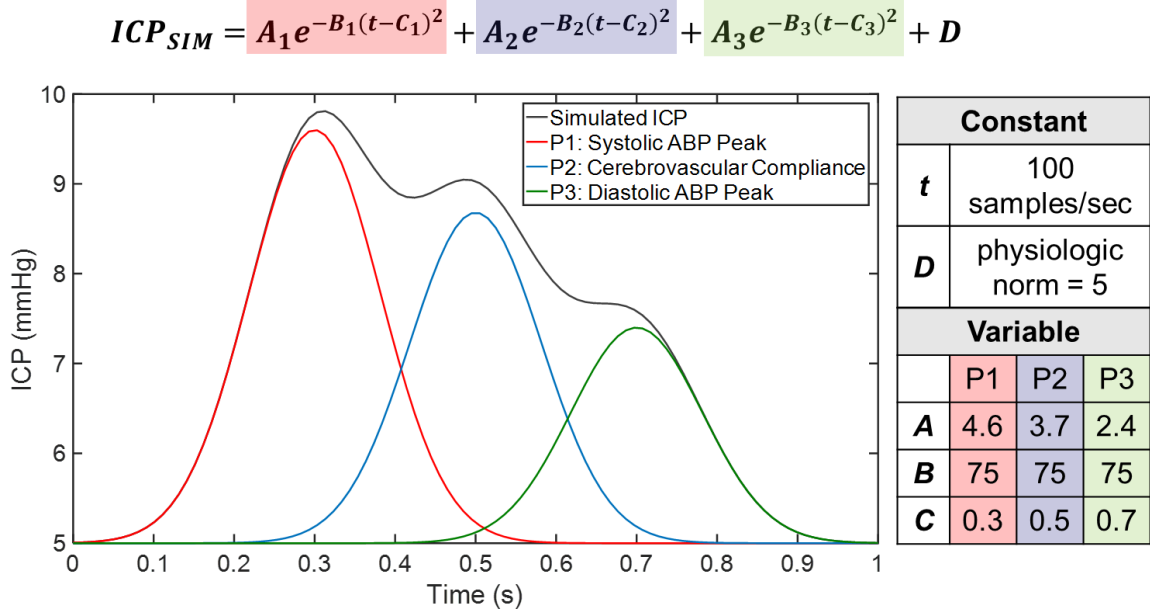
$$ICP_{SIM} = A_1 e^{-B_1(t-C_1)^2} + A_2 e^{-B_2(t-C)^2} + A_3 e^{-B_3(t-C_3)^2} + D$$

where t represents the time vector used to create the signal, A modulates the signal amplitude, B modulates signal width, C modulates the location of the Gaussian function relative to the start of the cycle, and D modulates the baseline

ICP. While the resulting clear tri-peaked curves are rarely seen in clinical data due to noise and physiological impairments, using “normal” ICP phenomena to understand phase plane analysis in ideal ICP data will yield insight into the interpretation of PAR in clinical settings.

While the literature includes images of the ideal ICP wave shape by identifying relative behavior of the peaks, numerical values for individual ICP features were not found; therefore, an idealized ICP was created by empirically modifying individual values of the parameters that yield an ICP_{SIM} that mimics the shape shown in literature and reflects available clinical recordings [7, 9, 12, 16, 41]. An exemplar of this technique is shown in Figure 5 with information on the parameters used, and the individual Gaussian sub-components are shown. While the offset represented by parameter D was necessary for morphological characterization in the time domain and the development of an accurate simulation necessitates its presence; in the clinical analysis presented in chapter 4, de-trended data were used to eliminate the role of this parameter. The PAR calculation is not affected by the presence or absence of an offset value. For these simulations, the offset was set to 11, the width of the cycle was maintained at one second, and sampling was simulated at 100 Hz. Given the relationship between ICP and ABP, these parameters are physiologically viable for resting heart rates of about 60 beats per minute.

Figure 5. Exemplar of ICP simulation with Three Gaussian Sub-Components Shown



In these simulations, Peak 2 width and amplitude (width model and amplitude model, respectively) were modulated to deviate from the empirical ideal, while Peak 1 and Peak 3 parameters remained fixed at the idealized conditions presented in Figure 5. The simulations were physiologically constrained to yield realistic morphologies. Peak 2 amplitudes were tested at values from [2.9452 - 4.5232] mmHg, and Peak 2 width was modulated between [571.2 - 1031.2] milliseconds.

The data were classified a priori into three levels: high, medium, and low for both width and amplitude models. The parameters used to define the boundaries in both models for each level are presented in Table 2. Within each level, 50 cycles were simulated for a total of 150 simulated cycles for each of the two models tested. For each of the resulting 300 simulated ICP wave cycles, peak 2 was identified and its width was measured using the MATLAB signal-

processing toolbox function “findpeaks” (‘WidthReference’ parameter set to ‘halfheight’) as shown in Figure 6. Visual exemplars of the ICP cycle for the lowest and highest parameter value for each modulation type are shown in Figures 7 & 8. As the width narrows, the AVP footprint and loop area both grow whereas as when the amplitude increases, only the loop area grows noticeably.

Figure 6. Exemplar @findpeaks with ICP simulation for Individual Peak Amplitudes and Widths

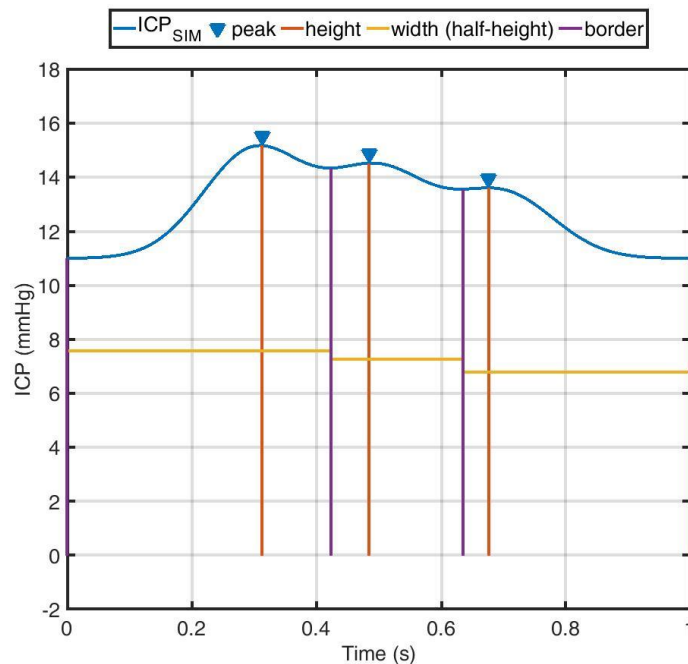


Table 2. Study Design Parameters

| LEVEL | MODEL 1: Width Modulation | MODEL 2: Amplitude Modulation |
|---------------|------------------------------|----------------------------------|
| Step Size | 0.01500 | 0.00015 |
| Low | [57.12000, 63.12000] | [2.94520, 3.00520] |
| Medium | [72.12000, 78.12000] | [3.54320, 3.60320] |
| High | [97.12000, 103.12000] | [4.46320, 4.52320] |
| Total Samples | 150 | 150 |

Figure 7. Simulated ICP Width Modulation Exemplars for Low (Red)[PAR2=0.43], Medium (Black)[PAR2=0.46], High (Blue)[PAR2=0.57] Time Domain, 1st & 2nd Derivatives, and Acceleration-Velocity Phase Plane

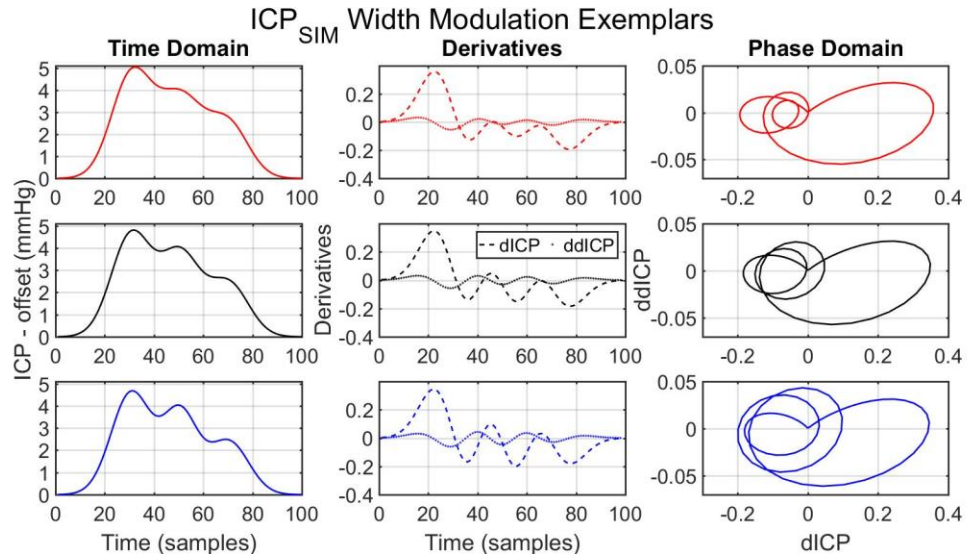
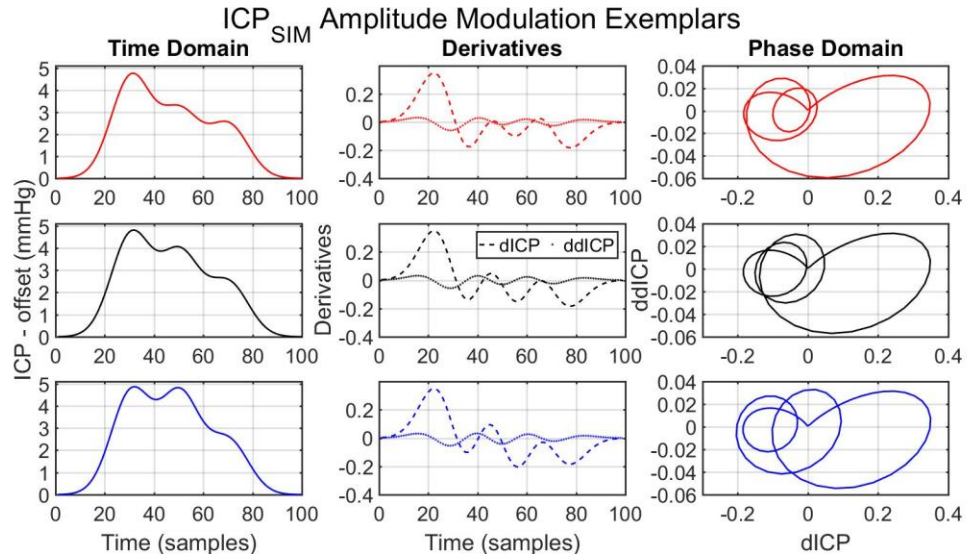


Figure 8. Simulated ICP Amplitude Modulation Exemplars for Low (Red)[PAR2=0.31], Medium (Black)[PAR2=0.46], High (Blue)[PAR2=0.44] Time Domain, 1st & 2nd Derivatives, and Acceleration-Velocity Phase Plane



3.2 Simulation: Experimental Design

3.2.1 Extraction of Time-Domain Features:

A total of eight features were extracted from each of the simulated ICP pulses: six time-domain and two phase-domain. The calculation of each feature is summarized in Table 3. Note that feature selection was based on earlier findings within the field as specified in Chapter 1. An established test of subtle variation in physiological signal data is sample entropy (SE), which is used here as a time-domain calculation that yields PAR-like information. The calculation of SE used here was based on an open-source algorithm from the Physionet database:

Equation 6. Sample Entropy

$$SE(k, r, N) = -\ln(A(k)/B(k-1)) \text{ for } k = 0, 1, \dots, m-1 \text{ with } B(0) = N$$

with the following parameters: N (epoch length) = 50 samples; r (tolerance) = (0.2 x standard deviation of epoch); and m (maximum template length) = 3 [36-38].

Table 3. Summary of features extracted from ICP pulses

| Feature | Domain | Description |
|--------------------------------------|--------|---|
| 1. VSP [dICP vs ICP] PAR (PAR1) | Phase | 1. OUT1=Equation 5: ICP Simulation 2. OUT2=Equation 2 (OUT1): dICP 3. PAR1=Equation 4 (OUT1, OUT2) |
| 2. AVP [ddICP vs dICP] PAR (PAR2) | Phase | 1. OUT3=Equation 2 (OUT1): dICP 2. OUT4=Equation 3 (OUT1): ddICP 3. PAR2=Equation 4 (OUT3, OUT4) |
| 3. Peak 2 Amplitude (A) | Time | 1. Matlab R2016b function: [A(1:3),~,~,~]=findpeaks(OUT1) 2. A=A(2) |
| 4. Peak 2 Width (W) | Time | 1. Matlab R2016b function: [~,~,W(1:3),~]=findpeaks(OUT1) 2. W=W(2) |
| 5. ICP Cycle Arithmetic Mean (mICP) | Time | $mICP = (\sum_{i=1}^n OUT1_i)/n$ where n=100 |
| 6. ICP Cycle Geometric Mean (gmICP) | Time | $gmICP = [\prod_{i=1}^n OUT1_i]^{1/n}$ where n=100 |
| 7. Amp. Peak 2/ Amp. Peak1 Ratio (S) | Time | 1. Matlab R2016b function: [A(1:3),~,~,~]=findpeaks(OUT1) 2. S=A(2)/A(1) |
| 8. Sample Entropy (SE) | Time | $SE(k, r, N) = -\ln(A(k)/B(k-1))$ for $k = 0, 1, \dots, m$ with $B(0) = N$ where N=50, r=0.2*stdev(1:N), m=3 |

3.2.2 Linear Modeling of Features

3.2.2.1. Amplitude of Peak 2

To analyze the results, five linear models were created with Amplitude of Peak 2 as the predicted output since this parameter has the most evidenced relationship to cerebral compliance and AR:

1. All Features

$$A \sim gmlCP + mICP + W + S + SE + PAR1 + PAR2$$

2. Time Domain Features

$$A \sim gmlCP + mICP + W + S + SE$$

3. Phase Domain Features

$$A \sim PAR1 + PAR2$$

4. Only Velocity Phase Feature

$$A \sim PAR1$$

5. Only Acceleration Phase Feature

$$A \sim PAR2$$

6. Only mean ICP Feature

$$A \sim mICP$$

Additionally, each feature was modeled independently: the full model results including scatter plots are included in the Appendix IV.

3.2.2.2. Mean ICP

Since the most commonly used clinical metric of ICP fluctuations is mean ICP and identifying individual peaks in clinical data is difficult, six linear models were created with mean ICP as the predicted output:

1. All Features

$mICP \sim gmlCP + A + W + S + SE + PAR1 + PAR2$

2. Time Domain Features

$mICP \sim gmlCP + A + W + S + SE$

3. Phase Domain Features

$mICP \sim PAR1 + PAR2$

4. Only Velocity Phase Feature

$mICP \sim PAR1$

5. Only Acceleration Phase Feature

$mICP \sim PAR2$

6. Only Amplitude Feature

$mICP \sim A$

Additionally, each feature was modeled independently: the full model results including scatter plots are included in the Appendix IV.

3.3 Simulation Results

The results of the 6 simulation conditions designed above are presented in two approaches. The first presentation demonstrates the mean, range, and quartiles, and outliers of the data sets using boxplots. The second presentation focuses on the linear model results from the two models to identify the strength of linear relationship between Peak 2 amplitude or mean ICP with the specified features.

3.3.1 Boxplots of Results

Figures 9 and 10 demonstrate the measured Amplitude and Width of Peak

2 for each specified level defined in Table 2 for each modulation case. When modulating the Width of Peak 2 artificially from wide to narrow, the interference from the adjacent and fixed Gaussians for Peak 1 and Peak 3 likely causes the overlap between the Low and Medium groups in width. While the Width is modulated, the measured Amplitude only fluctuates over a tiny range. Peak 2 Amplitude linearly relates to width, as expected. When modulating the Amplitude of the Peak 2, the measured amplitude and width both increase across all three levels in an expected fashion.

Figure 9. Measured Amplitude and Width for Model 1: Width Modulation

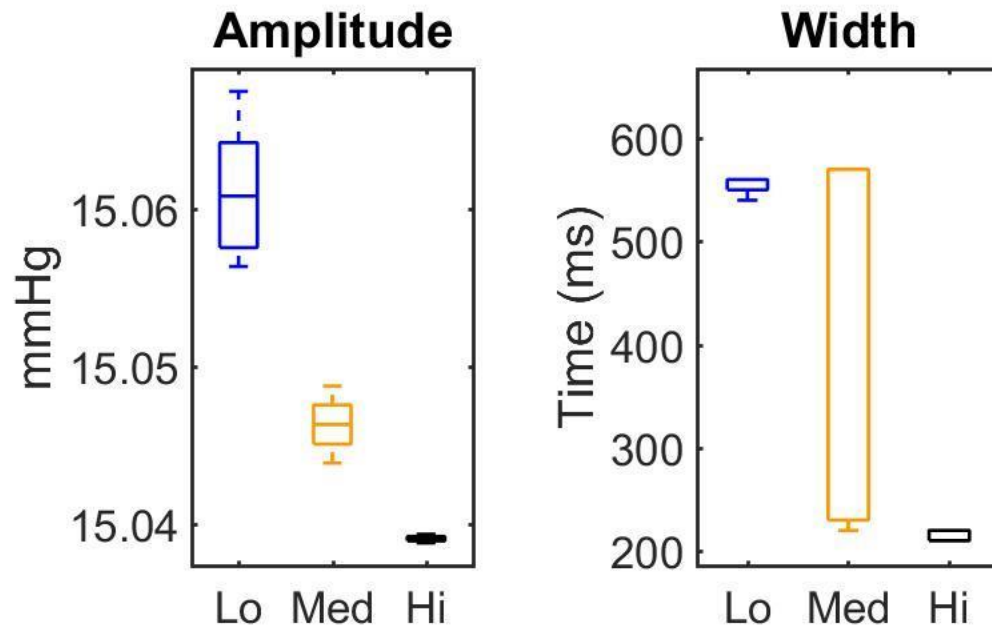
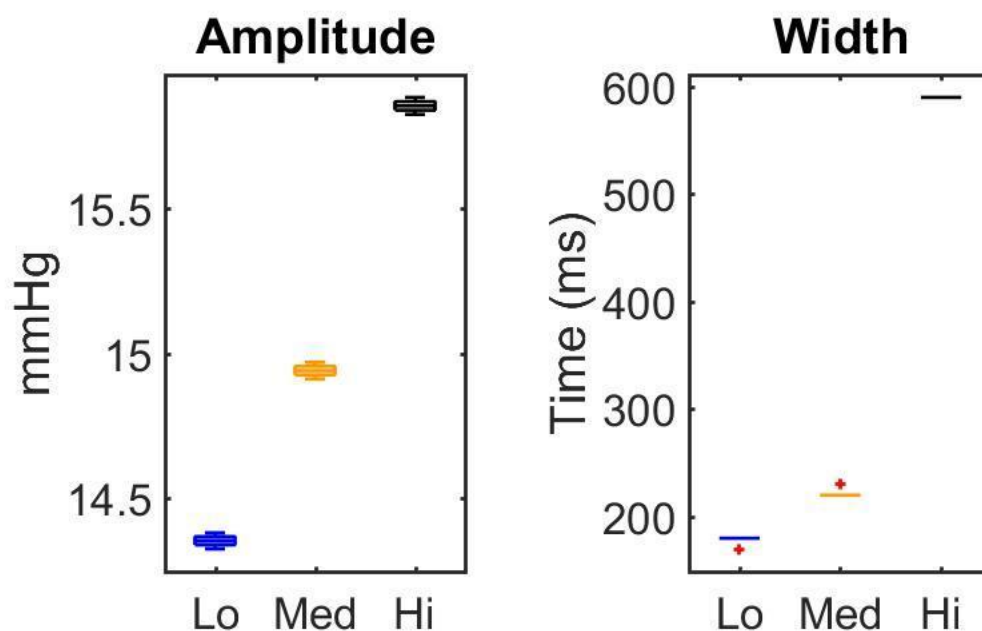


Figure 10. Measured Amplitude and Width for Model 2: Amplitude Modulation



Figures 11 and 12 present the two major time domain and phase domain parameters: mICP, gmICP, ratio P2/P1 (S), SE, PAR 1, and PAR 2. In the case of width modulation, except for PAR 1, the time domain features present a similar linear tendency from high to low whereas PAR 1 demonstrates a convex parabolic phenomena and PAR 2 demonstrates the opposite linear trend. For amplitude modulation, PAR 2 follows the linearly increasing trend demonstrated by arithmetic and geometric means while spanning a broader range of values than PAR 1. This is ultimately a trait that is more versatile as a singular ratio based metric that can be used to set thresholds for clinical alarms; as a reminder, the current gold standard for clinical care alarms for severe neurotrauma post-surgical intervention is only exceeding 25 mmHg. A full plot of metric versus metric behavior is available in Appendix IV.

Figure 11. Results from Simulated Width Modulation at Three Levels for

Time Domain Features and Phase Domain Features

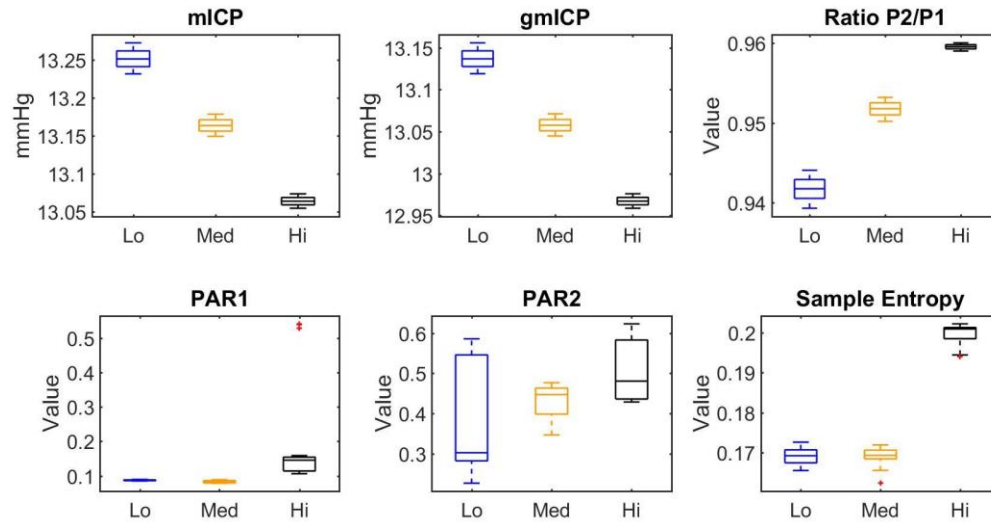
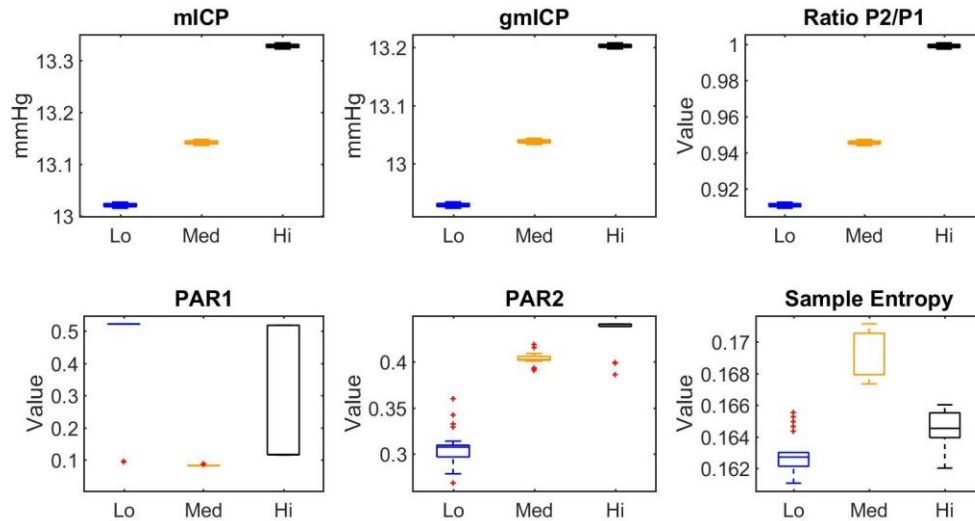


Figure 12. Results from Simulated Amplitude Modulation at Three Levels for Time Domain Features and Phase Domain Features



The results above demonstrate that PAR 2 demonstrates a negative correlation to mICP when modulating Width, whereas PAR 2 demonstrates a similar increasing trend when modulating Amplitude. In both cases, PAR 1 exhibits a parabolic trend across a narrower range of values.

3.3.2 *Linear Modeling of Results*

The full results of both sets of linear models are presented in Appendix IV, including models for each feature individually.

3.3.2.1 Amplitude of Peak 2

All models tested provided statistical significance with p-values below 0.05 as expected for a noise-free data set. An abbreviated summary of the model results is presented in Table 4 for the two models executed. These results indicate that all six of the models presented are robust enough to predict measured Peak 2 amplitude. PAR 2 alone yields a higher adjusted R-square value than PAR 1 alone for amplitude modulation but performs similarly low during the width modulation test. Note that Peak 2 and mICP have high correlation for both models with the following equations: Width Modulation ($A=13.50+0.12*mICP$) and Amplitude Modulation ($A=-49.07+4.87*mICP$)

Table 4. R-Squared Values for Linear Model Analysis of Peak 2 Amplitude

| Model Class | Model 1: Width Modulation | Model 2: Amplitude Modulation |
|--------------------------|---------------------------------|-------------------------------------|
| 1. All Features | 0.999 | 1.000 |
| 2. Time Domain Features | 0.999 | 1.000 |
| 3. Phase Domain Features | 0.200 | 0.786 |
| 4. Only PAR1 Feature | 0.128 | 0.036 |
| 5. Only PAR2 Feature | 0.127 | 0.758 |
| 6. Only mICP Feature | 0.932 | 1.000 |

3.3.2.2 Mean ICP

All models tested provided statistical significance with p-values below 0.05 except for SE by itself as a predictor of mean ICP (p-value=0.248). An abbreviated summary of the model results is presented in Table 5 for the two modulations cases executed in predicting mean ICP. These results indicate that all five of the models presented are robust enough to predict mean ICP. There is a perfect linear correlation between mean ICP and Peak 2 with an equations of (mICP= -105.89 + 7.916 * A) for width modulation and (mICP=10.074 + 0.205 *A) for amplitude modulation.

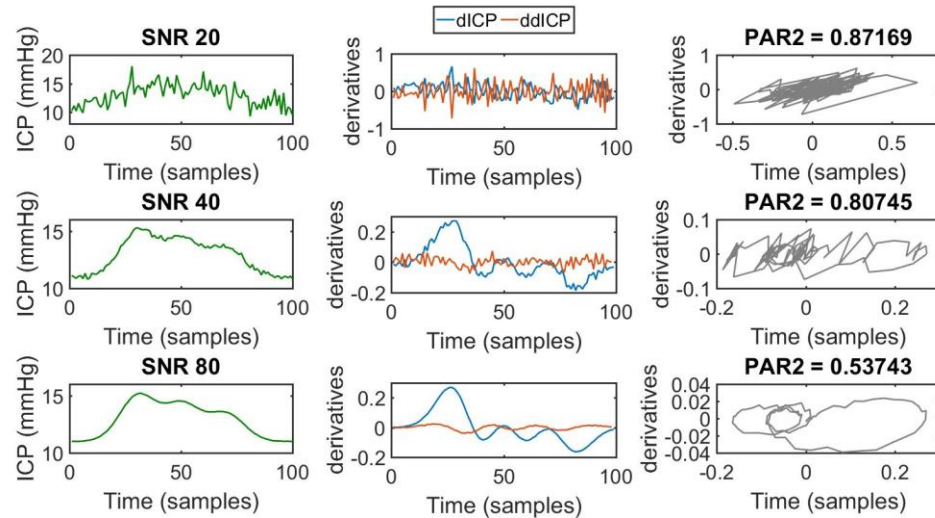
Table 5. R-Squared Values for Linear Model Analysis of mean ICP

| Model Class | Model 1: Width Modulation | Model 2: Amplitude Modulation |
|----------------------------------|---------------------------------|-------------------------------------|
| 1. All Features | 1.000 | 1.000 |
| 2. Time Domain Features | 1.000 | 1.000 |
| 3. Phase Domain Features | 0.324 | 0.788 |
| 4. Only PAR1 Feature | 0.198 | 0.037 |
| 5. Only PAR2 Feature | 0.215 | 0.761 |
| 6. Only Peak 2 Amplitude Feature | 0.932 | 1.000 |

3.4 Signal to Noise Ratio Performance of PAR

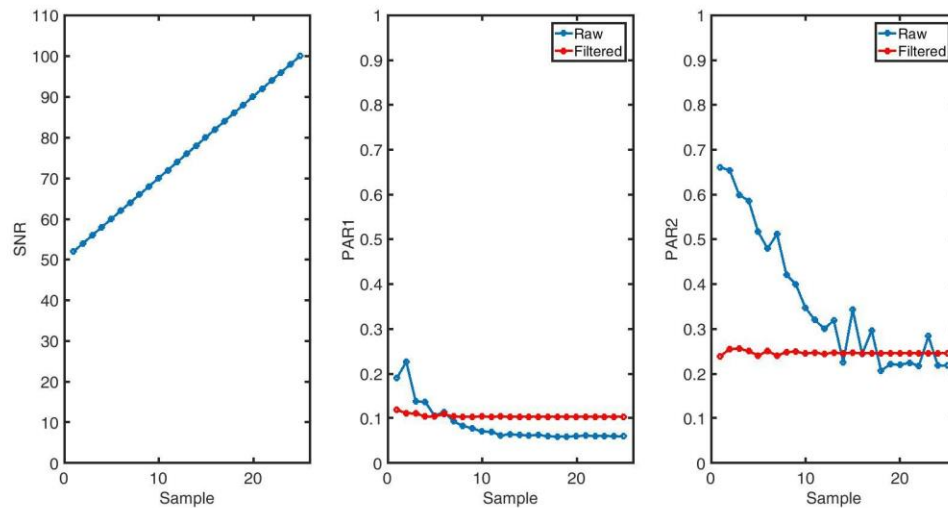
In order to evaluate PAR's tolerance to noise, the additional presence of white Gaussian noise was simulated to experimentally assess how well PAR1 and PAR2 perform under situations where filtering cannot happen prior to calculation. Additive white Gaussian noise presents with uniform power at all frequencies, which can be different than clinically recorded noise that can be higher at particular frequencies. Three representative samples of the input, process and output of the measure and the corresponding derivatives, phase domain, and PAR scores are displayed in Figure 13. Since analog methods are used to capture the data, after the analog-to-digital conversion is complete, the clinical data are appropriately filtered for smoothness that remove such noise from signals prior to calculating PAR - this will be discussed further in chapter 4.

Figure 13. Experimental SNR Modulation Exemplars for SNR of 20 (top row), 40 (middle row), and 80 (bottom row) with time domain (left column), derivatives (middle column), and acceleration phase plane (right column) with associated PAR 2



The experiment was executed at a finer resolution of 50 dB to 100 dB in increments of 2 dB (Figure 14). The results of this approach demonstrate that both PAR calculations are stable when a 10-point moving average filter is applied. Raw calculation of PAR 2 equilibrates at SNRs of greater than 86 dB. Raw PAR 1 is less sensitive to noise and equilibrates at 70 dB.

**Figure 14. SNR Modulation from 50 to 100 dB in increments of 2dB with the Raw PAR in Blue and the Filtered PAR in Red
SNR (Left), PAR1 (Middle), and PAR2 (Right) results**



Overall, as a higher SNR is preferred for reliable PAR calculation, data must be filtered prior to calculation of PAR to ensure reliable results. Both PAR1 and PAR2 metrics are sensitive to added noise. However, as demonstrated in Figures 4 and Section 3.3, PAR 2 demonstrates a distinct profile with a triple-peaked cycle than double-peaked or single-peaked cycle. Given the range of ICP simulations tested PAR 1 spans a smaller range of units than PAR 2. Because of this evidence, the clinical data in Chapter 4 will be analyzed using AVP and PAR 2 which hereafter will be referred to as PAR for simplicity.

CHAPTER 4. PHASE AREA RATIO PERFORMANCE IN CLINICAL TRAUMA RECORDINGS

The previous chapter demonstrates the benefits of using acceleration-velocity phase plane (AVP) analysis on simulated ICP data to resolve morphological changes between ICP cycles using a single metric, the phase area ratio (PAR). Previous studies indicate that ICP complexity measured by entropy decreases as the risk of IH increases and identifies decreased brain compliance, which can indicate dysfunction of cerebrovascular AR [7, 39]. Using clinical recordings from patients with acute and severe brain trauma, this chapter compares the performance of PAR against an existing waveform complexity measure, sample entropy (SE) that has previously been utilized in similar studies. The hypotheses tested here focus on the ability of PAR to predict IH in clinical recordings by focusing on PAR's behavior in the time preceding IH.

4.1 Sample Population

The study was approved by the Rutgers-RWJUH IRB in 2014 with one revision in 2015 and was conducted solely at Robert Wood Johnson University Hospital. The research team was assisted by Surgical Intensive Care Unit Nurses and the RWJUH Clinical Engineering Department. Patients who were indicated to have subdural bolt monitoring based on surgical assessment and who consented to the research study by proxy were collected between 2014-2017. Data were gathered on a total of 17 patients: 10 patients were excluded for ventriculostomy recordings, recording errors, changes in recording method, or records that were too short for analysis; this yielded 7 usable patient recordings

whose records are summarized in Table 6. All patients presented were placed on ventilators while ICP was being recorded. More than 400 hours of clinical data were analyzed, yielding over 1 million ICP cycles. The dataset includes 26 IH events which were isolated and examined to determine the correlation between mean ICP and PAR. In this analysis, 24 hours for one patient (Exemplar) is examined in depth for comparison of PAR versus SE. Cumulative test results for PAR in all seven patients are presented here; additional individual patient summaries are available in the Appendix V where only data on PAR is provided.

Table 6. Patient Summary Information

| Patient | Sex | Age | Race | Hispanic | Wt. (kg) | Ht. (in) | # of Events |
|----------|-----|-----|------|----------|----------|----------|-------------|
| Exemplar | M | 25 | W | Y | 73 | 67 | 4 |
| A | F | 66 | A | N | 65 | 61 | 2 |
| B | M | 47 | W | Y | 59 | 62 | 1 |
| C | M | 55 | W | N | 89 | 70 | 2 |
| D | M | 50 | W | N | 138 | 71 | 1 |
| E | M | 30 | W | Y | 80 | 62 | 5 |
| F | M | 60 | A | N | 62 | NA | 11 |

The patients' ages span a considerable range from 25 to 60 years old. The majority of the patients were White and the remainder Asian. Three of the White patients were Hispanic. One of the seven patients was female.

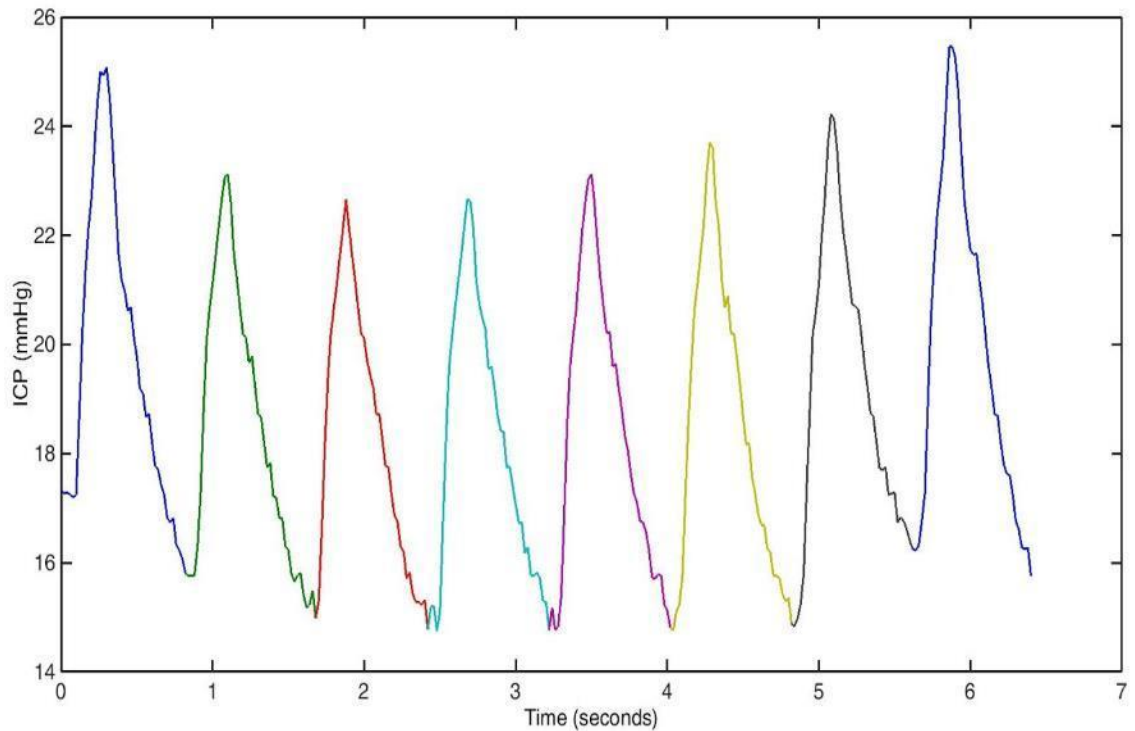
4.2 Data Collection & Conditioning

The data collection process for the following clinical data was described

previously, which used a custom data logging system that attached to the output of a clinical physiological monitor [34]. Briefly, ICP, ABP, ECG, and several other parameters, were recorded at a sampling rate of 50 Hz using software and hardware from National Instruments that interfaced with a General Electric TRAM Rac data monitor. ICP was measured continuously using a Camino Direct Pressure microtransducer that was inserted into the frontal cranium; ABP was measured using an Edwards Lifescience's fluid-filled catheter in the radial artery. All analytics presented in this manuscript were performed in Mathworks Matlab R2013a to 2016b or R x64 3.2.2.

Individual ICP beats were identified in raw data through a three-step process: Phase 1 cleaned the data by extracting only data that presented with variety of quantization (> 5 distinct quanta - exceeding noise in absent signal) and content prevalence ($>95\%$) when comparing total, early, and late histograms of small windows of data (less than 10 seconds) for numerical variation; Phase 2 refined the dataset by examining the periodicity of the sample windows and performed baseline detrending; and Phase 3 separated the ICP data into individual cycles by identifying relative minima of differentiated data and confirmation of time-offset minima in a second physiological signal, ABP. The results of the individual cardiac cycle identification process is shown in Figure 15 and Figure 18. Both visual and derivative-zero-crossing analysis verified the validity of this approach for cycle identification.

Figure 15. Abbreviated Sample of ICP Recording with Segmented Cardiac Cycles



A 10-point moving average filter was applied to each individual cycle to remove high frequency noise. To justify this approach, using an individual hour of clinical data as an exemplar, the frequency profile of the data in Figure 16 was identified by completing a Fast Fourier Transform (FFT) of the full vector with no zero padding or prior filtering, the results of which are in Figure 17. After zooming into the raw data to a 20-second window with individual cycle markers in Figure 18, the AVP is plotted for an individual cycle exemplar in Figure 19. For the exemplar patient presented in this chapter, each cycle was analyzed individually as represented in Figure 19.

The noise observed in Figure 19 is representative of commonly seen signals. Possibly because of this noise and possibly because of the clinical nature of the patients' physiologies, the natural three-peak phenomena are rarely

seen in clinical data. More often, two-peak and single-peak shapes are observed. While empirically selected values based on literature and clinical recordings were used to examine “normal” ICP phenomena in Chapter 3, understanding phase plane analysis in ideal ICP data yields insight into the interpretation of PAR in clinical data that is uncontrolled. As shown in Figure 19, a simple moving average filter with a length of 10 samples (equivalent to an analog lowpass filter with cutoff frequency = 0.94 Hz) was used to eliminate high frequency noise and ensure a smooth cycle prior to calculation of PAR and SE. This filtering method successfully reduces the amount of noise transferred from the time domain to the phase domain, permitting a more stable calculated PAR.

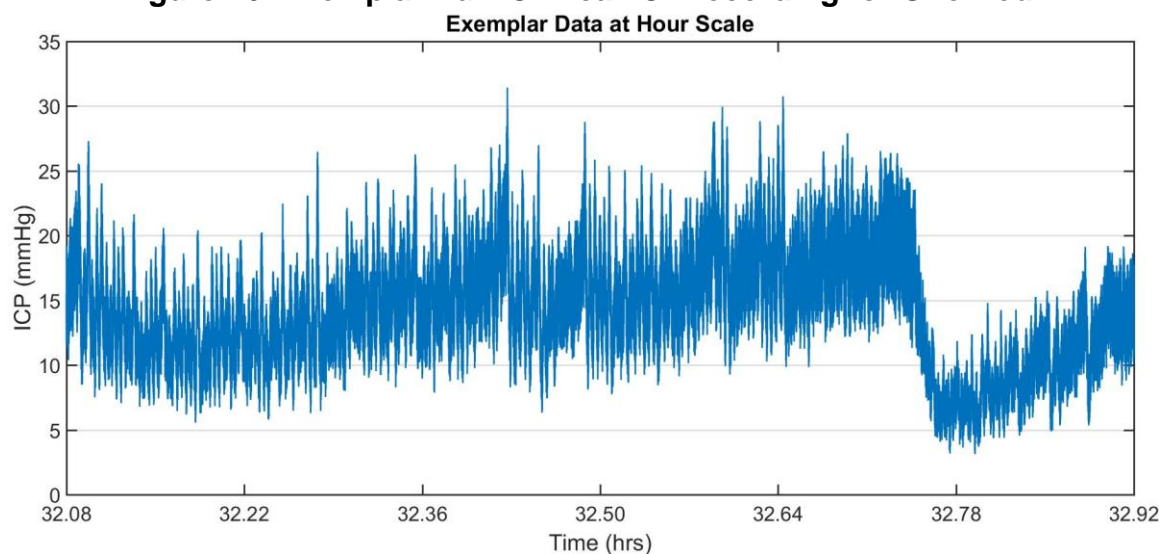
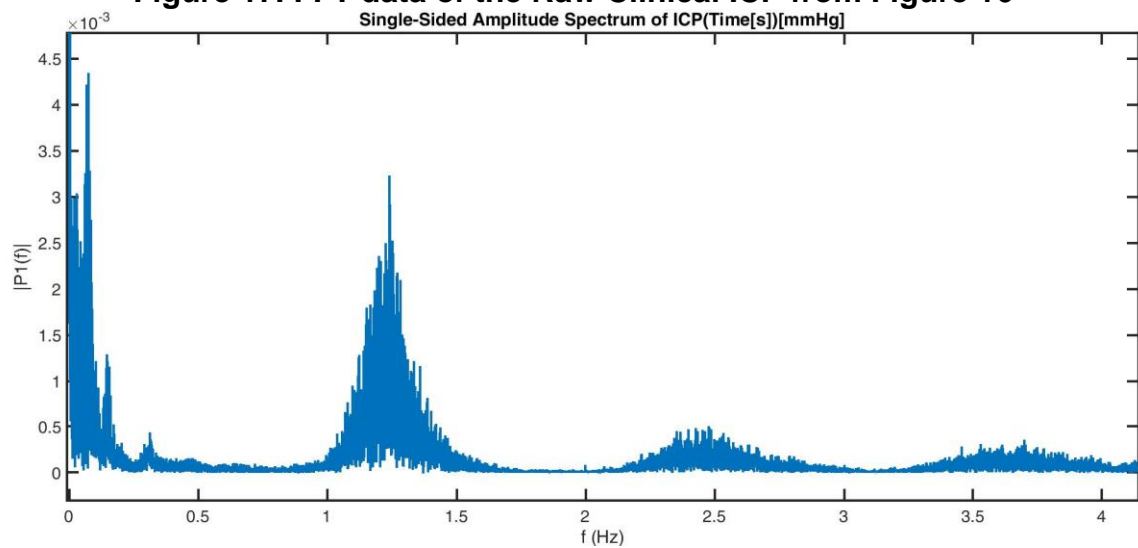
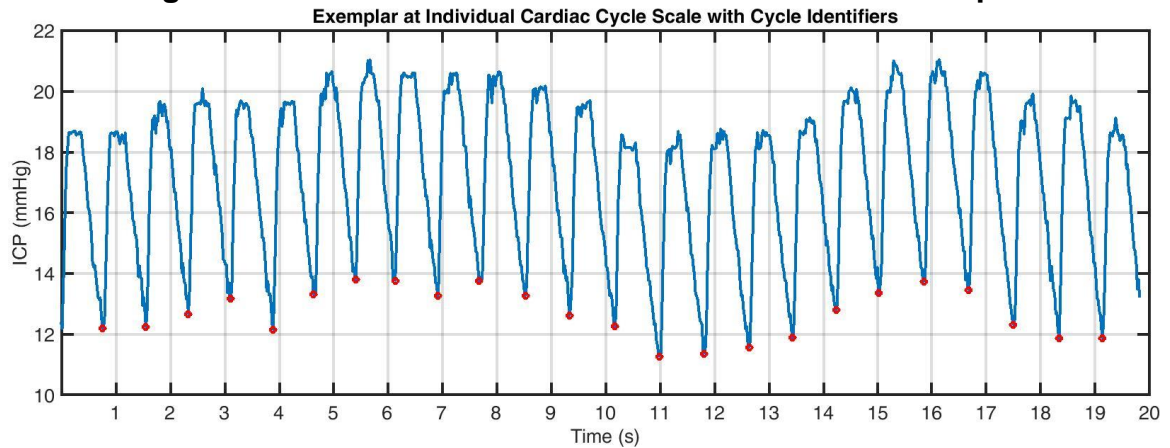
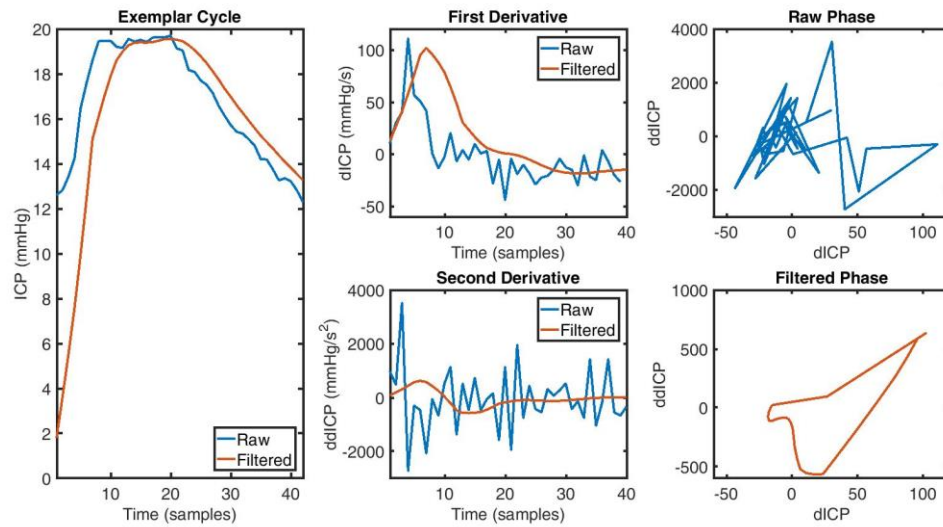
Figure 16. Exemplar Raw Clinical ICP recording for One Hour**Figure 17. FFT data of the Raw Clinical ICP from Figure 16**

Figure 18. 20-second Window of Raw Clinical ICP Exemplar**Figure 19. Clinical Exemplar of Raw (Blue) versus Filtered (Orange) ICP, dICP, & ddICP in Time Domain and Phase Domain for a single cardiac cycle**

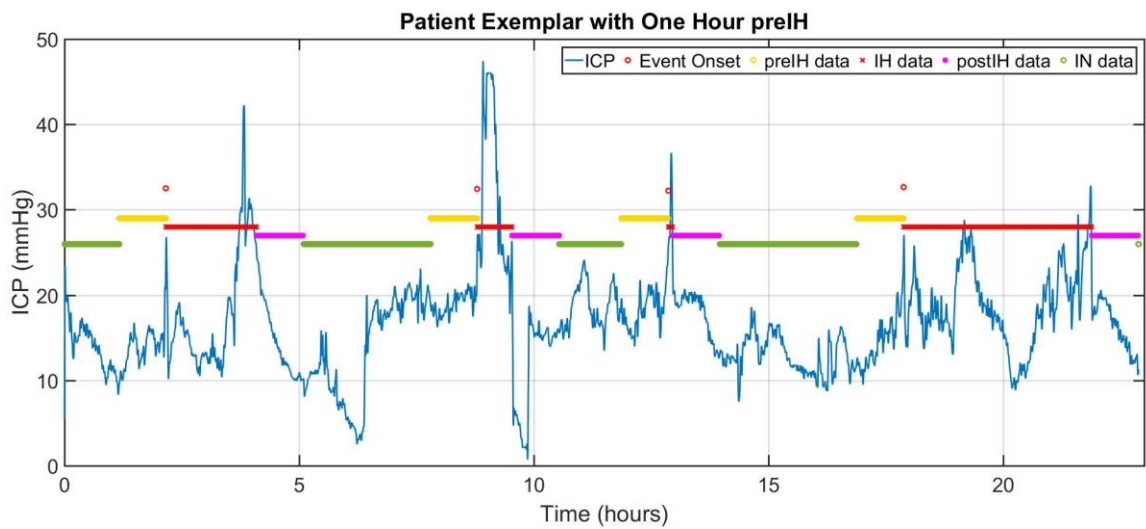
4.3 Analysis Methods and Results

4.3.1 Identifying *preIH* Timespans

In order to assess the clinical value of PAR, data were first categorized into IN, pre-IH, IH, or postIH data using the following criteria: IH data were considered any hour where ICP >25 mmHg; postIH time was set to an hour for all cases; pre-IH data were considered the specified time period (evaluated from 1- to 0.1-hours) prior to an individual event; two IH events were considered as a

unified singular event if a second event occurred during the postIH event time of the previous event. All other data not categorized by these conditions were considered IN data. Masking the data to identify periods of IN, preIH, IH, and postIH data according to the specifications is shown in Figure 20, with different time periods color coded.

Figure 20. Exemplar of Data Masking to Identify Onset of IH events & Classify IN (green), preIH (yellow), IH (red), and postIH (pink) time Periods



Pre-IH event data were analyzed at 1.0, 0.5, 0.25, and 0.1 hours scale

and analyzed in several approaches based on observed trends when zoomed in on IH events.

4.3.2 Relationship Between PAR and mICP via Linear Regression

As with the simulated data, the relationship between PAR and mean ICP was evaluated. To identify their relationship, a linear regression of PAR onto ICP was conducted using the exemplar patient's data. For this analysis, the preIH data for the exemplar patient was examined for each event separately and results are shown in Table 7. This event-wise processing gives us some insight into the stability of the relationship at hand and its generality across events

(although still limited to within a single patient).

Table 7. Linear Regression of PAR predicting ICP for Exemplar Patient

| Time period | R-sq% | R-sq (Adj)% | R-sq (Pred)% | SE Coef | P-Val | Regression Equation |
|------------------|-------|-------------|--------------|---------|-------|-------------------------|
| 1-hr pre Event 1 | 77.1 | 77.1 | 76.9 | 0.39 | 0.00 | ICP = 26.83 - 28.69*PAR |
| 1-hr pre Event 2 | 1.4 | 1.09 | 0.17 | 1.25 | 0.00 | ICP = 21.68 - 4.51*PAR |
| 1-hr pre Event 3 | 14.6 | 14.4 | 13.7 | 0.53 | 0.00 | ICP = 22.31 - 7.393*PAR |
| 1-hr pre Event 4 | 25.1 | 24.9 | 24.4 | 0.72 | 0.00 | ICP = 22.24 - 22.64*PAR |
| Full Data | 8.3 | 8.3 | 8.3 | 0.20 | 0.00 | ICP = 21.58 - 12.14*PAR |

The linear regression for the first event's data looks promising. The regression has a good fit with R-sq value of 77.2%, suggesting that a linear relationship between these variables accounts for about 77% of their variation, with a p value of 0.000 which show that it is significant (alpha fixed at .05). The regression equation for this best-fit linear model shows a negative relationship between ICP and PAR suggesting that as PAR increases, ICP decreases. Examining these statistics for the remaining events, the amount of variation accounted for by the regressions varies down to 1.4%, but the relationship is repeatedly suggested to be a negative one.

The linear regression analyses in summary suggests that ICP and PAR have an inverse relationship where PAR increases when ICP decreases. However, the magnitude of this relationship varies, from as strong as 77% in first event to 1% in the second event.

4.3.3 Correlation with ICP

A limitation of the linear regression analysis is that it assumes that the noise in the data specifically follow a Gaussian distribution. In this next analysis, I examine the possibility of a relationship that is not based in Gaussian distributions by using a non-parametric correlation coefficient, Spearman's Rho. A Spearman's Ranked Rho correlation coefficient was calculated for the all preIH + IH event data between mICP, PAR, and SE as follows:

Equation 7. Spearman's Correlation Coefficient

$$r_s = \rho_{rgX} \rho_{rgY} = \frac{\text{cov}(rgX, rgY)}{\sigma_{rgX} \sigma_{rgY}}$$

where ρ denotes the Pearson's correlation coefficient applied to the rank variables, $\text{cov}(rgX, rgY)$ is the covariance of the rank variables, and σ_{rgX} and σ_{rgY} are the standard deviations of the ranked variables. Significance of the correlation is assessed by p-values less than 0.05.

An exemplar of patient recording data with synchronous analysis of ICP, PAR, and SE is presented in Figure 21 for 24-hours. SE unlike PAR has discontinuities such as infinity and not a number values as seen near the 9 hour mark. This patient exemplar yielded 4 IH events and Figure 22 includes zoomed in ICP and PAR for two individual ICP elevations, where PAR appears to increase 10-30 minutes prior to the increase of ICP. SE behaves similarly to PAR with a characteristic increase 30-60 minutes in advance of IH. Based on this, the correlations of PAR and SE to ICP during periods of IN and prior to IH were examined for four different time scales in order to identify which time windows might yield clinical value when using PAR as an IH metric.

Figure 21. Patient Exemplar Recorded ICP & Analysis for 24 hours
Top: mICP; Middle: PAR; Bottom: SE

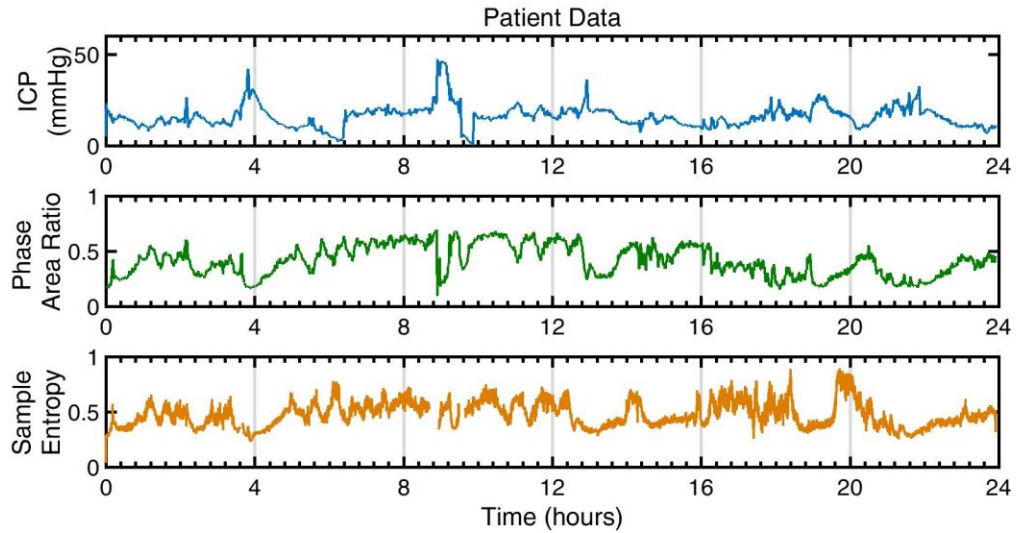
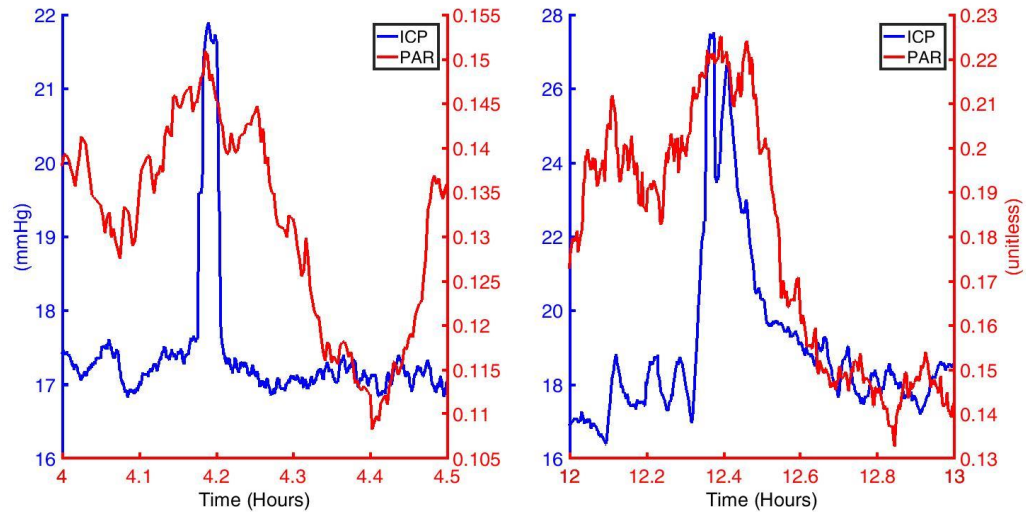


Figure 22. Patient Exemplar Zoomed In
Left: Event 1 at t~4 Hours; Right: Event at t~12 Hours



Spearman's rho correlation results on the exemplar patient are presented below in Figure 23 for IN segments and Figure 24 for IH segments. The following figures show ICP and PAR correlate more strongly than ICP and SE for both IN and pre-IH hours with the exception of 0.1-hr time point in preIH analysis. Asterisks exemplify statistically significant segments with a p-value < 0.05.

Figure 23. Spearman's Correlation of PAR (Blue) and SE (Yellow) to ICP during IN segments for Exemplar Patient at selected time increments

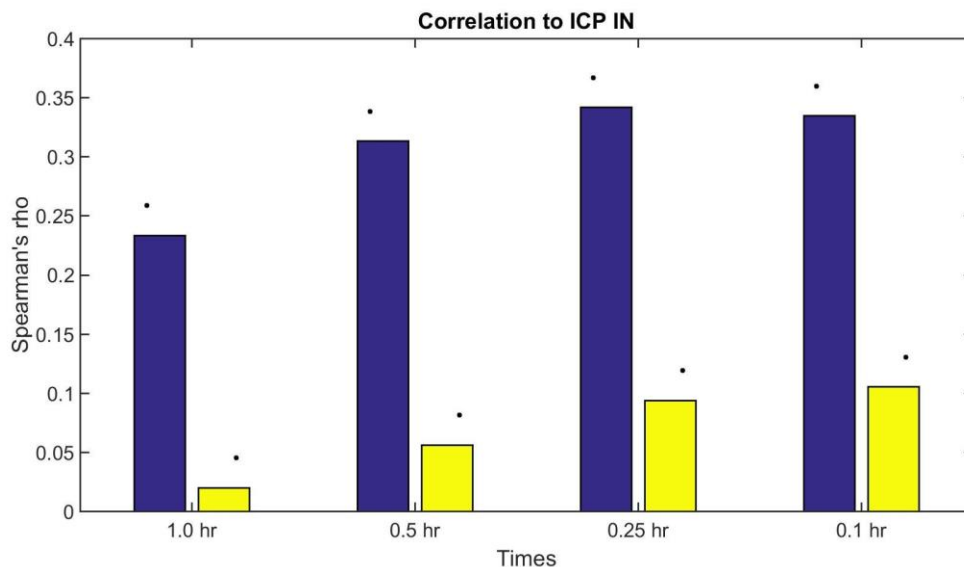
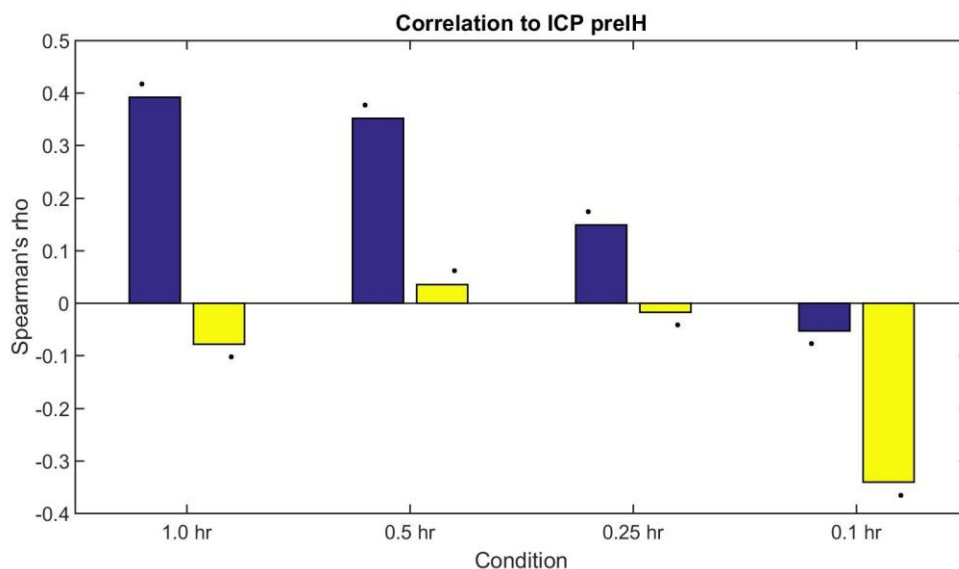


Figure 24. Spearman's Correlation of PAR (Blue) and SE (Yellow) to ICP during prelH segments for Exemplar Patient at selected time increments



Across all 7 patients analyzed, the Spearman's correlation results in Table 8 show PAR and mICP during IN hours and prelH hours are shown in Table 9. The comparative results indicate the positive correlations found in the exemplar are only found in patient E for IN hours. During IN hours and prelH hours, the strongest consistent correlations are in patient F, which also has the longest

dataset. For preIH hours, statistically significant correlations only occur in the Exemplar patient, patient E, and patient F. All correlations are still weak at below an absolute value of 0.55. These results indicate an absence of meaningful trends between patients, but trends do exist within patients particularly for IN hours.

Table 8. Spearman's Rank Correlation between PAR and mlCP during IN hours

| Time Segment (hr) | Exemplar | A | B | C | D | E | F |
|--------------------------|-----------------|----------|----------|----------|----------|----------|----------|
| 1.00 | 0.23* | -0.05* | -0.16* | -0.02 | -0.23* | 0.31* | -0.49* |
| 0.50 | 0.31* | -0.05* | -0.16* | -0.01 | -0.20* | 0.31* | -0.51* |
| 0.25 | 0.34* | -0.05* | -0.16* | -0.01 | -0.20* | 0.30* | -0.50* |
| 0.10 | 0.33* | -0.04* | -0.16* | -0.01 | -0.21* | 0.29* | -0.51* |

Table 9. Spearman's Rank Correlation between PAR and mICP during preIH hours

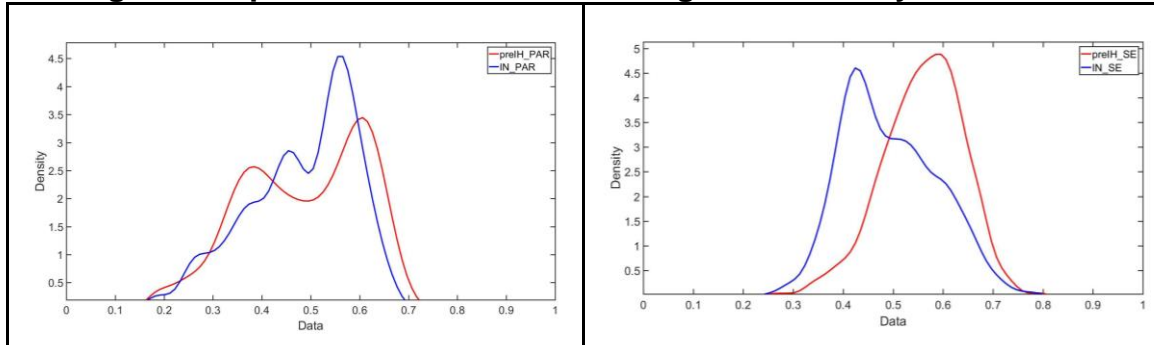
| Time Segment (hr) | Exemplar | A | B | C | D | E | F |
|-------------------|----------|-------|-------|------|-------|--------|--------|
| 1.00 | 0.40* | 0.09 | -0.10 | 0.20 | -0.10 | 0.08* | -0.48* |
| 0.50 | 0.36* | 0.18* | -0.12 | 0.22 | -0.12 | -0.09* | -0.41* |
| 0.25 | 0.15* | 0.06 | -0.30 | 0.27 | -0.30 | -0.26* | -0.40* |
| 0.10 | -0.05* | 0.06 | 1.00 | 0.19 | 1.00 | -0.55* | -0.42* |

4.3.4 Separation of preIH and IN Distributions

The previous analyses adopted the tactic from the simulations, which is to identify if and how PAR and ICP are related. The goal of the rest of the analyses is to examine the utility of PAR in predicting upcoming IH events. For this purpose, the remaining analyses will try to separate IN data from preIH data. First, the separability of preIH and IN PAR data was evaluated using a two-sample goodness of fit Kolmogorov-Smirnov (KS) test. This test identifies if a continuously-valued metrics from two datasets follow the same continuous distribution. If these datasets were identical (i.e., if the KS test returns a non-significant p-value), it would suggest that PAR had little if any usefulness in predicting HT events. The density of each set was plotted and fitted with a non-parametric distribution in Figure 25, and the corresponding cumulative density curves were calculated. The KS test evaluates how different these empirical cumulative density curves are and the computes the likelihood that they came from a single distribution.

Figure 25. Patient Exemplar KS Test of IN & preIH hours at 1-hour interval;

Left: Non-parametric distribution fitting of the density histograms for PAR
Right: Non-parametric distribution fitting of the density for SE data



The KS test results suggest that the pre-IH and IN distributions of PAR, SE, and their first-order time derivatives are distinct for all preIH windows. The full results of this analysis are presented in Table 10 where $H = 1$ demonstrates the null is successfully rejected along with the resulting numeric KS statistic. PAR and SE were successfully separated between IN and preIH hours for all four time periods.

Table 10. Results of Two-sided Kolmogorov Smirnov Test for PAR and SE at 1.0, 0.5, 0.25, and 0.1 preIH time periods versus IN time periods for Exemplar Patient

| | PAR | | SE | |
|--------------------|-----|---------|----|---------|
| preIH Time (hours) | H | KS Stat | H | KS Stat |
| 1.00 | 1* | 0.163 | 1* | 0.346 |
| 0.50 | 1* | 0.109 | 1* | 0.233 |
| 0.25 | 1* | 0.229 | 1* | 0.154 |
| 0.10 | 1* | 0.348 | 1* | 0.120 |

For the cohort of all 7 patients, the two-sided KS test was repeated to evaluate the generality of the results from the exemplar; these results are shown in Figure 26 and Table 11. The KS test was able to separate PAR during IN

hours from PAR during preIH hours at all 4 time periods for four of seven patients. The most separable time period was 1.00 hour and the least separable time period was 0.10 hours. The separation indicates higher repeatability than the correlations, meaning that while the predictive power may be relatively low, PAR still demonstrates an ability to separate between IN and preIH time points reliably.

Figure 26. Non-parametric distribution fitting of the density histograms for PAR for Patients A-F

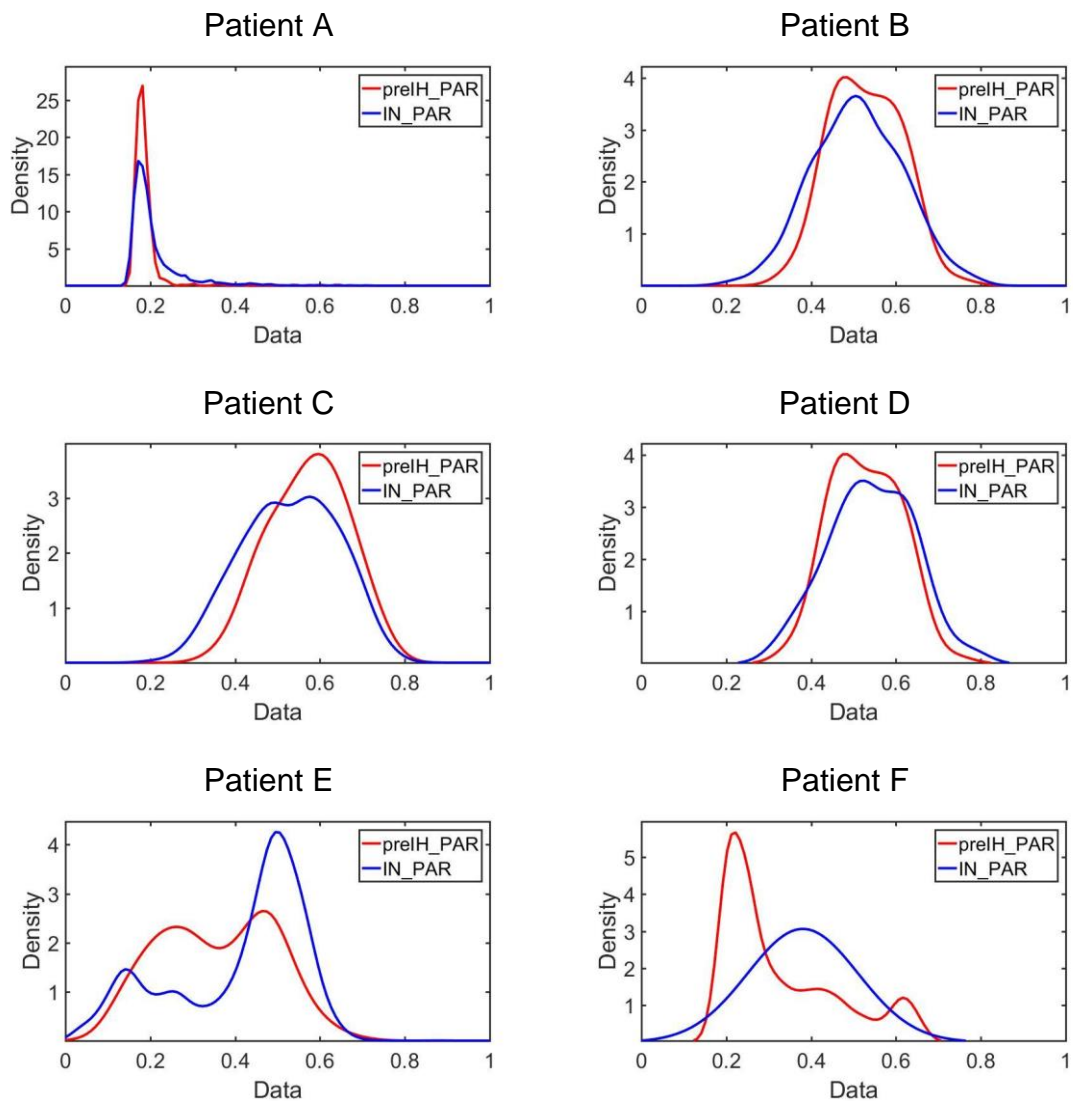


Table 11. Hypothesis Result of Two-Sided Kolmogorov-Smirnov Test for Patient Cohort. 1= PAR during IN and preIH hours are separable

| Time Segment (hr) | Exemplar | A | B | C | D | E | F | Mean |
|-------------------|----------|----|----|----|---|----|----|------|
| 1.00 | 1* | 1* | 1* | 1* | 0 | 1* | 1* | 0.86 |
| 0.50 | 1* | 1* | 1* | 0 | 0 | 1* | 1* | 0.71 |
| 0.25 | 1* | 1* | 0 | 0 | 0 | 1* | 1* | 0.71 |
| 0.10 | 1* | 1* | 0 | 0 | 0 | 1* | 1* | 0.33 |

Note that although the test suggests that the distributions are separable, it does not suggest any metric by which to do so. The KS test is sensitive to distribution differences in values (min, max, mean, etc.) and shape (kurtosis, skewness, peaks, modes, etc.). Creating a classification scheme of that evaluates PAR and determines whether or not the patient is about to have an IH event remains. However, this analysis also does not suggest that the differences are the same across the patients. A quick examination of all patients' PAR data in Figure 26 shows that in fact some patients do not have the same differences between their distributions as the patient exemplar. Some preIH distributions are left shifted from IN and some are right shifted, and all are non-normal.

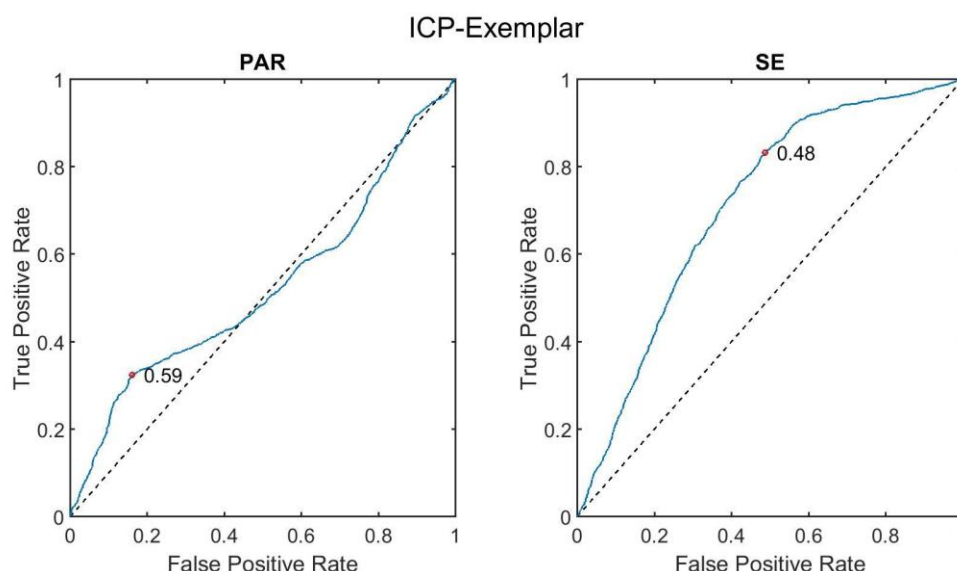
4.3.5 Receiver Operator Characteristic Curve

The previous analyses confirm that PAR has some ability to identify upcoming HT events. This analysis builds on this ability by identifying the general performance of a simple threshold method to identify upcoming IH events. The receiver operator characteristic (ROC) curve analysis examines the relationship between the true positive and false positive rate as the threshold value changes

in a classifier. The area under the curve (AUC) for ROC curves is a ready metric for evaluating the effectiveness of the classifier. A perfect classifier would have a curve at top of the graph, so that the AUC equaled 1.0. In contrast, a completely useless (i.e., random guessing) classifier would have an AUC of 0.5, and the curve would closely match the dashed reference line. Therefore, we can use AUC for both PAR and SE to determine the performance of each measure as a classifier of IH events.

The ROC curves for the 1-hr preIH window for the Exemplar patient are presented in Figure 27. As listed in Table 11, the AUC for PAR was 0.523 and for SE was 0.710, demonstrating that when using a simple threshold model, SE is a better classifier for separating IN and preIH data as it has a higher AUC ($AUC_{SE} - AUC_{PAR} = 0.187$). The maximum distance from the dashed reference line (e.g. maximum separation) occurs at a value of $PAR = 0.59$ with a False Positive Rate of 0.16 and the True Positive Rate for PAR is 0.32 whereas the maximum distance for SE occurs at a False Positive Rate of 0.49 and a True Positive Rate of 0.83, indicating that SE performs better as a classifier of true IH events for the Exemplar patient.

Figure 27. Receiver Operator Curves for PAR (left) and SE (right) for Exemplar Patient with 1-hr preIH window. Red circle indicates maximum distance from dashed line and labeled with corresponding PAR or SE value



In Figure 28, the ROC curves for Patients A through F are shown. Patients

A, E, and F demonstrate classifications where low PAR would be indicative of upcoming IH events whereas Patients B, C, and D follow the threshold line indicating that PAR performs as well as chance. These results would suggest that a patient specific approach should be used to analyzing these data when using PAR or SE. Table 12 shows all the AUC values for PAR, SE, and the difference between the two. In only two cases, Patient A and Patient C, PAR yields a negative value indicating that PAR would be a better classifier. However, patient A is one of the three cases where the ROC curve suggests a lower PAR and SE value corresponds to the onset of IH. Overall, the mean AUC values indicate that PAR and SE perform about the same as single threshold classifiers.

Figure 28. Receiver Operator Curves for PAR (left) and SE (right) for Patients A-F with 1-hr window. Red circle indicates maximum distance from dashed line and labeled with corresponding PAR or SE value

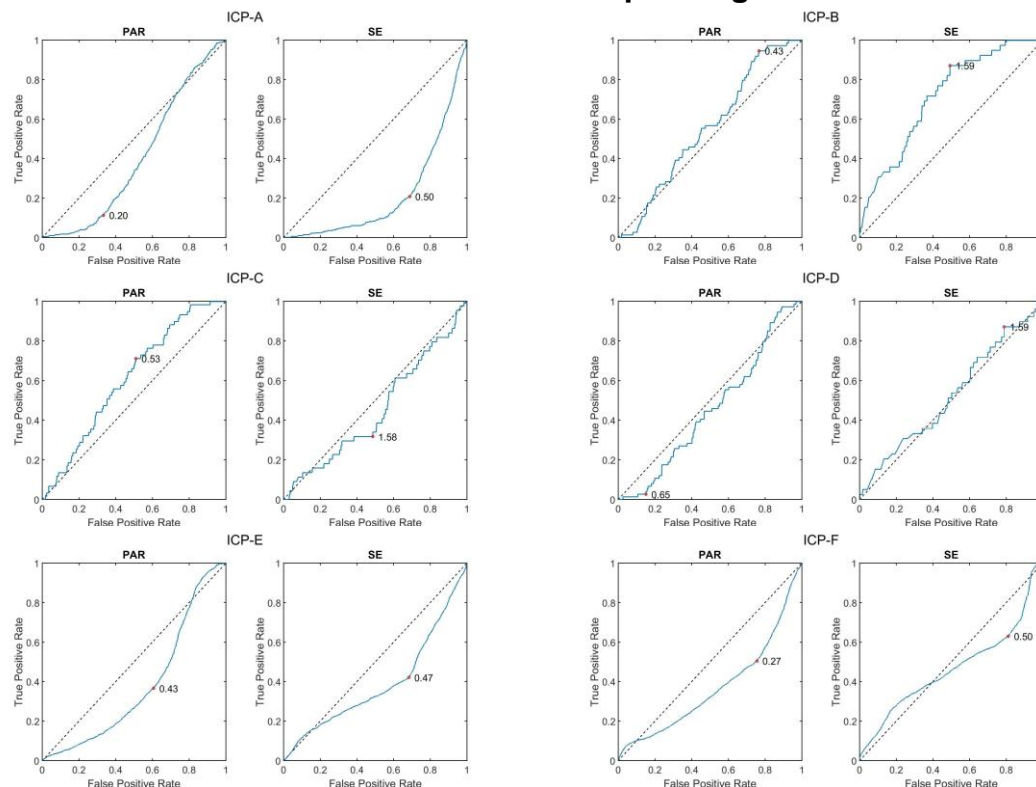
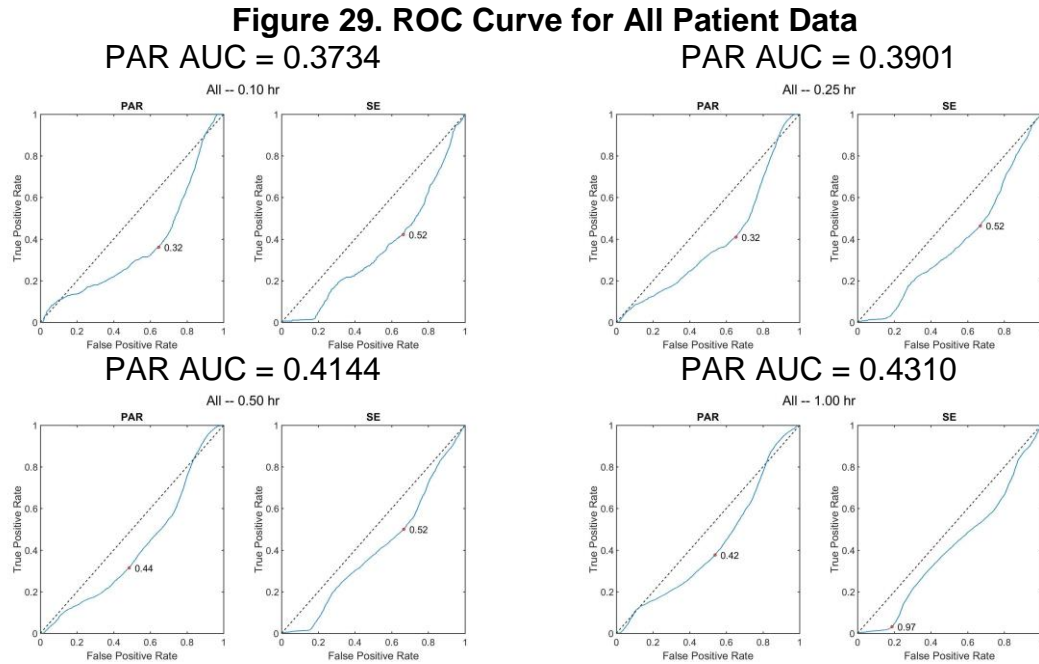


Table 12. Area Under the Curve for PAR, SE, & SE-PAR ROC Curves

| Patient | AUC PAR | AUC SE | AUC SE-PAR |
|----------|---------|--------|------------|
| Exemplar | 0.523 | 0.710 | 0.187 |
| A | 0.405 | 0.216 | -0.189 |
| B | 0.555 | 0.714 | 0.159 |
| C | 0.611 | 0.451 | -0.160 |
| D | 0.453 | 0.525 | 0.072 |
| E | 0.382 | 0.390 | 0.008 |
| F | 0.371 | 0.466 | 0.095 |
| Mean | 0.471 | 0.496 | 0.025 |

The overall ROC curve for all patient data is shown in Figure 29 for the

four time points. While the overall AUC approximates 0.4, all of the curve passes below the threshold that indicates that a lower bound threshold would be better for classification in this patient population.



4.3.6 Classification of Data Across Population

Also, a confusion matrix analysis was performed on the aggregate data to further elucidate the simple threshold classification parameters for PAR. Using the classification method outlined in Section 4.3.1, all data that was classified as IN or preIH was used to tally true positives, false positives, true negatives, and false negatives for the threshold values discovered in Section 4.3.5. Then summary statistics were calculated on the contingency tables [40].

In Table 13, two confusion matrices have been counted for PAR and for SE for the Exemplar patient. The Accuracy of both tests is at about 0.6 and the prevalence is 0.3 for both. The true positive rate is higher for SE but the positive predictive value is slightly higher for PAR. F1 is a harmonic mean between

precision and recall where a value of 1 equals perfect precision and recall - the statistic is higher for SE than PAR in the exemplar patient.

Table 13. Confusion Matrix Analysis for Exemplar Patient
Left Top: Confusion Matrix for PAR; Left Bottom: Confusion Matrix for SE;
Right: Summary Statistics

| | preIH | IN | |
|------------|-------|------|------|
| PAR > 0.59 | 458 | 459 | 917 |
| PAR < 0.59 | 952 | 2379 | 3331 |
| | 1410 | 2838 | 4248 |

| | preIH | IN | |
|----------------|-------|------|------|
| Entropy > 0.48 | 1175 | 1383 | 2558 |
| Entropy < 0.48 | 235 | 1455 | 1690 |
| | 1410 | 2838 | 4248 |

| | PAR | Entropy |
|---------------------------|-------|---------|
| Accuracy | 0.668 | 0.619 |
| Prevalence | 0.332 | 0.332 |
| Positive Predictive Value | 0.499 | 0.459 |
| False Discovery Rate | 0.501 | 0.541 |
| False Omission Rate | 0.335 | 0.083 |
| Negative Predictive Value | 0.714 | 0.861 |
| True Positive Rate | 0.325 | 0.833 |
| False Negative Rate | 0.675 | 0.167 |
| False Positive Rate | 0.162 | 0.487 |
| True Negative Rate | 0.838 | 0.513 |
| Positive Likelihood Ratio | 2.008 | 1.710 |
| Negative Likelihood Ratio | 0.805 | 0.325 |
| Diagnostic Odds Ratio | 2.494 | 5.260 |
| F1 Score | 0.394 | 0.592 |

In Table 14, two confusion matrices have been counted for PAR and for SE using all the patient data available. The Accuracy for SE stays the same at about 0.6 but the accuracy for PAR is as low as 0.4. The prevalence drops to 0.2 for both. The positive predictive value for both is under 0.2 as well. The F1 statistic for both is below 0.25 for both indicating poor precision and recall for a binary classification of all the patient data.

Table 14. Confusion Matrix Analysis for All Patient Data
Left Top: Confusion Matrix for PAR; Left Bottom: Confusion Matrix for SE;
Right: Summary Statistics

| | preIH | IN | | PAR | Entropy |
|------------|-------|-------|-------|-------|---------|
| PAR > 0.42 | 2472 | 12627 | 15099 | 0.443 | 0.627 |
| PAR < 0.42 | 4093 | 10803 | 14896 | 0.219 | 0.219 |
| | 6565 | 23430 | 29995 | 0.164 | 0.048 |
| | | | | 0.836 | 0.952 |
| | | | | 0.175 | 0.270 |
| | | | | 0.725 | 0.746 |
| | | | | 0.377 | 0.038 |
| | | | | 0.623 | 0.962 |
| | | | | 0.539 | 0.208 |
| | | | | 0.461 | 0.792 |
| | | | | 0.699 | 0.181 |
| | | | | 1.352 | 1.215 |
| | | | | 0.517 | 0.149 |
| | | | | 0.228 | 0.042 |

4.3.7 PAR General Utility in Predicting Hypertensive Events

The previous analyses focused on the momentary value of PAR for predicting upcoming IH events, primarily in a binary approach. For this next and final analysis, several modifications were made to this basic design.

The first modification is to supplement momentary PAR with various statistics of PAR over the previous 0.1 hours. This modification allows for more features that describe not only the value of PAR but also its recent behavior. For this purpose, six statistics were used: mean, median, min, max, range, and standard deviation. The standard deviation was computed as a population standard deviation, and the remainder followed their usual definitions. These six predictors were used in addition to the momentary PAR value for the next classifiers.

The second modification was to supplement PAR statistics with information about how PAR interacts with ICP. Specifically, Sections 4.3.1 and 4.3.2 highlight how the relationship between PAR and ICP can vary from fairly

positive to negative and strongly to weakly in different contexts. In this light, the Spearman's Rho Ranked correlation between PAR and ICP was also used as a predictor in the next classifiers. Again, this was computed using the data from the previous 0.1 hours. A second aspect of how PAR interacts with ICP was measured using cross-correlation. The cross-correlation between two signals is effectively the amount of correlation as one signal is lagged at different intervals. MATLAB's `xcorr` function was used to generate the cross correlation, and its max, min, their related time offsets, and the sum square cross correlation were used as additional predictors.

The third modification was to use the other values, ICP and SE, as predictors in the classifier as well. By including them in the classifier, this analysis can determine whether or not PAR has a utility that is not covered by the other measures. For example, if high SE is a good predictor of upcoming IH events, then it can dominate the classifier. However, if SE indicates an upcoming IH event, whether or not PAR also indicates an upcoming IH event can affect the decision. Thus, seven additional predictors were included for both ICP and SE (momentary value, mean, median, max, min, range, and standard deviation).

Finally, the fourth modification to this process was to examine the effect of changing statistics windows independently of changing the predictive interval. The predictive interval values are the same as in Section 4.3.3, at 1.0 hour, 0.5 hour, 0.25 hour, and 0.1 hour. The statistics windows, as used in the three previous modifications, used the same subset of values. This means that the mean, median, min, max, range, and standard deviations were computed over

these time windows, effectively increasing the scope of the analysis. Previously, the analysis would have used the past 0.1 hours to predict an event in the upcoming 1.0 hours. With this modification, this analysis will be repeated to examine the ability of the previous 0.1 to 1.0 hours of patient statistics to predict an IH event in the next 0.1 to 1.0 hours. Note, the statistic windows are not combined in a single classifier such that it uses both the 1-hour statistics and the 0.1 hour statistics in a single classifier simultaneously.

Given the results from Sections 4.3.4 - 4.3.6, it seems that the exemplar patient does not necessarily represent the remaining patients in terms of how ICP, PAR, and SE behave during preIH periods. Consequently, the data hereafter focuses on averages of overall analysis outcomes using all the patient data. This method allows the exemplar patient and the subsets of patients with divergent behavior to be well-represented in the results.

The goal of the current analysis is the same as Section 4.3.3: to discriminate preIH data from IN data using PAR and the other predictors described above. Up until this section, the assumption was that a simple threshold model of PAR would be sufficient to divide the data. For this section, a slightly more advanced classifier will be used: logistic regression. Logistic regression acts similar to the linear regression from Section 4.3.1, except that the “target” is the likelihood that the data belongs to one of two values (in this case, that the data comes from the preIH dataset or not). For this reason, logistic regression is preferred for problems that require classification between two states. The result from the logistic regression model is a function that provides

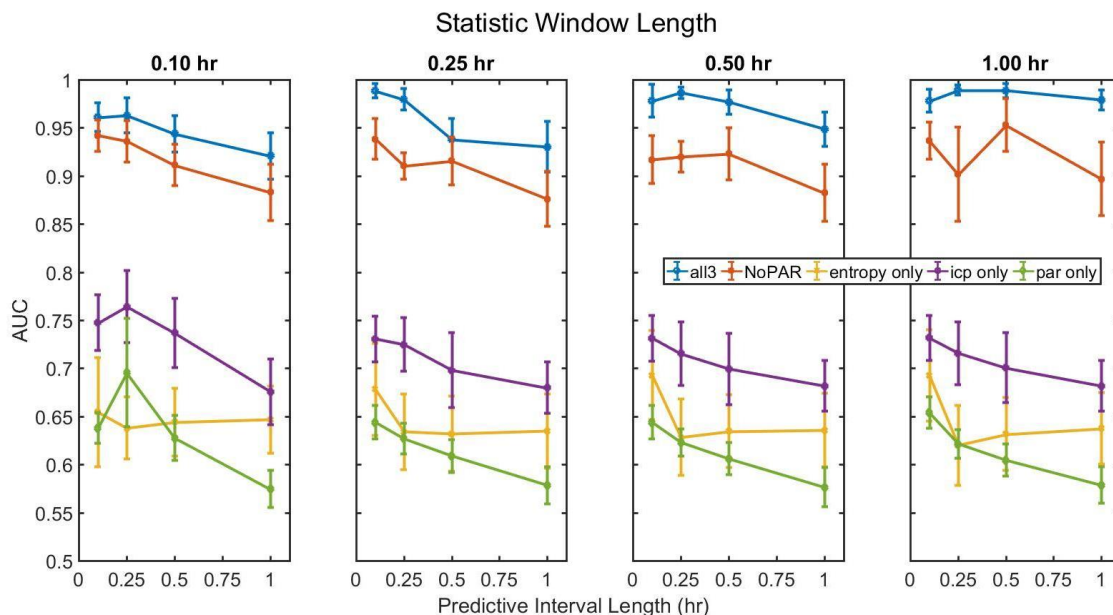
probabilities that a given data point comes from the preIH distribution. Given these probabilities, one can then use a simple threshold model on the probabilities to extract an ROC curve and evaluate the model. Given the number of models being evaluated here, each model will only be summarized using AUC, which is a good proxy for model fit. This analysis was conducted in R.

The first pass of this analysis focuses on establishing a proof-of-value for PAR. To complete this, five models were fit. The first three models test the utility of PAR, ICP, and SE separately. For these models, the results simply expand on the analyses from Section 4.3.4 and act as lower bounds on our understanding of how the analyses can function. The next model tests the utility of all predictors mentioned above, totaling 27 predictors, to establish an upper bound for the predictive ability of the dataset. Finally, the last model uses all 27 predictors less the 7 PAR measures, the 5 cross correlation metrics, and the Spearman correlation. By evaluating these five models, the raw utility of PAR as a predictor can be understood. It should be noted, however, that the idea of lower bounds and upper bounds are more conceptual than literal; there is not a strictly monotonic relationship between number of predictors and AUC as there is with other model evaluation metrics (i.e., R squared).

Examining the resulting plots in Figure 30 shows that, averaging across all the patients, the predictive model without PAR performs below the level of the model with all the metrics included. In this multi-paneled figure, each column shows the results for using statistics from different window lengths, from 0.1 hours to 1.0 hours. Within each panel, the data for each of the models is shown

across the different predictive intervals, with the error bars depicting standard error as computed across subjects. The single metric models cluster towards the bottom of the graphs, with ICP-based metrics yielding AUC about 0.71, SE-based metrics yielding 0.65, and PAR-based metrics yielding 0.62. Using all the metric produces a classifier that provides an AUC of about 0.97, but removing the PAR values reduces this to 0.91.

Figure 30. Mean Predictive Model Performance for 0.1, 0.25, 0.5, and 1 Hour statistic windows with error bars depicting standard error. PAR Only (Green), Entropy Only (Yellow), ICP Only (Purple), No PAR (Red), All Features (Blue)



Examining Figure 30 for optimal statistics window values and predictive interval lengths, the data suggest that shorter predictive intervals are better, and that longer statistics windows are better in terms of AUC values e.g. a longer amount of preIH information going in yields better IH predictions for shorter times into the future. However, as the statistic window length increases, so does the length of the error bars, and therefore the variability in the efficacy of the

classifier. As a compromise to these considerations, for the remaining analyses, a statistics window length of 0.25 hr and a predictive interval of 0.25 hr will be used.

4.3.8 PAR Specific Features Useful for Predicting Hypertensive Events

Having established a specific statistics window and predictive interval to use, the next issue to resolve is: which parameters are actually assisting in the classification problem and which are excessive? To answer this question, predictors were removed from the full model in a backwards stepwise regression analysis. This analysis determines which predictors contribute the least to the model and removes it. If the resulting reduced model performs as well as the original, the algorithm repeats the reduction step with the newly reduced model. If the reduction reduces the model's performance, it adds the removed predictor and halts the algorithm. For this purpose, the models are evaluated using Akaike Information Criterion (AIC) which is an information criterion metric that measures the variance in the remaining data after the model's predictions are accounted for, with a penalty included for each parameter included in the model. The parameter penalty scheme of AIC is part of its strength as a model evaluation metric: it has been shown to reasonably limit overfitting. This process was conducted using the stepAIC function in R. One depiction of these results are shown in Table 15 where all 28 features tested are presented; if 1 the variable was included in the model and if 0, the variable was excluded. Table 16 provides an easier summary of the process results.

Table 15. Feature Matrix Present in Models for All 7 Patients with Average Inclusion Colormap.

Green = High Presence and Red = Low Presence

| | Exemplar | A | B | C | D | E | F | | Average Inclusion |
|-----------------|----------|---|---|---|---|----|----|--|-------------------|
| icp.val | 1 | 1 | 0 | 0 | 0 | 0 | 1 | | 0.33 |
| icp.mean | 1 | 1 | 0 | 1 | 0 | 1 | 1 | | 0.67 |
| icp.median | 1 | 1 | 0 | 0 | 0 | 1 | 1 | | 0.50 |
| icp.range | 0 | 1 | 0 | 0 | 0 | 1 | 0 | | 0.33 |
| icp.stdev | 1 | 0 | 0 | 0 | 0 | 1 | 1 | | 0.33 |
| icp.max | 0 | 1 | 0 | 1 | 0 | 1 | 1 | | 0.67 |
| icp.min | 1 | 1 | 0 | 0 | 0 | 1 | 0 | | 0.33 |
| par.val | 1 | 0 | 0 | 0 | 0 | 0 | 1 | | 0.17 |
| par.mean | 1 | 1 | 1 | 0 | 0 | 1 | 1 | | 0.67 |
| par.median | 0 | 1 | 1 | 0 | 0 | 1 | 1 | | 0.67 |
| par.range | 1 | 1 | 1 | 0 | 1 | 1 | 1 | | 0.83 |
| par.stdev | 1 | 1 | 1 | 0 | 0 | 1 | 1 | | 0.67 |
| par.max | 1 | 1 | 1 | 0 | 1 | 0 | 1 | | 0.67 |
| par.min | 1 | 1 | 1 | 0 | 1 | 1 | 1 | | 0.83 |
| ent.val | 1 | 0 | 0 | 0 | 0 | 1 | 1 | | 0.33 |
| ent.mean | 1 | 1 | 0 | 0 | 0 | 1 | 1 | | 0.50 |
| ent.median | 0 | 1 | 0 | 0 | 0 | 1 | 1 | | 0.50 |
| ent.range | 1 | 1 | 0 | 1 | 0 | 1 | 1 | | 0.67 |
| ent.stdev | 1 | 1 | 0 | 1 | 1 | 1 | 1 | | 0.83 |
| ent.max | 1 | 1 | 0 | 0 | 0 | 0 | 1 | | 0.33 |
| ent.min | 1 | 0 | 0 | 0 | 0 | 1 | 1 | | 0.33 |
| corr | 0 | 0 | 0 | 1 | 0 | 1 | 1 | | 0.50 |
| xcorr.max | 1 | 1 | 0 | 0 | 0 | 0 | 1 | | 0.33 |
| xcorr.maxlag | 0 | 0 | 0 | 1 | 0 | 1 | 1 | | 0.50 |
| xcorr.min | 0 | 0 | 0 | 1 | 0 | 1 | 1 | | 0.50 |
| xcorr.minlag | 1 | 0 | 0 | 0 | 0 | 1 | 1 | | 0.33 |
| xcorr.sumsq | 1 | 0 | 0 | 0 | 0 | 1 | 1 | | 0.33 |
| NumParFeatures: | 9 | 7 | 6 | 3 | 3 | 10 | 13 | | |

Table 16. Features Present in Models by Number of Patients Using Each Feature

| Number of Patients Using Feature | Features |
|----------------------------------|---|
| 6 | par.range par.min ent.stdev |
| 5 | icp.mean par.mean par.stdev par.max ent.range |
| 4 | icp.median icp.max par.median ent.mean |
| 3 | xcorr.max xcorr.maxlag xcorr.min xcorr.minlag xcorr.sumsq icp.val icp.stdev icp.min ent.val ent.median ent.max ent.min corr |
| 2 | icp.range par.val |

The results for each patient are relatively distinct from each other with respect to which features are useful reinforcing the need for patient-specific classification approaches. Twelve features were found to be used in four of the seven patients tested. Three features tied for most used: PAR range, PAR min, and SE standard deviation. All of the PAR statistics were effective and included

for the majority of the seven patients from PAR, but the momentary PAR value was only included for two of the seven patients and was the weakest variable tested. For SE, the mean, range, and standard deviation were included, and for ICP, the mean, median, and max were included. Notably most of the cross-feature statistics from correlation and cross correlation were not used by the majority of the patients; however, the last row summary for Table 15 also shows that all the patients benefitted from the use of some PAR-based features.

4.3.9 Simulated Prediction of Hypertensive Events

The previous sections examined how PAR related to ICP, established the ability of PAR to help predict IH events, and isolated a set of features that could be used moving forward to create an IH alarm. The goal of this section is to implement a single such IH alarm based off the features useful for the majority of the patients.

One perspective on limiting the features used would say to include all the features in the potential alarm setup so as to provide the most power in the analysis. However, limiting the features used to a smaller subset prevents some amount of overfitting thus improving classifier generalization. Furthermore, the final results of this basic research is to create usable medical devices, and requiring large amounts of memory and processing for these devices could also increase their liability for errors and intrusions. Therefore, for this simulated IH alarm analysis, those features that were included for the majority (>50%) of the patients were included here.

This analysis will be done in three steps. First, the stated features will be

included in a logistic regression analysis of the pooled patient data using leave-one-out-cross-validation on a subject-wise basis. Second, the resulting model's ROC curve will be examined for a cutoff value. Third, the output of these first two steps will be used to evaluate the patient data when used as an alarm.

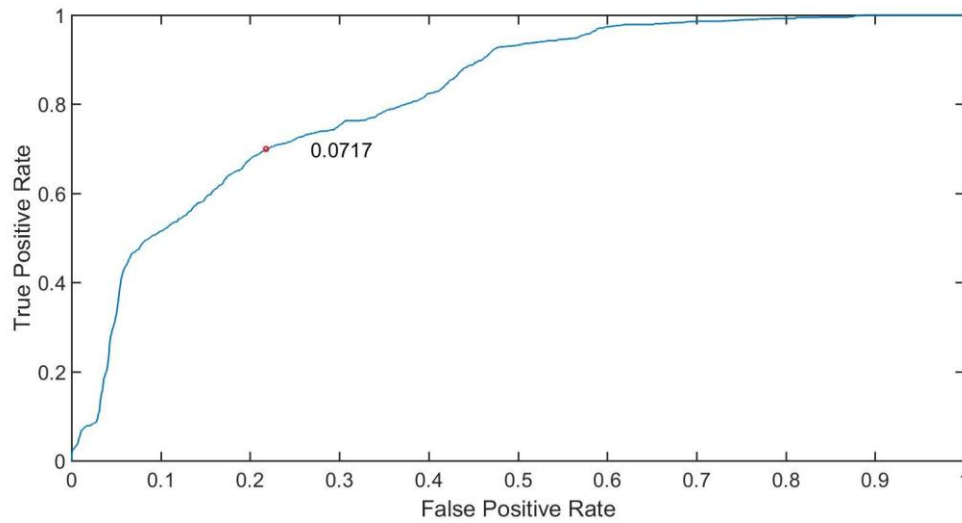
For the first step, the logistic regression is conducted seven times, each time with a single patient's data omitted. This method, known as leave-one-out-cross-validation (LOOCV), has been shown to be effective in preventing overfitting of classifiers in many other contexts [41]. The final classifier will use the averages of all the patients' model parameters. This process yielded the following coefficients:

Table 17. 12 Parameter Logistic Regression Coefficients

| | | | |
|------------|----------------------|------------|---------|
| PAR.range | 1.082×10^4 | ICP.max | 0.186 |
| PAR.min | 1.083×10^4 | ICP.median | -0.218 |
| PAR.mean | -32.540 | ICP.mean | 29.900 |
| PAR.stdev | 37.634 | ENT.stdev | -21.707 |
| PAR.max | -1.082×10^4 | ENT.range | 2.565 |
| PAR.median | 23.112 | ENT.mean | 1.016 |
| | | Intercept | -6.778 |

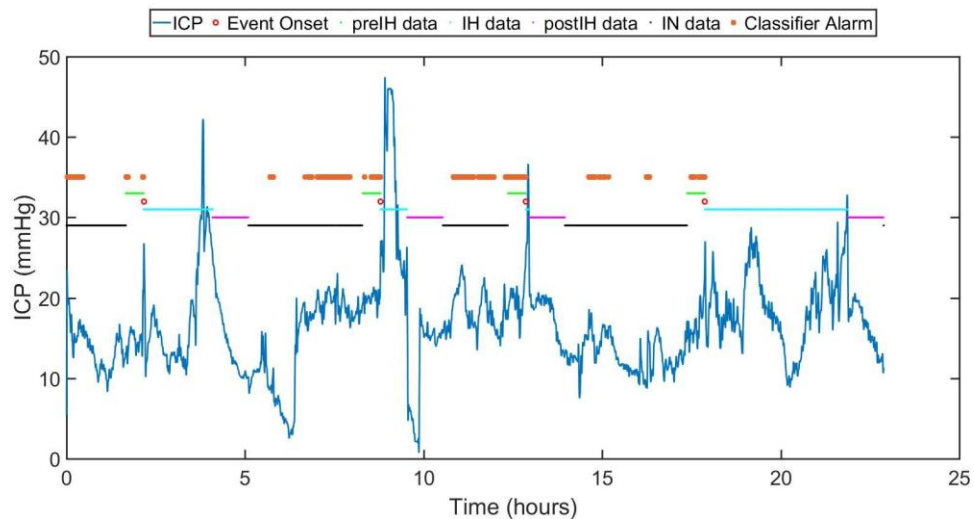
The next step evaluated an ROC curve based off the results from this setup. The ROC curve associated with this classifier when tested against the entire dataset looks as follows:

Figure 31. ROC of 12 Parameter Classifier



This ROC analysis suggests that a good threshold to use is 0.0717; this means that when the classifier exceeds 7% probability that there is an IH event upcoming, the alarm will go off. The result of this is shown in Figure 32 and the result for all of the other patients is presented in Appendix VI.

Figure 32. Mock Alarm Results in Exemplar Patient.
Alarm on (Red Star), preIH (green), IH (cyan), postIH (purple), IN (Black)



This result is not perfect. There are several times when it suggests to alarm that are not necessary (false positives), and although not visible in this dataset, there are IH events that it does not alarm for as shown in Table 18 (false negatives).

Establishing a correct level for the involvement of PAR may be difficult, and will require coordination with practitioners to determine acceptable levels of false alarms and acceptable procedures for dealing with alarms.

Table 18. Number of Events with Simulated Alarm before Event

| Patient | Number of Events | Alarm in 5 minutes before event |
|----------|------------------|---------------------------------|
| Exemplar | 4 | 4 |
| A | 2 | 1 |
| B | 1 | 0 |
| C | 2 | 1 |
| D | 1 | 0 |
| E | 5 | 4 |
| F | 11 | 10 |

4.4 Overall Results

Looking across the patients, there are limited inter-subject trends within this set of 7 patients. The issue is further complicated due to the inherent physiological variation in age, gender, injury severity, comorbidity, and length of stay. Each patient demonstrated variation from the exemplar patient in either KS or Spearman's rank results. The linear regression approach demonstrated negative trends between PAR and ICP during preIH periods whereas Spearman's rank correlation demonstrated a positively ranked relationship for the exemplar patient at the majority of IN and IH periods; the Spearman's results across the other six patients yielded low agreement between patients and fewer demonstrated significant correlations (IN: 85% preIH 46%). The KS test shows evidence that preIH and IN timespans are separable for the majority of conditions

and patients. Only patient D failed at separation at all four time points and four of the seven patients passed at separability at all four time points. Of 28 time points tested across 7 patients, 67.9% of time periods tested yielded evidence to reject the null hypothesis.

Overall, these results demonstrate that for the exemplar subject, AVP PAR at all time segments correlates marginally better than SE to mean ICP at both IN and preIH segments, though significantly for all time periods with the exception of 0.1-hr segments for preIH data. SE correlates positively for IN data significantly for time periods less than 1-hr and correlates negatively at 1-hr and 0.1-hr for preIH analysis. These results along with the KS test results establish that PAR is comparable to the established cycle variability measure, SE, and can be used to identify time periods to focus on within the hour preceding IH when designing alarms based on PAR in the future.

The aggregate patient results also reiterate the need for a patient-specific approach to applying a metric like PAR for predictive alarm design. While the ROC results indicate that PAR performs poorly as a classifier as a single threshold metric, this is likely due to the variability in distribution shape compared to normal distributions. Ultimately, PAR requires smaller data buffers than several existing metrics and does not yield discontinuous values like sample entropy does. The multiple regression analyses confirms that even when considering the value of the other predictors such as ICP and SE, including PAR enables better prediction of IH events.

An important limitation to these analytic methods should also be

considered. The methods used here, (regression, correlation, KS-based separation, etc.) assume the independence of data points. However, given the nature of the data as time-series from a patient(s), this assumption is questionable. A further analysis with a style of Monte-Carlo resampling of the data could preserve the validity of these analytic methods and provide a refined estimation for the predictive value of PAR.

CHAPTER 5. FUTURE DIRECTIONS AND CONCLUSIONS

5.1 Future Directions

Future directions for PAR analysis include simulations to identify the relationship between PAR scores and simulated ICP signals mimicking specific known long-term pathologies, to better interpret the behavior of PAR in impaired physiologies for longer time periods. Also, by further examining PAR trends in segments before and after ICP hypertensive events, the presence of clinically-relevant and unique patterns in PAR can precede cerebrovascular crisis diagnosis. Another avenue for exploration is the implementation of PAR analysis on alternative phase planes of other vascular metrics or combinations of multiple cerebrovascular metrics.

5.1.1 Alternative Phase Domain Metrics

While this body of work focuses on one ratio metric feature in one of two tested phase domains, VSP and AVP, several alternative phase domain metrics are possible. For instance, phase path length comparing loop path length to total path length could be a viable feature for measure in ICP analysis. A similar ratio metric feature based on path length would be low for smooth ICP cycles and high for ICP cycles where multiple peaks are present. One challenge that arises particularly with clinical data is how to analyze figures where multiple-peaks are absent, which could be overcome by comparing path length to the path length of a convex hull as well.

5.1.2 Multiparameter Phase Domain Analysis

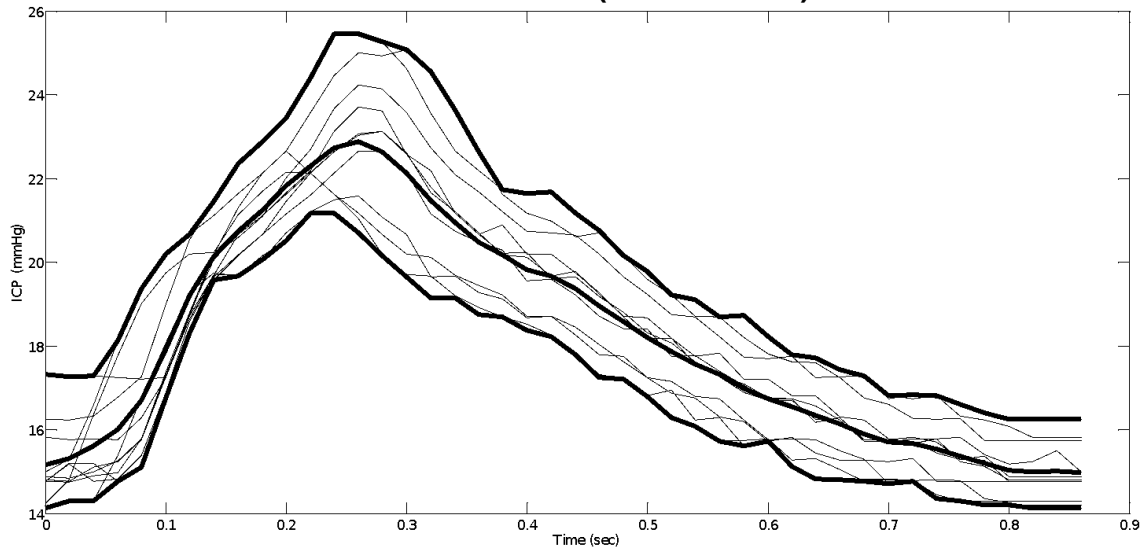
To address the complexity of AR, a future approach could focus on

analyzing the phase relationships between ICP and ABP. Much of the work in cardiovascular physiology focuses on the behavior of pressure-volume curves. A persistent challenge with neurovascular analyses is that volume measurements are difficult to derive without continuous imaging. A solution to bridge the relationship between ABP and ICP is to analyze co-phase domains, e.g. dICP vs dABP, ddICP vs ddABP, or even ABP vs dICP. While a known lag exists between ABP and ICP wave timing, analyzing the lag is an entirely unique body of research. By examining the consistency between adjacent cycles, a combined phase domain analysis of these two physiological metrics could magnify miniscule timing changes that are integral to AR function.

5.1.3 Accelerating PAR Score Calculation Time and Increasing SNR

Since calculating PAR scores has a high computational cost of ~1 minute per computation and there are usually ~60 cycles per minute from any given patient, a method of compressing data in order to shorten computational time is necessary for implementation in clinical monitors; one proposed method averages ~10 adjacent cycles prior to calculation of PAR scores. An example of the aggregation is displayed in Figure 33. This pre-treatment of data into aggregated profile costs significantly less computational time compared to PAR score calculation for each cycle individually: the computational time is reduced by approximately 70% according to Matlab.

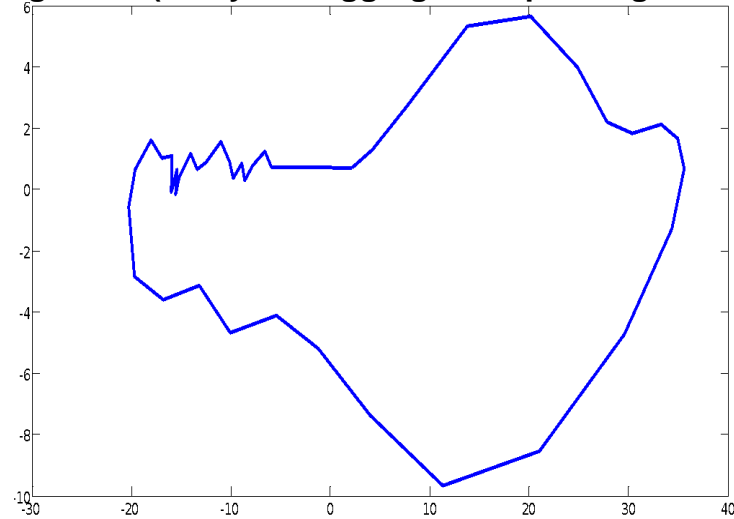
Figure 33. Example of Multiple Cycles Aggregated: Individual Cycles (Thin Solid), Mean Cycle (Thick Solid), Absolute Maximum and Absolute Minimum Values (Thick Dotted)



After cycles have been aggregated in approximately 10 second chunks,

the PDA approach can still be applied on the acceleration-velocity (A-V) phase plane of the arithmetic mean of the ICP cycles. For the example data shown in Figure 33, the corresponding phase plane is shown in Figure 34. The number of loops inside and outside the loop as well as the general shape of the A-V phase plane still varies based on prominence of peaks in the cycle; this approach can increase the signal to noise ratio without using a digital filter.

Figure 34. Acceleration-Velocity Phase Plane of Mean ICP signal from Figure 27 (11 Cycles Aggregated Spanning 9 seconds)



Other approaches to accelerating the PAR calculation include non-graphical calculation methods as well as integrating the digital signal processing techniques into the analog-to-digital conversion process at the data collection stage.

5.1.4 Combinatorial Approach to Cerebrovascular AR Monitoring

The complexity of human physiology and metrics of physiological change is that the measured behaviors are time- and frequency-limited. The current state of ICP analyses focuses on creating intricate and highly-specific algorithms that combine several time- and frequency- domain parameters into a single index for treatment and prediction that often focus on long-duration analyses and have ignored information available on smaller time scales. While PAR advances information about shorter time changes in ICP than other current modalities like PRx and RAP, an approach that combines multiple metrics with unique weighting factors when applied to the same data set would capture the most information

about current and future ICP behavior.

5.2 Conclusions

This research advances a novel approach to analyzing intracranial pressure monitoring metrics developed on earlier studies on (1) signal processing techniques for cyclical waves, (2) physiological variability related to the timing of vascular phenomena, and (3) intracranial pressure waveform morphology. As previously demonstrated, particularly in ICP monitoring, a morphological parameter(s) can address the issue of underscoring subtle time-domain changes in the sub peaks of ICP between cardiac cycles. Patterns in the rate of change for ICP were identified by transformation of ICP waves from the time domain to the phase domain for 300 simulated cycles and 7 clinical cases spanning over 400 hours.

For the morphological simulation of ICP cycles, the data demonstrated a strong linear correlation of 0.93 or greater between Amplitude of Peak 2 and mICP for both cases tested as well as a linear correlation of 0.76 R-Squared between acceleration-velocity phase plane PAR for amplitude modulation as demonstrated in Chapter 3.2 and 3.3. Signal noise creates notable distortion in the phase domain, and accurate PAR calculations demand high SNR or sufficient filtering as demonstrated in Section 3.4.

In the exemplar case study, both SE and PAR demonstrated the ability to separate IN from preIH hours according to the two sample Kolmogorov-Smirnov test. SE offers a higher area under the curve measure of the receiver operator curve (ROC) in the exemplar patient, but not in Patients A or C. These results

demonstrate that phase domain analysis can detect IH using PAR to conflicting reliability when used as a simple threshold measure.

Further analysis of PAR classification using multiple PAR-based metrics yields better results than classifiers without PAR along with long information windows forecasting at short times into the future. PAR was found to add value when compared to a classifier without PAR. While a 27 feature parameter vector was tested across all seven patients, 15 of the features were found useful in less than half the patients and were excluded from further analysis. In simulating the prediction of IH events, the classifier was successful in alarming before all four events in the exemplar patient but also incorrectly alarmed during periods of IN; further refinement of the classifier or incorporation of other existing parameters like RAP and PRx may improve the performance as suggested in the future directions chapter.

The invasive and heterogeneous nature of current ICP sensing technologies creates a major challenge for research and development of novel analytics. Noise and heterogeneity is introduced by variations in: (1) neurosurgical sensor types, manufacturers, and sensor placement; (2) recording tools and sampling rate; and (3) signal storage, preprocessing, and secondary data acquisition. In many existing databases, ICP recordings are noisy, data are typically inaccessible, limited to recordings of less than 10 minutes, and recorded at too low of a sampling rate to analyze cycle-to-cycle ICP behavior using this approach. The simulation based approach demonstrated in Chapter 3 fills this existing gap to afford the validation of beat-to-beat metrics. PAR and PAR-based

metrics are found to contribute unique information when compared to SE and raw ICP metrics during classification as explained in Chapter 4.

PAR is a single ratio metric unit less feature bounded from 0 to 1 that magnifies small changes in timing typically classified by large multi-parameter feature vectors that adds unique information to time-domain algorithms. By analyzing ICP behavior in the phase domain, PAR showed relationships to ICP as shown by the linear regression, Spearman's rank correlation, Kolmogorov-Smirnov test, and Receiver Operator Characteristic Curves as well as predictive accuracy with a confusion matrix analysis, logistic regression, and simulated alarm models. The above evidence demonstrates that PAR adds value and address real-world medical challenges best when using multi-parameter logistic algorithms; further investigation is needed to couple the changes in PAR to mechanistic physiological drivers of such changes likely using animal models or modulation of a driven model of ICP. Ultimately, this body of work quantifies the utility of phase domain analysis in simulated and clinical ICP data and shows that PAR-based metrics add unique information when classifying preIH correctly within the seven patients analyzed in this dissertation in comparison to SE and ICP metrics.

APPENDIX I. REFERENCES

1. Taylor et al., "Traumatic Brain Injury–Related Emergency Department Visits, Hospitalizations, and Deaths — United States, 2007 and 2013." https://www.cdc.gov/traumaticbraininjury/get_the_facts.html
2. Brain Trauma Foundation. TBI Statistics: Facts About TBI in the USA. www.braintrauma.org/tbi-facts/tbi-statistics/.
3. Traumatic Brain Injury.com, LLC. "TBI: Glasgow Coma Scale." <http://www.traumaticbraininjury.com/symptoms-of-tbi/glasgow-coma-scale/>
4. Sternbach, "The Glasgow Coma Scale." J Emerg Med. 2000 Jul;19(1):67-71. <https://www.ncbi.nlm.nih.gov/pubmed/10863122>
5. Ryan M. McAdams and Sandra E. Juul, "The Role of Cytokines and Inflammatory Cells in Perinatal Brain Injury," Neurology Research International, vol. 2012, Article ID 561494, 15 pages, 2012. doi:10.1155/2012/561494 <https://www.hindawi.com/journals/nri/2012/561494/>
6. Cipolla MJ. The Cerebral Circulation. San Rafael (CA): Morgan & Claypool Life Sciences; 2009. Chapter 5, Control of Cerebral Blood Flow. Available from: <https://www.ncbi.nlm.nih.gov/books/NBK53082/>
7. Le Roux P. Intracranial Pressure Monitoring and Management. In: Laskowitz D, Grant G, editors. Translational Research in Traumatic Brain Injury. Boca Raton (FL): CRC Press/Taylor and Francis Group; 2016. Chapter 15. Available from: <https://www.ncbi.nlm.nih.gov/books/NBK326713/>
8. Rangel-Castillo L, Gopinath S, Robertson CS. Management of Intracranial Hypertension. Neurologic clinics. 2008;26(2):521-541. doi:10.1016/j.ncl.2008.02.003. <https://www.ncbi.nlm.nih.gov/pmc/articles/PMC2452989/>
9. AANN Care of the Patient Undergoing Intracranial Pressure Monitoring/ External Ventricular Drainage or Lumbar Drainage; American Association of Neuroscience Nurses: 2011; pp 1-36. <http://aann.org/publications/clinical-practice-guidelines>
10. Andrews, P. J.; Citerio, G.; Longhi, L.; Polderman, K.; Sahuquillo, J.; Vajkoczy, P., NICEM consensus on neurological monitoring in acute neurological disease. Intensive Care Med 2008, 34 (8), 1362-70. <https://www.ncbi.nlm.nih.gov/pubmed/18398598>
11. Güiza F, Depreitere B, Piper I, Van den Berghe G, Meyfroidt G., "Novel methods to predict increased intracranial pressure during intensive care and long-term neurologic outcome after traumatic brain injury: development and validation in a multicenter dataset" Critical Care Medicine 2013, 41 (2), 688-689. <https://www.ncbi.nlm.nih.gov/pubmed/23263587>

12. Hawthorne C, Piper I. "Monitoring of Intracranial Pressure in Patients with Traumatic Brain Injury." *Frontiers in Neurology*. 2014;5:121. doi:10.3389/fneur.2014.00121. <https://www.ncbi.nlm.nih.gov/pmc/articles/PMC4100218/>
13. Bullock, M. R.; Povlishock, J. T., "Guidelines for the management of severe traumatic brain injury." 4th ed.; Brain Trauma Foundation: 2016. <https://braintrauma.org/guidelines/guidelines-for-the-management-of-severe-tbi-4th-ed#:~:guideline/12-intracranial-pressure-monitoring>
14. Czosnyka, M.; Brady, K.; Reinhard, M.; Smielewski, P.; Steiner, L. A., "Monitoring of Cerebrovascular Autoregulation: Facts, Myths, and Missing Links." *Neurocritical Care* 2009, 10 (3), 373-386. <https://www.ncbi.nlm.nih.gov/pubmed/19127448>
15. Soehle, M.; Gies, B.; Smielewski, P.; Czosnyka, M., "Reduced complexity of intracranial pressure observed in short time series of intracranial hypertension following traumatic brain injury in adults." *J Clin Monit Comput* 2013, 27 (4), 395-403. <https://www.ncbi.nlm.nih.gov/pubmed/23306818>
16. Hu, X.; Xu, P.; Scalzo, F.; Vespa, P.; Bergsneider, M., "Morphological Clustering and Analysis of Continuous Intracranial Pressure." *IEEE Transactions on Biomedical Engineering* 2009, 56 (3), 696-705. <https://www.ncbi.nlm.nih.gov/pmc/articles/PMC2673331/>
17. Kim et al., "Inter-Subject Correlation Exists between Morphological Metrics of Cerebral Blood Flow Velocity and Intracranial Pressure Pulses." *Neurocrit Care*. 2011 Apr;14(2):229-37. doi: 10.1007/s12028-010-9471-x. Epub 2010 Dec 7. <https://www.ncbi.nlm.nih.gov/pubmed/21136207>
18. Scalzo et al., "Intracranial Pressure Signal Morphology." *IEEE Pulse*. 2012 Mar;3(2):49-52. doi: 10.1109/MPUL.2011.2181024. <https://www.ncbi.nlm.nih.gov/pubmed/22481746>
19. Tian et al., "Intracranial Pressure Variability Predicts Short-Term Outcome after Intracerebral Hemorrhage." *J Neurol Sci*. 2013 Jul 15;330(1-2):38-44. doi:10.1016/j.jns.2013.04.001. Epub 2013 Apr 28. <https://www.ncbi.nlm.nih.gov/pubmed/23628469>
20. Le Roux, P., Intracranial pressure after the BEST TRIP trial: a call for more monitoring. *Current Opinion in Critical Care* 2014, 20 (2), 141-147 <https://www.ncbi.nlm.nih.gov/pubmed/24584171>
21. Farahvar, A.; Gerber, L. M.; Chiu, Y.-L.; Carney, N.; Haertl, R.; Ghajar, J., Increased mortality in patients with severe traumatic brain injury treated without intracranial pressure monitoring Clinical article. *Journal of Neurosurgery* 2012, 117 (4), 729-734. <https://www.ncbi.nlm.nih.gov/pubmed/22900846>
22. Kirkman, M. A.; Smith, M., Intracranial pressure monitoring, cerebral perfusion pressure estimation, and ICP/CPP-guided therapy: a standard of care or optional extra after brain injury? *Br J Anaesth* 2014, 112 (1), 35-46. <https://www.ncbi.nlm.nih.gov/pubmed/24293327>
23. T. Takemae, et al. A Simulation Study of Intracranial Pressure Increment Using an Electrical Circuit Model of Cerebral Circulation." *IEEE*

- Transactions on Biomedical Engineering. 1987, BME-34, 12: 958-962, DOI: 10.1109/TBME.1987.325935
<https://www.ncbi.nlm.nih.gov/pubmed/24584171>
24. Ursino M, Lodi CA. "A simple mathematical model of the interaction between intracranial pressure and cerebral hemodynamics." J Appl Physiol (1985). 1997 Apr;82(4):1256-69.
<https://www.ncbi.nlm.nih.gov/pubmed/9104864>
 25. Giulioni M, Ursino M. "Impact of cerebral perfusion pressure and autoregulation on intracranial dynamics: a modeling study." Neurosurgery. 1996 Nov;39(5):1005-14; discussion 1014-5.
<https://www.ncbi.nlm.nih.gov/pubmed/8905758>
 26. Drzewiecki, Gary M., Li, John K-J. Analysis and Assessment of Cardiovascular Function. Springer. ISBN 978-1-4612-1744-2. 1998.
<http://www.springer.com/us/book/9780387982823>
 27. Cheitlin MD. "Cardiovascular physiology-changes with aging." Am J Geriatr Cardiol. 2003 Jan-Feb;12(1):9-13.
<https://www.ncbi.nlm.nih.gov/pubmed/12502909>
 28. Diedrich FJ, Warren WH Jr. "Why change gaits? Dynamics of the walk-run transition" J Exp Psychol Human Percept Perform, 21 (1995), pp. 183-202. <https://www.ncbi.nlm.nih.gov/pubmed/7707029>
 29. Varlet M, Richardson MJ. "Computation of continuous relative phase and modulation of frequency of human movement." J Biomech. 2011 Apr 7;44(6):1200-4. doi:10.1016/j.jbiomech.2011.02.001.
<https://www.ncbi.nlm.nih.gov/pubmed/21329929>
 30. Wininger MT. Decomposition and metrical analysis of single-joint movement of the hemiparetic upper-limb. Rutgers, The State University of New Jersey. 2009. <http://dx.doi.org/doi:10.7282/T3SJ1KSG>
 31. Moradi MK. Evaluation of Features and Quantitative Assessment of Hemiparetic Upper-Limb Movement through Phase Plane Analysis. Rutgers, The State University of New Jersey. 2015.
<http://dx.doi.org/doi:10.7282/T31J9CS6>
 32. A. Goshtasby and D. Schonfeld, "Signal representation based on a Gaussian decomposition," Conference on Information Sciences and Systems, The Johns Hopkins University, pp. 613-618, March 20-22, 1991.
<http://cecs.wright.edu/~agoshtas/ISS91.pdf>
 33. Han et al., "An Online Approach for Intracranial Pressure Forecasting Based on Signal Decomposition and Robust Statistics." IEEE Int. Conf. on Acoustics, Speech, and Sig. Process. 2013
<http://dx.doi.org/doi:10.1109/ICASSP.2013.6638865>
 34. Kim, N., Krasner, A., Kosinski, C. et al. Trending autoregulatory indices during treatment for traumatic brain injury. J Clin Monit Comput (2016) 30: 821. <http://dx.doi.org/doi:10.1007/s10877-015-9779-3>

35. Pimentel et al., "Outcome Prediction for Patients with Traumatic Brain Injury with Dynamic Features from Intracranial Pressure and Arterial Blood Pressure Signals: A Gaussian Process Approach." *Acta Neurochir Suppl.* 2016;122:85-91 http://dx.doi.org/doi:10.1007/978-3-319-22533-3_17
36. Lake, D. E., J. S. Richman, M. P. Griffin, and J. R. Moorman. Sample entropy analysis of neonatal heart rate variability. *Am J Physiol* 2002; 283(3):R789-R797; <http://ajpregu.physiology.org/content/283/3/R789.abstract>
37. Richman, J. S. and J. R. Moorman. Physiological time series analysis using approximate entropy and sample entropy. *Am J Physiol* 2000; 278(6):H2039-H2049; <http://ajpheart.physiology.org/content/278/6/H2039.abstract>
38. Lake DK, Moorman JR, Hanqing C. "Sample Entropy estimation using sampen." *Physionet: Physiotoools.* <https://physionet.org/physiotoools/sampen/>
39. Gao L, Smielewski P, Czosnyka M, Ercole A. Cerebrovascular Signal Complexity Six Hours after Intensive Care Unit Admission Correlates with Outcome after Severe Traumatic Brain Injury. *J Neurotrauma.* 2016 Nov 15;33(22):2011-2018. Epub 2016 Apr 19. <https://www.ncbi.nlm.nih.gov/pubmed/26916703>
40. Fawcett, Tom. "An Introduction to ROC Analysis." *Pattern Recognition Letters.* 2006. 27 (8): 861–874. <https://doi.org/10.1016/j.patrec.2005.10.010>
41. Hu X, Xu P, Asgari S, Vespa P, Bergsneider M. "Forecasting ICP elevation based on prescient changes of intracranial pressure waveform morphology." *IEEE Trans Biomed Eng.* 2010 May;57(5):1070-8. doi: [10.1109/TBME.2009.2037607](https://doi.org/10.1109/TBME.2009.2037607).

APPENDIX II. ABBREVIATIONS

A: Amplitude

ABP: Arterial Blood Pressure

AVP: Acceleration-Velocity Phase Plane [e.g. PAR 2]

AR: Homeostatic Cerebrovascular Autoregulation

FFT: Fast Fourier Transform

ICP: Intracranial Pressure

IH: Intracranial Hypertension

IN: Intracranial Normotension

KS: Kolmogorov-Smirnov

PAR: Phase Area Ratio

PDA: Phase Domain Analysis

preIH: 1-hour preceding ICP hypertension

S: Peak 2 to Peak 1 Amplitude Ratio

SE: Sample Entropy

TBI: Traumatic Brain Injury

VSP: Velocity-Signal Phase Plane [e.g. PAR 1]

W: Width

APPENDIX III. PEER-REVIEWED MANUSCRIPTS, CONFERENCE PROCEEDINGS, AND PRESENTATIONS

Publications

1. Kim NH, Krasner A, Kosinski C, Wininger M, Qadri M, Kappus Z, Danish S, Craelius W. "Trending Autoregulatory Indices During Treatment for Traumatic Brain Injury." *Journal of Clinical Monitoring and Computing*. 2016 Dec;30(6):821-831. Epub 2015 Oct 7.
<https://www.ncbi.nlm.nih.gov/pubmed/26446002>

In Preparation

1. MJ Qadri, N.H. Kim, M. Wininger, S. Danish, W. Craelius. "In-Silico Study of Time- and Phase-Domain Morphological Features of Intracranial Pressure"
2. MJ Qadri, B. Pineda, C. Kosinski, Z. Kappus, N.H. Kim, M. Wininger, S. Danish, W. Craelius. "Multi-scale Time-, Frequency-, and Phase-Domain Analysis of Clinical Intracranial Pressure"

Peer Reviewed Conference Proceedings

1. Qadri MJ, S Danish, W Craelius. "Creating a Validation Dataset for Intracranial Pressure Monitoring Metrics using Gaussian Fitting" BMES Annual Meeting 2016; Translation Biomedical Engineers: Models, Phantoms and Surrogates for Device Validation, Oct 2016; Minneapolis, MN. Poster Presentation.
<http://submissions.mirasmart.com/SecureView/BMESArchive/rad3qleccps.pdf>
2. Kim NH, Qadri M, Danish S, Craelius W. "Assessing Autoregulatory Indices During Traumatic Brain Injury Monitoring." 16th International Symposium on Intracranial Pressure and Neuromonitoring; Cerebrovascular Autoregulation; Jun 2016 ; Massachusetts Institute of Technology, Cambridge, MA. Abstract 123. Poster Presentation.
<http://www.rle.mit.edu/icp2016/programme/>
3. Pineda B, Qadri M, Kosinski C, Kim N, Danish S, Craelius W. "RAP as an Index of Cerebral Hemodynamic Stability after Brain Injury." 16th International Symposium on Intracranial Pressure and Neuromonitoring; Cerebrovascular Autoregulation; Jun 2016 ; Massachusetts Institute of Technology, Cambridge, MA. Abstract 115. Poster Presentation.
<http://www.rle.mit.edu/icp2016/programme/>
4. Qadri MJ, Danish SD, Craelius W. Phase Plane Metric for Quantifying Cycle-to-Cycle ICP Fluctuations. 16th International Symposium on Intracranial Pressure and Neuromonitoring; Track: Neurocritical Care Informatics, Jun 2016; Massachusetts Institute of Technology, Cambridge,

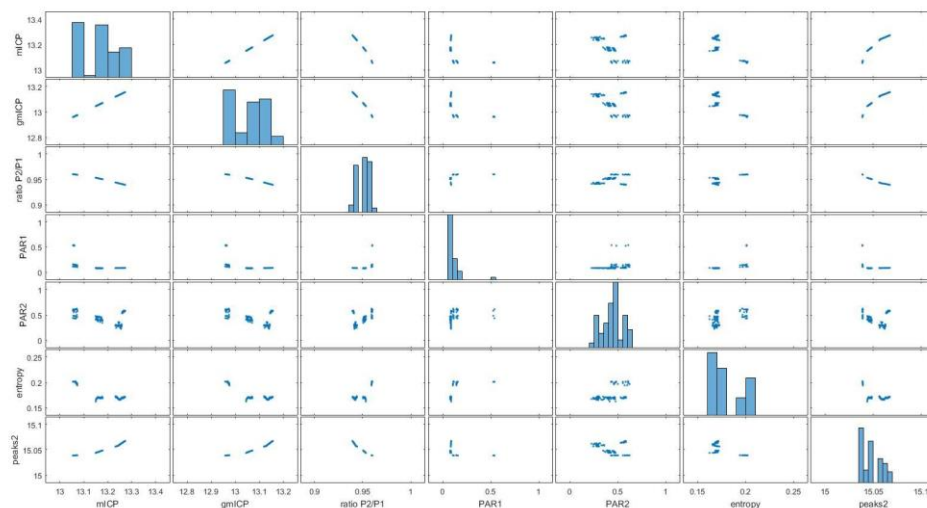
MA. Abstract 119. Poster Presentation.

<http://www.rle.mit.edu/icp2016/programme/>

5. Qadri MJ, NH Kim, M Wininger, S Danish, W Craelius. "Monitoring Cerebrovascular Systems After Traumatic Brain Injury." Rutgers SWE Grad Research Symposium. March 2016; Piscataway, NJ. Poster Presentation: **First Place Winner**
6. Qadri M, Kim NH, Danish S, Craelius W. "A Phase Plane Metric For Intracranial Pressure After Traumatic Brain Injury." Translational Biomedical Engineering: Biomedical Device Design in Translational Research Posters. Biomedical Engineering Society Annual Meeting 2015; Oct 2015, Tampa, FL. Poster Presentation.
<http://submissions.mirasmart.com/SecureView/BMESArchive/radzbdplh0.pdf>
7. Qadri MJ, Kim NH, Kosinski C, Danish S., Wininger M., Craelius W. "Development of Improved Metric for Traumatic Brain Injury Monitoring." Rutgers Joint Molecular Biosciences Graduate Student Association Annual Symposium 2015. Mar 2015; Piscataway, NJ. **Selected Oral Presentation**

APPENDIX IV. FULL RESULTS OF SIMULATION LINEAR MODEL

Width Modulation



Width variation -- Output:mICP

Linear regression model:

$mICP \sim 1 + PAR1 + PAR2 + ratioP1P2 + gmICP + peaks2 + widths2 + entropy$

Estimated Coefficients:

| | Estimate | SE | tStat | pValue |
|-------------|------------|------------|---------|-------------|
| (Intercept) | -0.97058 | 0.010117 | -95.936 | 5.3407e-131 |
| PAR1 | 1.0072e-05 | 4.8271e-06 | 2.0865 | 0.038724 |
| PAR2 | 5.6709e-06 | 4.7436e-06 | 1.1955 | 0.23389 |
| ratioP1P2 | -0.18664 | 0.0019192 | -97.25 | 7.9563e-132 |
| gmICP | 1.0851 | 0.00020177 | 5377.9 | 0 |
| peaks2 | 0.0095183 | 0.00050138 | 18.984 | 8.5881e-41 |
| widths2 | 2.8644e-08 | 4.1981e-08 | 0.68231 | 0.49616 |
| entropy | -0.0013042 | 0.00016822 | -7.7527 | 1.5782e-12 |

Number of observations: 150, Error degrees of freedom: 142

Root Mean Squared Error: 3.64e-06

R-squared: 1, Adjusted R-Squared 1

F-statistic vs. constant model: 9.68e+09, p-value = 0

Linear regression model:

$mICP \sim 1 + PAR1 + PAR2$

Estimated Coefficients:

| | Estimate | SE | tStat | pValue |
|-------------|----------|----------|---------|-------------|
| (Intercept) | 13.322 | 0.023144 | 575.62 | 2.2957e-248 |
| PAR1 | -0.35866 | 0.073675 | -4.8681 | 2.8755e-06 |
| PAR2 | -0.27777 | 0.053114 | -5.2298 | 5.7351e-07 |

Number of observations: 150, Error degrees of freedom: 147

Root Mean Squared Error: 0.0642

R-squared: 0.324, Adjusted R-Squared 0.315

F-statistic vs. constant model: 35.2, p-value = 3.21e-13

Linear regression model:

mICP ~ 1 + ratioPlP2 + gmICP + peaks2 + widths2 + entropy

Estimated Coefficients:

| | Estimate | SE | tStat | pValue |
|-------------|------------|------------|---------|-------------|
| (Intercept) | -0.97675 | 0.0075379 | -129.58 | 5.677e-151 |
| ratioPlP2 | -0.18633 | 0.0016784 | -111.02 | 2.1232e-141 |
| gmICP | 1.0851 | 0.00019378 | 5599.4 | 0 |
| peaks2 | 0.0099483 | 0.00035834 | 27.762 | 1.1154e-59 |
| widths2 | 3.2258e-08 | 4.1877e-08 | 0.77031 | 0.44238 |
| entropy | -0.0013659 | 0.00016834 | -8.114 | 1.9685e-13 |

Number of observations: 150, Error degrees of freedom: 144

Root Mean Squared Error: 3.68e-06

R-squared: 1, Adjusted R-Squared 1

F-statistic vs. constant model: 1.32e+10, p-value = 0

Linear regression model:

mICP ~ 1 + PAR2 + entropy

Estimated Coefficients:

| | Estimate | SE | tStat | pValue |
|-------------|-----------|----------|---------|-------------|
| (Intercept) | 13.98 | 0.039254 | 356.15 | 9.7425e-218 |
| PAR2 | -0.047958 | 0.034771 | -1.3792 | 0.16992 |
| entropy | -4.4555 | 0.24546 | -18.151 | 2.2819e-39 |

Number of observations: 150, Error degrees of freedom: 147

Root Mean Squared Error: 0.0384

R-squared: 0.758, Adjusted R-Squared 0.754

F-statistic vs. constant model: 230, p-value = 5.5e-46

Linear regression model:

mICP ~ 1 + PAR1

Estimated Coefficients:

| | Estimate | SE | tStat | pValue |
|-------------|----------|----------|---------|-------------|
| (Intercept) | 13.212 | 0.010312 | 1281.3 | 3.0379e-301 |
| PAR1 | -0.46478 | 0.076872 | -6.0462 | 1.1548e-08 |

Number of observations: 150, Error degrees of freedom: 148

Root Mean Squared Error: 0.0697

R-squared: 0.198, Adjusted R-Squared 0.193

F-statistic vs. constant model: 36.6, p-value = 1.15e-08

Linear regression model:

mICP ~ 1 + PAR2

Estimated Coefficients:

| | Estimate | SE | tStat | pValue |
|-------------|----------|----------|---------|-------------|
| (Intercept) | 13.313 | 0.02478 | 537.27 | 2.1411e-245 |
| PAR2 | -0.34899 | 0.054835 | -6.3643 | 2.3205e-09 |

Number of observations: 150, Error degrees of freedom: 148

Root Mean Squared Error: 0.0689

R-squared: 0.215, Adjusted R-Squared 0.21

F-statistic vs. constant model: 40.5, p-value = 2.32e-09

Linear regression model:

mICP ~ 1 + peaks2

Estimated Coefficients:

| | Estimate | SE | tStat | pValue |
|--|----------|----|-------|--------|
|--|----------|----|-------|--------|

```

      (Intercept)   -105.89      2.6502   -39.953   3.5913e-81
      peaks2        7.9106      0.17611   44.919   3.949e-88
Number of observations: 150, Error degrees of freedom: 148
Root Mean Squared Error: 0.0203
R-squared: 0.932, Adjusted R-Squared 0.931
F-statistic vs. constant model: 2.02e+03, p-value = 3.95e-88
*****
Linear regression model:
      mICP ~ 1 + widths2

Estimated Coefficients:
              Estimate          SE          tStat          pValue
      (Intercept)           13      0.0091089      1427.2   3.5479e-308
      widths2       0.0038398      0.00020295      18.92   2.424e-41
Number of observations: 150, Error degrees of freedom: 148
Root Mean Squared Error: 0.0421
R-squared: 0.707, Adjusted R-Squared 0.706
F-statistic vs. constant model: 358, p-value = 2.42e-41
*****
Linear regression model:
      mICP ~ 1 + gmICP

Estimated Coefficients:
              Estimate          SE          tStat          pValue
      (Intercept)   -1.2798      0.0026091   -490.52   1.5095e-239
      gmICP          1.1061      0.00019987    5534.3      0
Number of observations: 150, Error degrees of freedom: 148
Root Mean Squared Error: 0.000171
R-squared: 1, Adjusted R-Squared 1
F-statistic vs. constant model: 3.06e+07, p-value = 0
*****
Linear regression model:
      mICP ~ 1 + ratioPlP2

Estimated Coefficients:
              Estimate          SE          tStat          pValue
      (Intercept)    23.063      0.091159      253      4.7912e-197
      ratioPlP2     -10.414      0.095853   -108.64   4.9045e-143
Number of observations: 150, Error degrees of freedom: 148
Root Mean Squared Error: 0.00866
R-squared: 0.988, Adjusted R-Squared 0.988
F-statistic vs. constant model: 1.18e+04, p-value = 4.9e-143
*****
Linear regression model:
      mICP ~ 1 + entropy

Estimated Coefficients:
              Estimate          SE          tStat          pValue
      (Intercept)    13.988      0.038955      359.08   1.6232e-219
      entropy       -4.6169      0.2164      -21.335   5.2682e-47
Number of observations: 150, Error degrees of freedom: 148
Root Mean Squared Error: 0.0385
R-squared: 0.755, Adjusted R-Squared 0.753
F-statistic vs. constant model: 455, p-value = 5.27e-47

```

```

*****
Width variation -- Output:peaks2

```



```
*****
Linear regression model:
peaks2 ~ 1 + PAR1 + PAR2 + ratioP1P2 + gmICP + mICP + widths2 + entropy
```

Estimated Coefficients:

| | Estimate | SE | tStat | pValue |
|-------------|-------------|------------|----------|------------|
| (Intercept) | 78.223 | 3.1809 | 24.592 | 4.8625e-53 |
| PAR1 | -0.00088316 | 0.0004311 | -2.0486 | 0.042341 |
| PAR2 | 0.0014811 | 0.00040702 | 3.639 | 0.0003824 |
| ratioP1P2 | 13.378 | 0.84053 | 15.916 | 2.2371e-33 |
| gmICP | -81.598 | 4.3125 | -18.921 | 1.2061e-40 |
| mICP | 75.173 | 3.9777 | 18.899 | 1.3621e-40 |
| widths2 | -9.8103e-07 | 3.7529e-06 | -0.26141 | 0.79416 |
| entropy | 0.11209 | 0.01522 | 7.3648 | 1.3216e-11 |

Number of observations: 150, Error degrees of freedom: 142

Root Mean Squared Error: 0.000325

R-squared: 0.999, Adjusted R-Squared 0.999

F-statistic vs. constant model: 1.81e+04, p-value = 4.62e-206

Linear regression model:

peaks2 ~ 1 + PAR1 + PAR2

Estimated Coefficients:

| | Estimate | SE | tStat | pValue |
|-------------|-----------|-----------|---------|------------|
| (Intercept) | 15.064 | 0.0030724 | 4903 | 0 |
| PAR1 | -0.035802 | 0.0097806 | -3.6605 | 0.00035028 |
| PAR2 | -0.02559 | 0.007051 | -3.6293 | 0.00039158 |

Number of observations: 150, Error degrees of freedom: 147

Root Mean Squared Error: 0.00852

R-squared: 0.2, Adjusted R-Squared 0.189

F-statistic vs. constant model: 18.3, p-value = 7.78e-08

Linear regression model:

peaks2 ~ 1 + ratioP1P2 + gmICP + mICP + widths2 + entropy

Estimated Coefficients:

| | Estimate | SE | tStat | pValue |
|-------------|-------------|------------|---------|------------|
| (Intercept) | 85.421 | 2.4741 | 34.526 | 1.5485e-71 |
| ratioP1P2 | 15.427 | 0.64853 | 23.787 | 9.7505e-52 |
| gmICP | -91.746 | 3.3211 | -27.626 | 2.0286e-59 |
| mICP | 84.544 | 3.0626 | 27.605 | 2.2169e-59 |
| widths2 | -3.9177e-06 | 3.8766e-06 | -1.0106 | 0.31391 |
| entropy | 0.12899 | 0.015432 | 8.3587 | 4.9047e-14 |

Number of observations: 150, Error degrees of freedom: 144

Root Mean Squared Error: 0.000341

R-squared: 0.999, Adjusted R-Squared 0.999

F-statistic vs. constant model: 2.29e+04, p-value = 7.35e-207

Linear regression model:

peaks2 ~ 1 + PAR2 + entropy

Estimated Coefficients:

| | Estimate | SE | tStat | pValue |
|-------------|------------|-----------|----------|-----------|
| (Intercept) | 15.132 | 0.0067527 | 2240.9 | 0 |
| PAR2 | -0.0014944 | 0.0059816 | -0.24984 | 0.80306 |
| entropy | -0.46185 | 0.042226 | -10.938 | 9.581e-21 |

Number of observations: 150, Error degrees of freedom: 147

Root Mean Squared Error: 0.00661

R-squared: 0.519, Adjusted R-Squared 0.512

F-statistic vs. constant model: 79.2, p-value = 4.66e-24

Linear regression model:

peaks2 ~ 1 + PAR1

Estimated Coefficients:

| | Estimate | SE | tStat | pValue |
|-------------|-----------|-----------|---------|------------|
| (Intercept) | 15.054 | 0.0013121 | 11474 | 0 |
| PAR1 | -0.045579 | 0.0097813 | -4.6598 | 6.9977e-06 |

Number of observations: 150, Error degrees of freedom: 148

Root Mean Squared Error: 0.00887

R-squared: 0.128, Adjusted R-Squared 0.122

F-statistic vs. constant model: 21.7, p-value = 7e-06

Linear regression model:

peaks2 ~ 1 + PAR2

Estimated Coefficients:

| | Estimate | SE | tStat | pValue |
|-------------|-----------|-----------|---------|------------|
| (Intercept) | 15.063 | 0.0031888 | 4723.8 | 0 |
| PAR2 | -0.032699 | 0.0070565 | -4.6339 | 7.8092e-06 |

Number of observations: 150, Error degrees of freedom: 148

Root Mean Squared Error: 0.00887

R-squared: 0.127, Adjusted R-Squared 0.121

F-statistic vs. constant model: 21.5, p-value = 7.81e-06

Linear regression model:

peaks2 ~ 1 + widths2

Estimated Coefficients:

| | Estimate | SE | tStat | pValue |
|-------------|------------|------------|--------|------------|
| (Intercept) | 15.031 | 0.0013457 | 11170 | 0 |
| widths2 | 0.00042099 | 2.9982e-05 | 14.041 | 5.2663e-29 |

Number of observations: 150, Error degrees of freedom: 148

Root Mean Squared Error: 0.00622

R-squared: 0.571, Adjusted R-Squared 0.568

F-statistic vs. constant model: 197, p-value = 5.27e-29

Linear regression model:

peaks2 ~ 1 + mICP

Estimated Coefficients:

| | Estimate | SE | tStat | pValue |
|-------------|----------|-----------|--------|-------------|
| (Intercept) | 13.499 | 0.034505 | 391.22 | 5.0822e-225 |
| mICP | 0.11777 | 0.0026219 | 44.919 | 3.949e-88 |

Number of observations: 150, Error degrees of freedom: 148

Root Mean Squared Error: 0.00248

R-squared: 0.932, Adjusted R-Squared 0.931

F-statistic vs. constant model: 2.02e+03, p-value = 3.95e-88

Linear regression model:

peaks2 ~ 1 + gmICP

Estimated Coefficients:

| | Estimate | SE | tStat | pValue |
|-------------|----------|-----------|--------|-------------|
| (Intercept) | 13.349 | 0.038153 | 349.88 | 7.5199e-218 |
| gmICP | 0.1302 | 0.0029227 | 44.548 | 1.2363e-87 |

Number of observations: 150, Error degrees of freedom: 148

Root Mean Squared Error: 0.0025
 R-squared: 0.931, Adjusted R-Squared 0.93
 F-statistic vs. constant model: 1.98e+03, p-value = 1.24e-87

Linear regression model:
 peaks2 ~ 1 + ratioP1P2

Estimated Coefficients:

| | Estimate | SE | tStat | pValue |
|-------------|----------|----------|---------|-------------|
| (Intercept) | 16.248 | 0.016358 | 993.3 | 6.9593e-285 |
| ratioP1P2 | -1.2613 | 0.0172 | -73.333 | 3.0533e-118 |

Number of observations: 150, Error degrees of freedom: 148

Root Mean Squared Error: 0.00155

R-squared: 0.973, Adjusted R-Squared 0.973

F-statistic vs. constant model: 5.38e+03, p-value = 3.05e-118

Linear regression model:

peaks2 ~ 1 + entropy

Estimated Coefficients:

| | Estimate | SE | tStat | pValue |
|-------------|----------|-----------|--------|------------|
| (Intercept) | 15.133 | 0.0066599 | 2272.2 | 0 |
| entropy | -0.46688 | 0.036996 | -12.62 | 3.0187e-25 |

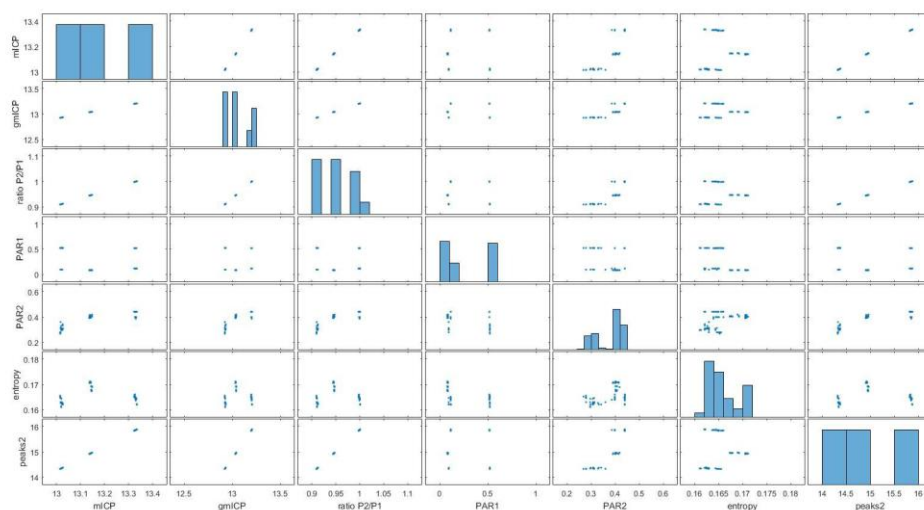
Number of observations: 150, Error degrees of freedom: 148

Root Mean Squared Error: 0.00659

R-squared: 0.518, Adjusted R-Squared 0.515

F-statistic vs. constant model: 159, p-value = 3.02e-25

Amplitude Modulation



Amplitude variation -- Output:mICP

Linear regression model:

mICP ~ 1 + PAR1 + PAR2 + ratioP1P2 + gmICP + peaks2 + widths2 + entropy

Estimated Coefficients:

| | Estimate | SE | tStat | pValue |
|-------------|-------------|------------|---------|------------|
| (Intercept) | 9.2768 | 0.11308 | 82.037 | 1.617e-121 |
| PAR1 | 4.4542e-06 | 3.6702e-06 | 1.2136 | 0.22691 |
| PAR2 | -7.5693e-05 | 3.5766e-05 | -2.1164 | 0.036059 |
| ratioP1P2 | 4.8859 | 0.12505 | 39.072 | 7.4079e-78 |
| gmICP | 0.046083 | 0.011755 | 3.9201 | 0.00013718 |
| peaks2 | -0.090685 | 0.0053415 | -16.977 | 5.3759e-36 |
| widths2 | 8.9082e-06 | 8.3226e-07 | 10.704 | 5.6964e-20 |
| entropy | -0.0043904 | 0.00044252 | -9.9215 | 5.974e-18 |

Number of observations: 150, Error degrees of freedom: 142

Root Mean Squared Error: 6.05e-06

R-squared: 1, Adjusted R-Squared 1

F-statistic vs. constant model: 9.36e+09, p-value = 0

Linear regression model:

mICP ~ 1 + PAR1 + PAR2

Estimated Coefficients:

| | Estimate | SE | tStat | pValue |
|-------------|----------|----------|--------|-------------|
| (Intercept) | 12.338 | 0.038332 | 321.87 | 2.7669e-211 |
| PAR1 | 0.10902 | 0.025113 | 4.3411 | 2.6244e-05 |
| PAR2 | 2.1048 | 0.092241 | 22.819 | 3.6492e-50 |

Number of observations: 150, Error degrees of freedom: 147

Root Mean Squared Error: 0.0589

R-squared: 0.788, Adjusted R-Squared 0.785

F-statistic vs. constant model: 273, p-value = 3.17e-50

Linear regression model:

mICP ~ 1 + ratioP1P2 + gmICP + peaks2 + widths2 + entropy

Estimated Coefficients:

| Estimate | SE | tStat | pValue |
|----------|----|-------|--------|
|----------|----|-------|--------|

```

(Intercept)      9.2748      0.11239      82.526      3.8486e-123
ratioP1P2        4.8789      0.12624      38.648      6.5999e-78
gmICP            0.046351     0.0117      3.9617      0.00011667
peaks2           -0.090341     0.0053995   -16.731      1.4019e-35
widths2          9.3861e-06    7.3146e-07   12.832      1.3053e-25
entropy          -0.0042208    0.00044091  -9.5729      4.1947e-17
Number of observations: 150, Error degrees of freedom: 144
Root Mean Squared Error: 6.12e-06
R-squared: 1, Adjusted R-Squared 1
F-statistic vs. constant model: 1.28e+10, p-value = 0
*****
Linear regression model:
      mICP ~ 1 + PAR2 + entropy

Estimated Coefficients:
              Estimate      SE      tStat      pValue
(Intercept)    14.779      0.21086      70.091    7.3888e-115
PAR2            2.3211     0.073953      31.386    4.8417e-67
entropy        -15.059     1.3396     -11.242    1.5074e-21
Number of observations: 150, Error degrees of freedom: 147
Root Mean Squared Error: 0.0459
R-squared: 0.871, Adjusted R-Squared 0.87
F-statistic vs. constant model: 498, p-value = 3.53e-66
*****
Linear regression model:
      mICP ~ 1 + PAR1

Estimated Coefficients:
              Estimate      SE      tStat      pValue
(Intercept)    13.194     0.016446     802.3    3.6842e-271
PAR1           -0.11629    0.049044     -2.371    0.019026
Number of observations: 150, Error degrees of freedom: 148
Root Mean Squared Error: 0.125
R-squared: 0.0366, Adjusted R-Squared 0.0301
F-statistic vs. constant model: 5.62, p-value = 0.019
*****
Linear regression model:
      mICP ~ 1 + PAR2

Estimated Coefficients:
              Estimate      SE      tStat      pValue
(Intercept)    12.426     0.034392     361.3    6.5242e-220
PAR2            1.9474     0.08978     21.691    8.2387e-48
Number of observations: 150, Error degrees of freedom: 148
Root Mean Squared Error: 0.0623
R-squared: 0.761, Adjusted R-Squared 0.759
F-statistic vs. constant model: 470, p-value = 8.24e-48
*****
Linear regression model:
      mICP ~ 1 + peaks2

Estimated Coefficients:
              Estimate      SE      tStat      pValue
(Intercept)    10.074     0.00078092   12901      0
peaks2          0.20529    5.1847e-05   3959.5      0
Number of observations: 150, Error degrees of freedom: 148
Root Mean Squared Error: 0.000391
R-squared: 1, Adjusted R-Squared 1
F-statistic vs. constant model: 1.57e+07, p-value = 0

```

```
*****
Linear regression model:
mICP ~ 1 + widths2
```

Estimated Coefficients:

| | Estimate | SE | tStat | pValue |
|-------------|-----------|------------|--------|------------|
| (Intercept) | 12.948 | 0.0063674 | 2033.5 | 0 |
| widths2 | 0.0065336 | 0.00016837 | 38.805 | 1.8507e-79 |

Number of observations: 150, Error degrees of freedom: 148

Root Mean Squared Error: 0.0381

R-squared: 0.911, Adjusted R-Squared 0.91

F-statistic vs. constant model: 1.51e+03, p-value = 1.85e-79

```
*****
Linear regression model:
mICP ~ 1 + gmICP
```

Estimated Coefficients:

| | Estimate | SE | tStat | pValue |
|-------------|----------|------------|---------|-------------|
| (Intercept) | -1.5582 | 0.0085001 | -183.32 | 2.0967e-176 |
| gmICP | 1.1276 | 0.00065099 | 1732.1 | 1.2786e-320 |

Number of observations: 150, Error degrees of freedom: 148

Root Mean Squared Error: 0.000895

R-squared: 1, Adjusted R-Squared 1

F-statistic vs. constant model: 3e+06, p-value = 1.28e-320

```
*****
Linear regression model:
mICP ~ 1 + ratioP1P2
```

Estimated Coefficients:

| | Estimate | SE | tStat | pValue |
|-------------|----------|------------|-------|--------|
| (Intercept) | 9.8413 | 0.00022467 | 43803 | 0 |
| ratioP1P2 | 3.4908 | 0.00023588 | 14799 | 0 |

Number of observations: 150, Error degrees of freedom: 148

Root Mean Squared Error: 0.000105

R-squared: 1, Adjusted R-Squared 1

F-statistic vs. constant model: 2.19e+08, p-value = 0

```
*****
Linear regression model:
mICP ~ 1 + entropy
```

Estimated Coefficients:

| | Estimate | SE | tStat | pValue |
|-------------|----------|---------|--------|------------|
| (Intercept) | 12.527 | 0.54838 | 22.844 | 2.2185e-50 |
| entropy | 3.8422 | 3.3094 | 1.161 | 0.24751 |

Number of observations: 150, Error degrees of freedom: 148

Root Mean Squared Error: 0.127

R-squared: 0.00903, Adjusted R-Squared 0.00233

F-statistic vs. constant model: 1.35, p-value = 0.248

```
*****
Amplitude variation -- Output:peak2
*****
```

Linear regression model:

peaks2 ~ 1 + PAR1 + PAR2 + ratioP1P2 + gmICP + mICP + widths2 + entropy

Estimated Coefficients:

| | Estimate | SE | tStat | pValue |
|-------------|----------|--------|--------|------------|
| (Intercept) | 74.9 | 3.3106 | 22.624 | 6.1831e-49 |

```

PAR1          3.6489e-05      3.312e-05      1.1017      0.27244
PAR2         -0.00061685      0.0003234     -1.9074      0.058488
ratioPlP2          43.787        1.2165      35.993      2.9508e-73
gmICP          -0.31916        0.10833     -2.9463      0.0037605
mICP           -7.3959         0.4349     -17.006      4.5812e-36
widths2         4.8965e-05      9.2193e-06      5.3111      4.1134e-07
entropy        -0.020757        0.0048943     -4.2411      3.9883e-05
Number of observations: 150, Error degrees of freedom: 142
Root Mean Squared Error: 5.46e-05
R-squared: 1, Adjusted R-Squared 1
F-statistic vs. constant model: 2.73e+09, p-value = 0
*****
Linear regression model:
peaks2 ~ 1 + PAR1 + PAR2

Estimated Coefficients:
              Estimate          SE          tStat          pValue
(Intercept)    11.027         0.1875         58.81      4.8613e-104
PAR1           0.53562        0.12284         4.3602      2.4299e-05
PAR2           10.245         0.4512        22.707      6.4169e-50
Number of observations: 150, Error degrees of freedom: 147
Root Mean Squared Error: 0.288
R-squared: 0.786, Adjusted R-Squared 0.783
F-statistic vs. constant model: 270, p-value = 5.87e-50
*****
Linear regression model:
peaks2 ~ 1 + ratioPlP2 + gmICP + mICP + widths2 + entropy

Estimated Coefficients:
              Estimate          SE          tStat          pValue
(Intercept)    74.351         3.3201        22.394      9.2373e-49
ratioPlP2       43.579         1.2203        35.712      1.9775e-73
gmICP          -0.34011        0.10702        -3.1779      0.001816
mICP           -7.3184         0.43661       -16.762      1.1785e-35
widths2         5.1661e-05      8.6147e-06      5.9968      1.5473e-08
entropy        -0.018693        0.0048256       -3.8737      0.00016221
Number of observations: 150, Error degrees of freedom: 144
Root Mean Squared Error: 5.5e-05
R-squared: 1, Adjusted R-Squared 1
F-statistic vs. constant model: 3.77e+09, p-value = 0
*****
Linear regression model:
peaks2 ~ 1 + PAR2 + entropy

Estimated Coefficients:
              Estimate          SE          tStat          pValue
(Intercept)    23.006         1.0297        22.342      4.0774e-49
PAR2           11.305         0.36115        31.304      6.7762e-67
entropy        -73.882         6.5418       -11.294      1.0964e-21
Number of observations: 150, Error degrees of freedom: 147
Root Mean Squared Error: 0.224
R-squared: 0.871, Adjusted R-Squared 0.869
F-statistic vs. constant model: 495, p-value = 5.13e-66
*****
Linear regression model:
peaks2 ~ 1 + PAR1

Estimated Coefficients:
              Estimate          SE          tStat          pValue

```

| | | | | |
|-------------|----------|----------|---------|-------------|
| (Intercept) | 15.197 | 0.080138 | 189.63 | 1.4226e-178 |
| PAR1 | -0.56107 | 0.23899 | -2.3477 | 0.020213 |

Number of observations: 150, Error degrees of freedom: 148

Root Mean Squared Error: 0.609

R-squared: 0.0359, Adjusted R-Squared 0.0294

F-statistic vs. constant model: 5.51, p-value = 0.0202

Linear regression model:

peaks2 ~ 1 + PAR2

Estimated Coefficients:

| | Estimate | SE | tStat | pValue |
|-------------|----------|---------|--------|-------------|
| (Intercept) | 11.461 | 0.16832 | 68.09 | 1.3048e-113 |
| PAR2 | 9.4719 | 0.43939 | 21.557 | 1.6519e-47 |

Number of observations: 150, Error degrees of freedom: 148

Root Mean Squared Error: 0.305

R-squared: 0.758, Adjusted R-Squared 0.757

F-statistic vs. constant model: 465, p-value = 1.65e-47

Linear regression model:

peaks2 ~ 1 + widths2

Estimated Coefficients:

| | Estimate | SE | tStat | pValue |
|-------------|----------|------------|--------|-------------|
| (Intercept) | 13.998 | 0.030718 | 455.7 | 8.0993e-235 |
| widths2 | 0.031856 | 0.00081228 | 39.218 | 4.4291e-80 |

Number of observations: 150, Error degrees of freedom: 148

Root Mean Squared Error: 0.184

R-squared: 0.912, Adjusted R-Squared 0.912

F-statistic vs. constant model: 1.54e+03, p-value = 4.43e-80

Linear regression model:

peaks2 ~ 1 + mICP

Estimated Coefficients:

| | Estimate | SE | tStat | pValue |
|-------------|----------|-----------|---------|--------|
| (Intercept) | -49.073 | 0.016195 | -3030.1 | 0 |
| mICP | 4.8711 | 0.0012302 | 3959.5 | 0 |

Number of observations: 150, Error degrees of freedom: 148

Root Mean Squared Error: 0.00191

R-squared: 1, Adjusted R-Squared 1

F-statistic vs. constant model: 1.57e+07, p-value = 0

Linear regression model:

peaks2 ~ 1 + gmICP

Estimated Coefficients:

| | Estimate | SE | tStat | pValue |
|-------------|----------|-----------|---------|-------------|
| (Intercept) | -56.662 | 0.059431 | -953.41 | 2.9973e-282 |
| gmICP | 5.4923 | 0.0045516 | 1206.7 | 2.17e-297 |

Number of observations: 150, Error degrees of freedom: 148

Root Mean Squared Error: 0.00626

R-squared: 1, Adjusted R-Squared 1

F-statistic vs. constant model: 1.46e+06, p-value = 2.17e-297

Linear regression model:

peaks2 ~ 1 + ratioP1P2

Estimated Coefficients:

| | Estimate | SE | tStat | pValue |
|-------------|----------|-----------|---------|-------------|
| (Intercept) | -1.1353 | 0.003001 | -378.31 | 7.2569e-223 |
| ratioP1P2 | 17.004 | 0.0031507 | 5397 | 0 |

Number of observations: 150, Error degrees of freedom: 148

Root Mean Squared Error: 0.0014

R-squared: 1, Adjusted R-Squared 1

F-statistic vs. constant model: 2.91e+07, p-value = 0

Linear regression model:

peaks2 ~ 1 + entropy

Estimated Coefficients:

| | Estimate | SE | tStat | pValue |
|-------------|----------|--------|--------|------------|
| (Intercept) | 12.037 | 2.6719 | 4.5052 | 1.3371e-05 |
| entropy | 18.18 | 16.125 | 1.1275 | 0.26138 |

Number of observations: 150, Error degrees of freedom: 148

Root Mean Squared Error: 0.618

R-squared: 0.00852, Adjusted R-Squared 0.00182

F-statistic vs. constant model: 1.27, p-value = 0.261

APPENDIX V. CLINICAL DATA - PATIENT A-F SUMMARIES

Patient A:

Recording Time: 27.38 hours

Number of Cycles: 1.0902e+05

Number of Events: 2

KS Test Results:

| preIH Time (hr) | H | P | KS stat |
|-----------------|---|--------|---------|
| 1 | 1 | 0.0000 | 0.2206 |
| 0.5 | 1 | 0.0000 | 0.2619 |
| 0.25 | 1 | 0.0000 | 0.2829 |
| 0.1 | 1 | 0.0001 | 0.3200 |

Spearman's Ranked Corr. Results:

| preIH Time (hr) | Spearman's Rho for IN | P for IN | Spearman's Rho for preIH | P for IH |
|-----------------|-----------------------|----------|--------------------------|----------|
| 1 | -0.0478 | 0.0027 | 0.0896 | 0.0605 |
| 0.5 | -0.0473 | 0.0023 | 0.1762 | 0.0094 |
| 0.25 | -0.0449 | 0.0034 | 0.0614 | 0.5143 |
| 0.1 | -0.0440 | 0.0038 | 0.0587 | 0.6846 |

Patient B:

Recording Time: 49.08 hours

Number of Cycles: 1.7669e+05

Number of Events: 1

KS Test Results:

| preIH Time (hr) | H | P | KS stat |
|-----------------|---|--------|---------|
| 1 | 1 | 0.0186 | 0.1779 |
| 0.5 | 1 | 0.0119 | 0.3326 |
| 0.25 | 0 | 0.1500 | 0.3611 |
| 0.1 | 0 | 0.7957 | 0.4019 |

Spearman's Ranked Corr. Results:

| preIH Time (hr) | Spearman's Rho for IN | P for IN | Spearman's Rho for preIH | P for IH |
|-----------------|-----------------------|----------|--------------------------|----------|
| 1 | -0.1611 | 0.0000 | -0.1034 | 0.3799 |
| 0.5 | -0.1604 | 0.0000 | -0.1214 | 0.5891 |
| 0.25 | -0.1630 | 0.0000 | -0.3000 | 0.4366 |
| 0.1 | -0.1645 | 0.0000 | 1.0000 | 1.0000 |

Patient C:

Recording Time: 70.46 hours

Number of Cycles: 2.5366e+05

Number of Events: 2

KS Test Results:

| preIH Time (hr) | H | P | KS stat |
|-----------------|---|--------|---------|
| 1 | 1 | 0.0156 | 0.2011 |
| 0.5 | 0 | 0.1615 | 0.1768 |
| 0.25 | 0 | 0.2354 | 0.1766 |
| 0.1 | 0 | 0.7240 | 0.2320 |

Spearman's Ranked Corr. Results:

| preIH Time (hr) | Spearman's Rho for IN | P for IN | Spearman's Rho for preIH | P for IH |
|-----------------|-----------------------|----------|--------------------------|----------|
| 1 | -0.0188 | 0.2882 | 0.2031 | 0.1229 |
| 0.5 | -0.0118 | 0.5028 | 0.2246 | 0.1692 |
| 0.25 | -0.0111 | 0.5294 | 0.2729 | 0.1244 |
| 0.1 | -0.0091 | 0.6061 | 0.1905 | 0.6646 |

Patient D:

Recording Time: 30.28 hours

Number of Cycles: 1.0900e+05

Number of Events: 1

KS Test Results:

| preIH Time (hr) | H | P | KS stat |
|-----------------|---|--------|---------|
| 1 | 0 | 0.2461 | 0.1244 |
| 0.5 | 0 | 0.1834 | 0.2299 |
| 0.25 | 0 | 0.4303 | 0.2786 |
| 0.1 | 0 | 0.9002 | 0.3547 |

Spearman's Ranked Corr. Results:

| preIH Time (hr) | Spearman's Rho for IN | P for IN | Spearman's Rho for preIH | P for IH |
|-----------------|-----------------------|----------|--------------------------|----------|
| 1 | -0.2341 | 0.0000 | -0.1034 | 0.3799 |
| 0.5 | -0.2018 | 0.0000 | -0.1214 | 0.5891 |
| 0.25 | -0.2049 | 0.0000 | -0.3000 | 0.4366 |
| 0.1 | -0.2076 | 0.0000 | 1.0000 | 1.0000 |

Patient E:

Recording Time: 186.78

Number of Cycles: 6.7240e+05

Number of Events: 5

KS Test Results:

| preIH Time (hr) | H | P | KS stat |
|-----------------|---|--------|---------|
| 1 | 1 | 0.0000 | 0.2409 |
| 0.5 | 1 | 0.0000 | 0.2682 |
| 0.25 | 1 | 0.0000 | 0.3103 |
| 0.1 | 1 | 0.0000 | 0.3398 |

Spearman's Ranked Corr. Results:

| preIH Time (hr) | Spearman's Rho for IN | P for IN | Spearman's Rho for preIH | P for IH |
|-----------------|-----------------------|----------|--------------------------|----------|
| 1 | 0.3161 | 0.0000 | 0.0837 | 0.0009 |
| 0.5 | 0.3094 | 0.0000 | -0.0939 | 0.0092 |
| 0.25 | 0.3017 | 0.0000 | -0.2631 | 0.0000 |
| 0.1 | 0.2926 | 0.0000 | -0.5462 | 0.0000 |

Patient F:

Recording Time: 82.51

Number of Cycles: 2.7997e+05

Number of Events: 11

KS Test Results:

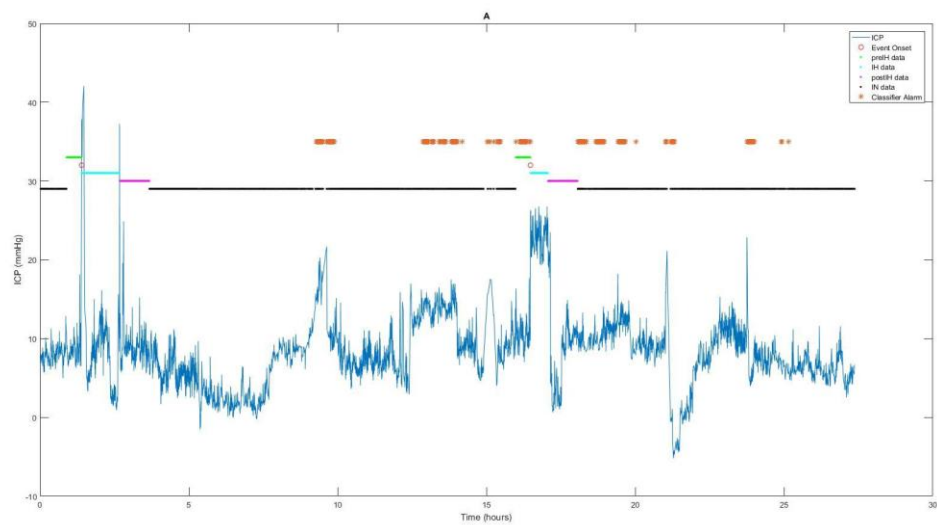
| preIH Time (hr) | H | P | KS stat |
|-----------------|---|--------|---------|
| 1 | 1 | 0.0000 | 0.2508 |
| 0.5 | 1 | 0.0000 | 0.2738 |
| 0.25 | 1 | 0.0000 | 0.3313 |
| 0.1 | 1 | 0.0000 | 0.3378 |

Spearman's Ranked Corr. Results:

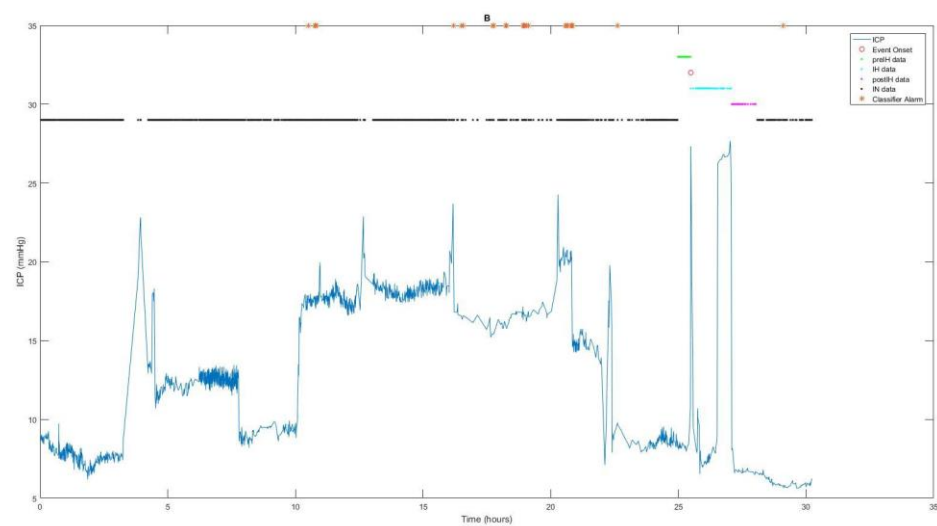
| preIH Time (hr) | Spearman's Rho for IN | P for IN | Spearman's Rho for preIH | P for IH |
|-----------------|-----------------------|----------|--------------------------|----------|
| 1 | -0.4948 | 0.0000 | -0.4819 | 0.0000 |
| 0.5 | -0.5115 | 0.0000 | -0.4058 | 0.0000 |
| 0.25 | -0.5052 | 0.0000 | -0.3983 | 0.0000 |
| 0.1 | -0.5121 | 0.0000 | -0.4171 | 0.0000 |

APPENDIX VI. MOCK ALARM FOR PATIENTS A-F

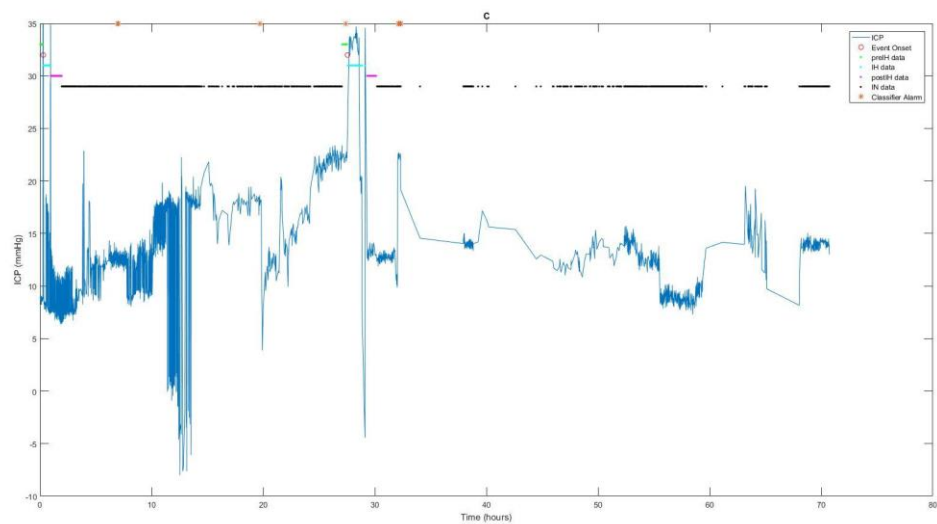
Patient A



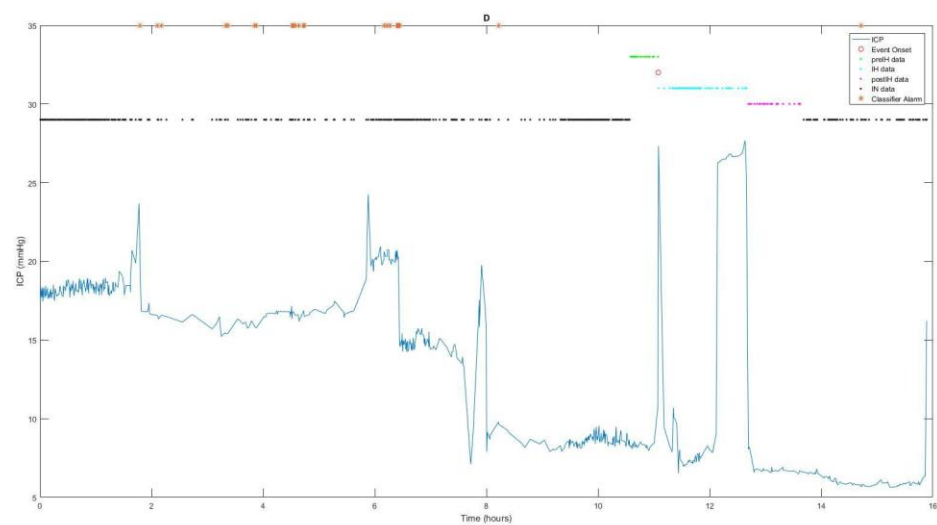
Patient B



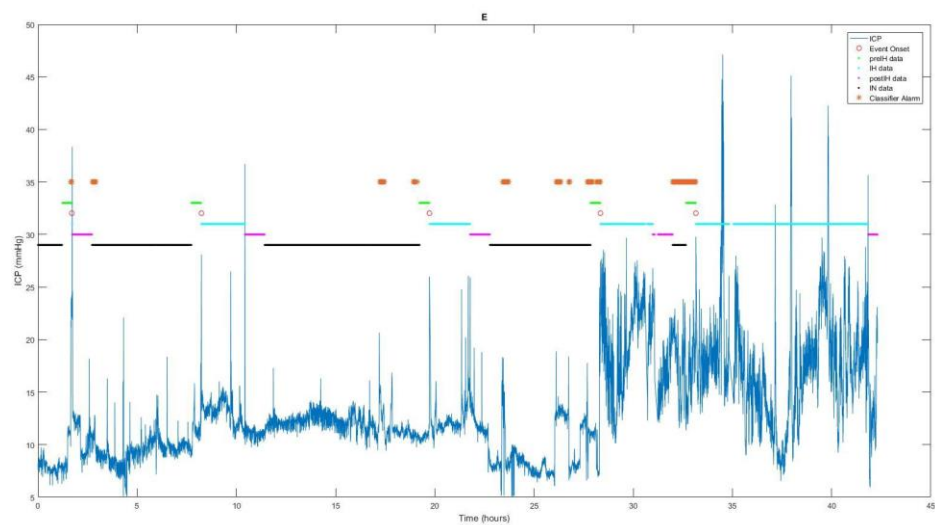
Patient C



Patient D



Patient E



Patient F

